FUNCTIONAL PROPERTIES OF METALLOTHIONEIN EXPRESSION IN MITOCHONDRIAL NADH:UBIQUINONE OXIDOREDUCTASE DEFICIENCY

By

Fimmie Reinecke, Hons. B.Sc.

Dissertation submitted for the degree Magister Scientiae in Biochemistry at the North-West University

Supervisor: Dr. F.H. van der Westhuizen
Co-supervisor: Prof. A. Olckers

The financial assistance of the National Research Foundation (NRF) towards this research is hereby acknowledged. Opinions expressed and conclusions arrived at, are those of the author and are not necessarily to be attributed to the NRF.

2004
Potchefstroom

FUNKSIONELE EIENSKAPPE VAN METALLOTIONEIN UITDRUKKING IN MITOCHONDRIALE NADH:UBIQUNOON OKSIDOREDUKTASE DEFEK

Deur

Fimmie Reinecke, Hons. B.Sc.

Verhandeling voorgelê vir die graad Magister Scientiae in Biochemie aan die Noordwes-Universiteit

Studieleier: Dr. F.H. van der Westhuizen
Medestudieleier: Prof. A. Olckers

Die finansiële bystand van die Nasionale Navorsings Stigting (NRF) vir hierdie navorsing word hiermee erken. Opinies uitgedruk en gevolgtrekkings gemaak is die van die outeur en wourd nie noodwendig deur die NRF erken nie.

2004
Potchefstroom

"The thing that is really hard, and really amazing,
is giving up on being perfect and beginning the work of becoming yourself."

Anna Quindlen

To my mom and dad

OPSOMMING

NADH:ubiqunoon oksidoreduktase (kompleks I) defekte is een van die mees algemene oorsake van 'n mitochondriale respiratoriese ketting defek. Een van die belangrikste gevolge van kompleks I defekte is die produksie van hoë vlakke van reaktiewe suurstof spesies (ROS) en die skadelike effek daarvan op die mitochondrion en induksie van apoptose. Daar is gevind dat metallotioniene (MTs), waarskynlik a.g.v. hul unieke strukturele eienskappe, ROS kan bind en reduseer.

Die doel van hierdie studie was om hierdie voorgestelde beskermende rol van metallotionien deur ooruitdrukking in 'n sellyn met 'n kompleks I defek te ondersoek en te bepaal of hierdie proteïne teen ROS of ROS-verwante skade kan beskerm. Verder is die bydrae van verskillende MT isovorme tot verskillende vlakke van beskerming in hierdie selle ondersoek. MT-1B en MT-2A cDNA volgordes is onderskeidelik in the pIRESneo2 uitdrukkings-vektor gekloneer en getransfekteer na HeLa selle. Die uitdrukkingsvlakke is gekarakteriseer en selektiewe biochemiese analises uitgevoer.

Kaspase 3/7 aktiwiteit en sel-lewensvatbaarheidsanalises op rotenoon-geïnduseerde kompleks I-defektiewe selle het onthul dat MT-1B en veral MT-2A teen apoptose induksie beskerm, terwyl MT-2A ook addisionele beskerming teen ROS-geïnduseerde nekrose getoon het. Direkte ROS kwantifisering kon nie MT beskerming in hierdie selle ondersteun nie, maar dit het wel laer vlakke van ROS produksie in *t*-BHP-behandelde selle getoon. In kompleks I defektiewe selle waarin MTs teen verhoogde vlakke uitgedruk is, was die verlaging van membraanpotensiaal ook baie minder en hierdie selle het ook 'n beter sellulêre morfologie getoon in vergelyking met kontrole selle. Die resultate wat in hierdie studie gegenereer is ondersteun die hipotese dat beide MT-1B en MT-2A 'n spesifieke beskermende effek in selle met 'n kompleks I defek het. Dit blyk egter dat MT-2A 'n effens groter beskerming teen ROS, mtPTP vorming, apoptose en ROS-geïnduseerde nekrose bied as MT-1B.

ABSTRACT

NADH:ubiquinone oxidoreductase (complex I) deficiency is one of the most frequently encountered causes of mitochondrial respiratory chain disorders. One of the major consequences of such a complex I deficiency is the production of high levels of reactive oxygen species (ROS) and its deleterious effects on the mitochondria and induction of apoptosis. Metallothioneins have been identified as scavengers of ROS, probably due to its unique structural characteristics that provide the ability to bind and reduce ROS.

The study investigated the putative protective role of metallothionein overexpression in a complex I deficient cell line and establish whether this protection was targeted against ROS or ROS-related consequences. It was also necessary to establish whether different MT isoforms would lead to different levels of protection in complex I deficient cells. MT-1B and MT-2A cDNA sequences were respectively cloned into the pIRESneo2 expression vector and transfected into HeLa cells. The expression levels were characterised and selected biochemical assays conducted.

Caspase 3/7 activity measurement and cell viability assays of rotenone-induced complex I deficient cells revealed MT-1B and especially MT-2A to protect against apoptosis induction, whilst MT-2A also showed additional protection against ROS-induced necrosis. Direct ROS quantification could not confirm MT protection in rotenone-induced complex I deficient cells, but showed lower levels of ROS production in *t*-BHP treated cells. Decreases in membrane potential also appeared to be much less in MT-overexpressed complex I deficient cells. These cells also showed a tendency towards better cellular morphology. Hence, the results presented in this study support the hypothesis that both MT-1B and MT-2A has some protective effect in complex I deficient cells. It does appear, however, that MT-2A seems to be somewhat more effective in protection against ROS, mtPTP formation, apoptosis and ROS-induced necrosis than MT-1B.

TABLE OF CONTENTS

LIST OF ABBREVIATIONS AND SYMBOLS

LIST OF SYMBOLS

α	alpha
β	beta
λ	lambda
$\Delta\psi$	electrochemical gradient, membrane potential
ψ	pseudogene
I	complex I, NADH:ubiquinone oxidoreductase
II	complex II, succinate:ubiquinone oxidoreductase
III	complex III, ubiquinol:ferricytochrome *c* oxidoreductase, *cytochrome bc_1 complex*
IV	complex IV, ferrycytochrome:oxygen oxidoreductase, *cytochrome c oxidase*, COX
V	complex V, F_1F_0-ATP synthase
#	number
µ	micro: 10^{-6}
n	nano:10^{-9}
e^-	electron
~	approximately
%	percent
E^0	standard redox potential

LIST OF ABBREVIATIONS

A	adenine
A	alanine
acetyl-CoA	acetyl-coenzyme A
ADP	adenosine diphosphate
Ag	silver
Ag^+	silver monovalent ion
Ag^{2+}	silver divalent ion
Age I	*Agrobacterium gelatinovorum* restriction endonuclease, isoschizomer of *Pin* AI
AIF	apoptosis-inducing factor
Ala	alanine
Amp^r	ampicillin resistance

A_{nm}	absorbance at specific wavelength (in nm)
ANT	adenine nucleotide translocator
Apaf-1	apoptotic peptidase activating factor 1
apo-MT	metal-free thionein
ARE	antioxidant - or electrophile response element
Arg	arginine
Asn	asparagine
Asp	aspartic acid
ATP	adenosine triphosphate
ATPase 6 and 8	ATP synthase subunits 6 and 8
b	base
*Bam*H I	*Bacillus amyloliquefaciens* H restriction endonuclease
BCA	Bicinchoninic acid
Bi^{3+}	bismuth trivalent ion
β-2-MG	β-2-microglobulin
bp	base pair
BSA	bovine serum albumin
C	cysteine
°C	degrees centigrade
Ca^{2+}	calsium ion
$CaCl_2$	calcium chloride
Cd	cadmium
Cd^{2+}	cadmium divalent ion
cDNA	complementary DNA
CK	creatine kinase
CMV	cytomegalovirus
Cph D	cyclophilin D
Co	cobalt
Co^{2+}	cobalt divalent ion
CO_2	carbon dioxide
Col E1 ori	*E.coli* replication origin
CoQ	coenzyme Q, ubiquinone
$CoQH_2$	ubiquinol
COX1-3	ferricytochrome:oxygen oxidoreductase or *cytochrome c oxidase* subunits 1, 2 and 3
Cr	creatine
Cr-P	creatine phosphate
CsA	cyclosporine A
CsTFA	caesium trifluoroacetate

Ct	cycle threshold value
Cu	copper
Cu^+	copper monovalent ion
Cys	cysteine
Da	Dalton
dATP	2'-deoxyadenosine-5'-triphosphate
D	aspartic acid
DCF	2',7'-dichlorofluorescin
DCFDA	2',7'-dichlorofluorescin diacetate
dCTP	2'-deoxycytidine-5'-triphosphate
ddH_2O	double distilled water
DEPC	diethyl pyrocarbonate
dGTP	2'-deoxyguanosine-5'-triphosphate
DMEM	Dulbecco's Modified Eagle's Medium
DMSO	dimethyl sulphoxide
DNA	deoxyribonucleic acid
ds	double stranded
DTNB	5,5'-dithiobis-(2-nitrobenzoic acid)
dTTP	2'-deoxythymidine-5'-triphosphate
E	glutamic acid
E	PCR efficiency
ECMV	encephalomyocarditis virus
E.coli	*Escherichia coli*
E.coli DH10B	*Escherichia coli* strain DH10B
*Eco*R I	*Escherichia coli* RY13 restriction enzyme
*Eco*R V	*Escherichia coli* J62P7G74 restriction enzyme
EDTA	ethlyene diamine tetra-acetic acid di-sodium salt
ELISA	enzyme-linked immunosorbent assay
ETC	electron transport chain
ETF	electron transfer flavoprotein
EtOH	ethanol
F	forward
F_0	F_0 subunit of ATPase complex
FAD^+	flavin adenine dinucleotide (oxidised)
$FADH_2$	flavin adenine dinucleotide (reduced)
FBS	fetal bovine serum
Fe^{2+}	iron divalent ion
FeS	iron-sulphur clusters
FMN	flavin mononucleotide

FP	flavoprotein fraction
fwd	forward primer
g	grams
g	gravitational force of the earth (~10m.s^{-1})
G	guanine
G	glycine
GAPDH	glyceraldehyde-3-phosphate dehydrogenase
gDNA	genomic DNA
Gln	glutamine
Glu	glutamic acid
glucose-6-P	glucose-6-phosphate
Gly	glycine
GPx	glutathione peroxidase
GSH	reduced glutathione
HCl	hydrochloric acid
H_2O	water
H_2O_2	hydrogen peroxide
Hg	mercury
Hg^{2+}	mercury divalent ion
HG	housekeeping gene
Hind III	*Haemophilus influenzae* R_d, restriction endonuclease
His	histidine
HK	hexokinase
hMT	human metallothionein
hMT-1 A to X	human metallothionein subform 1, isoforms A, B, C, D, E, F, G, H, I, J, K, L and X
ΨhMT-1C	human metallothionein subform 1, isoform C, pseudogene
ΨhMT-1D	human metallothionein subform 1, isoform D, pseudogene
ΨhMT-1G	human metallothionein subform 1, isoform G, pseudogene
ΨhMT-1H	human metallothionein subform 1, isoform h, pseudogene
hMT-2 A	human metallothionein subform 2, isoform A
ΨhMT-2B	human metallothionein subform 2, isoform B, pseudogene
hMT-3	human metallothionein subform 3
hMT-4	human metallothionein subform 4
HP	hydrophobic-protein fractions
Ile	isoleucine
IP	iron–protein fraction
IRES	the internal ribosome entry site
IT_{H1}	heavy strand initiation of transcription sites 1

IT_{H2}	heavy strand initiation of transcription sites 2
IT_L	light stand initiation of transcription site
IVS	synthetic intron
K	lysine
KAc	potassium acetate
kb	kilo base pairs (thousand base pairs)
KCl	potassium chloride
KCN	potassium cyanide
KDa	kilo Dalton
KH_2PO_4	potassium phosphate monobasic
K_2HPO_4	potassium phosphate dibasic
KPi	potassium phosphate
LB	Luria broth
LDH	lactate dehydrogenase
Leu	leucine with anticodon CUN
Leu $^{(UUR)}$	leucine with anticodon UUR
LHON	Leber's hereditary optic neuropathy
LiCl	lithium chloride
Ln	natural logarithm
Lys	lysine
M	methionine
M	molar (moles/litre)
MCS	multiple cloning site
Me	methyl group (-CH_3)
MELAS	mitochondrial encephalomyopathy with lactic acidosis and stroke-like episodes
MERRF	myoclonus epilepsy with ragged red fibres
Met	methionine
$MgCl_2$	magnesium chloride
µl	micro litres (10^{-6})
µm	micro meters (10^{-6})
min	minutes
ml	millilitres (10^{-3})
MLTF	adenomajor late transcription factor, or USF
mM	milli molar
mm	millimetre
M-MLV RT	Moloney Murine Leukemia virus reverse transcriptase
MnSOD	manganese superoxide dismutase
MP	metallo-regulatory protein

MRE	metal responsive element
MREa-g	non-identical copies of metal responsive elements a to g
mRNA	messenger RNA
MT	metallothionein
MT-1B	metallothionein isoform1B
MT-2A	metallothionein isoform 2A
mtDNA	mitochondrial DNA
MT-E	metallothionein subgroup 5
MTF-1	metal-responsive element-binding transcription factor 1
MTL-5	metallothionein-like 5
MT-M	metallothionein subgroup 5
mtPTP	mitochondrial permeability transition pore
MTT	3-(4,5-Dimethylthiazol-2-yl)-2,5-diphenyltetrazolium bromide
mtTERM	binding site for the mitochondrial transcription terminator
N	asparagine
n	number
NaCl	sodium chloride
NAD^+	nicotinamide adenine dinucleotide (oxidised)
NADH	nicotinamide adenine dinucleotide (reduced)
NADPH	nicotinamide adenine dinucleotide phosphate (reduced)
NaOAc	sodium acetate
NaOH	sodium hydroxide
$NaHCO_3$	sodium bicarbonate
ND1-6	NADH:ubiquinone oxidoreductase subunits 1, 2, 3, 4, 4L, 5, 6
nDNA	nuclear DNA
NE	normalized expression of target genes
Neo^r	neomycin phosphotransferase coding sequence
NF	normalization factor
Ni	nickel
Ni^{2+}	nickel divalent ion
$NO^{\cdot}$	nitric oxide
O_2	oxygen
$O_2^{\cdot-}$	superoxide
OD	optical density / Absorbance
O_H	heavy strand origin or replication
$OH^{\cdot}$	hydroxyl free radical
O_L	light strand origin of replication
$ONOO^{\cdot}$	peroxynitrite
OXPHOS	oxidative phosphorylation

P	proline
Pb	lead
Pb^{2+}	lead divalent ion
PBS	phosphate buffered saline
P CMV IE	human cytomegalovirus (CMV) major immediate early promoter
PCR	polymerase chain reaction
PDH_c	pyruvate dehydrogenase complex
Phe	phenylalanine
Pi	inorganic phosphate
Pin AI	*Pseudomonas inequalis* restriction endonuclease, isoschizomer of *Age* I
pmol	picomoles (10^{-12})
PolyA	fragment containing bovine growth hormone poly-A signal
Pro	proline
P/S	penicillin/streptomycin
Pt^{+}	platinum monovalent ion
Q	glutamine
Q	relative expression quantities
R	arginine
R	reverse
rev	reverse primer
RNA	ribonucleic acid
ROS	reactive oxygen species
rpm	rounds per minute
rRNA	ribosomal RNA
16s rRNA	16 Svedberg units ribosomal RNA
12s rRNA	12 Svedberg units ribosomal RNA
S	serine
Sb^{3+}	antimony trivalent ion
SD	standard deviation
SDS	sodium dodecylsulfate
Ser	serine
T	thymine
T	threonine
T_a	experimentally determined optimal annealing temperature
TAE	Tris-acetate buffer
t-BHQ	*tert*-butyl hydroquinone
TCA	tricarboxylic acid cycle
t-BHP	*t*-butylhydroperoxide
T_m	calculated melting temperature

TMB	3,5,3',5'-tetramethylbenzidine
TMRM	tetramethylrhodamine methylester
Tris®[1]	tris(hydroxymethyl)aminomethane
tRNA	transfer RNA
Trp	tryptophan
Tyr	tyrosine
U	units
USF	upstream stimulatory factor
UV	ultraviolet light
V	valine
V	Volt
Val	valine
VDAC	voltage dependant anion channel, porin
v/v	volume per volume
w/v	weight per volume
Zn	zinc
Zn^{2+}	zinc divalent ion

[1] Tris® is a registered trademark of the United States Biochemical Corporation, Cleveland, OH, U.S.A.

LIST OF EQUATIONS

LIST OF FIGURES

LIST OF TABLES

ACKNOWLEDGEMENTS

The completion of this dissertation would not have been possible without the following people and institutions whom I would like to thank sincerely:

- My supervisor, Dr. F.H. van der Westhuizen, for his guidance and being the most enthusiastic supervisor ever.
- My co-supervisor, Prof. A. Olckers, for always making time for me and welcoming me at the Centre for Genome Research and her company.
- Financial support from the National Research Foundation.
- Dr. Annelize van der Merwe and the students at the Centre for Genome Research for their help with the sequencing. Also a special thanks to Dr. Boitumelo Semete, not only for the sequencing, but also for all the small things she helped with.
- Ann Grobler for her assistance with the confocal microscopy.
- The molecular biology laboratory at Dept. of Pharmacy for letting us use the iCycler, photo documentation system and confocal microscope.
- The staff of the Mitochondrial laboratory for always lending a helping hand, especially Leigh who was a big help with the cell cultures when I didn't have the time.
- Yolanda for her work on the ELISA and OXPHOS analyses.
- Most of all, I would like to thank Dr. Oksana Levanets for coaching me in molecular biology and never being too busy to help me.
- Finally, I couldn't leave out a big thanks to my mom, for always just being there for me.

CHAPTER ONE

INTRODUCTION

Mitochondria oxidise hydrogen rich molecules in food to produce over 90% of the ATP our cells use. ATP is the form of energy utilised universally by all life on earth (Perkins & Frey, 2000). Keilin's concept of the respiratory chain in the early 1960s included a complex of sequentially acting redox carriers that reduces substrates and finally also molecular oxygen (Mitchell, 1979). Mitchell included the production of ATP into this concept and today this is called the chemiosmotic theory (Mitchell, 1979). The first concept of mitochondrial disease, or disorders of this respiratory chain, was introduced in the 1960s by Luft and co-workers when accumulation of mitochondria was observed in patients with exercise intolerance (DiMauro, 2004b). Since then five complexes have been identified and deficiencies of these complex activities differ in cause, incidence, mode of inheritance (Mendelian or maternal), severity and clinical manifestation. Complex I (NADH:ubiquinone oxidoreductase) deficiencies are frequently encountered amongst these and often results in multi-system disorders, often fatal at a young age (Pitkanen *et al.*, 1996).

The mitochondrial electron transport chain has been recognized as one of the major cellular generators of reactive oxygen species (ROS) and under normal physiological conditions ROS are produced by leakage of electrons from the chain and produce subtle or transient changes in the cellular redox state (Wallace, 1999). However, when the electron transport chain is inhibited as with a complex I deficiency, accumulated electrons are donated to oxygen to form superoxide radicals and other reactive oxygen species (Piccolo *et al.*, 1991; Ide *et al.*, 1999; Raha & Robinson, 2000). Some of the consequences of ROS production are mitochondrial permeability transition pore formation, lipid peroxidation, protein oxidation, mitochondrial DNA (mtDNA) damage and it could also influence both mitochondrial and nuclear transcription processes, which could finally lead to apoptosis or programmed cell death (Wallace, 1999).

Metallothioneins (MTs) belong to a superfamily of intracellular metal-binding proteins, present in virtually all living organisms. Their unique structural characteristics include a very high cysteine content of almost one in three amino acids. Many studies regarding MTs capacity for zinc homeostasis and cadmium detoxification has been conducted since its discovery. However, since 1974 some researchers such as Kägi and co-workers proposed MTs might play a role in maintaining oxidation-reduction potential, perhaps analogous to the functions of glutathione (Kägi *et al.*, 1974). Since then MTs mechanism of scavenging ROS has been a hot topic of debate. Some suggest that free thiol groups bind ROS, whilst others contemplate zinc release to be predominant.

Mitochondrial-specific ROS generators are known to induce MT synthesis (Haq *et. al.*, 2003) and investigations carried out by Kondoh and co-workers (2001) suggested that MTs particularly play a major role in protection against oxidative stress induced in mitochondria. Work conducted by van der Westhuizen *et al.* (2003) showed a marked induction of MTs in complex I deficient cells cultured under conditions favouring oxidative metabolism rather than glycolytic metabolism. Seeing that complex I deficiencies produce an increase in ROS, it is hypothesised that MTs may have a protective response to ROS-mediated damage in complex I deficient cell lines.

In a study conducted parallel to this one, the expression levels of MTs with rotenone-induced complex I deficiency was examined (Olivier, 2004). It was found that MT-2A showed significant levels of induction with such a complex I deficiency in HeLa cells, confirming previous work of van der Westhuizen and co-workers (2003). This leaves the question whether MTs indeed have a protective role in complex I deficiency and whether this protection is ROS-related.

This study therefore aimed to investigate the putative protective role of metallothionein overexpression in a complex I deficient cell line. It was necessary to establish whether this protection was targeted against ROS or ROS-related consequences, and also whether different MT isoforms would lead

to different levels of protection in complex I deficient cells. Two isoforms of metallothioneins, MT-1B and MT-2A, respectively was cloned into the pIRESneo2 vector and transfected into HeLa cells to establish an *in vitro* MT-overexpression model. Complex I deficiency was then induced by rotenone treatment and the effect of the MT overexpression on ROS levels and apoptosis established. ROS levels were quantified and apoptosis were investigated by measuring caspase activity and visualising decreases in membrane potential indicating formation of mitochondrial permeability transition pores.

Chapter two describes the general aspects of mitochondria, complex I and metallothioneins. Chapter 3 describes the cloning and characterisation of MT-expression vectors, after which the expression of MTs (Chapter 4) and biochemical analyses (Chapter 5) are described. The final discussions and conclusions follow in Chapter 6.

CHAPTER TWO

LITERATURE REVIEW

The primary mechanism of energy transduction in mitochondria, called chemi-osmosis or oxidative phosphorylation, uses the free energy of oxidation of carboxylic acids to phosphorylate ADP to produce ATP (Frey & Mannella, 2000). Current epidemiological data have revealed that diseases due to a defect of this oxidative phosphorylation pathway has a prevalence of one in 8 500, suggesting these deficiencies are the most frequent metabolic disorder (Chinnery, 2002). One of the consequences of such respiratory chain deficiencies is the production of reactive oxygen species (ROS), which is a major cause of multiple types of damage in the mitochondria (Wallace, 1999). Recent evidence has revealed the putative protective function of metallothioneins against ROS, both of which are elevated in defects of the oxidative phosphorylation system (van der Westhuizen *et al.*, 2003; Olivier, 2004). It is therefore likely that metallothioneins could facilitate a protective role in some of these oxidative phosphorylation deficiencies, specifically complex I deficiencies.

In this chapter an overview of mitochondria and oxidative phosphorylation will be given, as well as the role of complex I and consequences of complex I deficiency. The properties of metallothioneins, their function and induction during oxidative stress are also discussed. The chapter concludes with a problem statement, hypothesis, aims, strategy and experimental design.

2.1. THE MITOCHONDRION

Mitochondria use over 80% of the oxygen we inhale to oxidise hydrogen rich molecules in food to produce over 90% of the energy-rich molecules ATP our cells need. In this process water and carbon dioxide is also released (Perkins & Frey, 2000).

2.1.1. Evolution of mitochondria

The universal consensus is that the mitochondrion is a residue of a prokaryotic cell involved in symbiosis with another cell in early evolution (Scheffler, 2001a; Scheffler, 2001b). However, the present mitochondrion is completely dependant on its "host". The revised current view postulates that two bacteria, an anaerobic archeo-bacterium and a respiration-competent proteo-bacterium fused (Scheffler, 2001a; Scheffler, 2001b). From this organism, all eukaryotes are thought to have evolved. It is also believed that the mitochondrion has a monophyletic origin, that is to say the endosymbiosis occurred just once during the evolution on earth from a common ancestor of all existing eukaryotes. This theory also includes the possibility that the mitochondrion originated at essentially the same time as the nuclear component of the eukaryotic cell, rather than in a separate, succeeding event, and therefore denies the existence of a distinct amitochondrial eukaryote as postulated by the serial endosymbiont theory, which was the prevailing postulate until recently (Gray *et al.*, 1999; Scheffler, 2001a; Scheffler, 2001b).

2.1.2. Structure of mitochondria

Every cell in the human body contains hundreds of mitochondria. (Scheffler, 2001b) The overall shape of the mitochondrion is somewhat variable, but generally it is either spherical or cylindrical, and range from 0.5 - 5 μm in diameter and 1 - 20 μm in length (Perkins & Frey, 2000).

During the first elucidations of the structure of mitochondria in the 1960s, two competing models arose (Perkins & Frey, 2000). Both included an outer membrane and a folded inner membrane. The model introduced by Palade in 1952, the most popular model until recently, described the cristae (folds of the inner membrane that serves to increase the surface area of this membrane) to be "baffle-like" as depicted in Figure 2.1 (as reviewed by Perkins & Frey, 2000). Recent investigations with electron microscopy however, have deemed it

necessary to accept the model introduced by Sjostrand (1953) instead, as indicated in Figure 2.1.

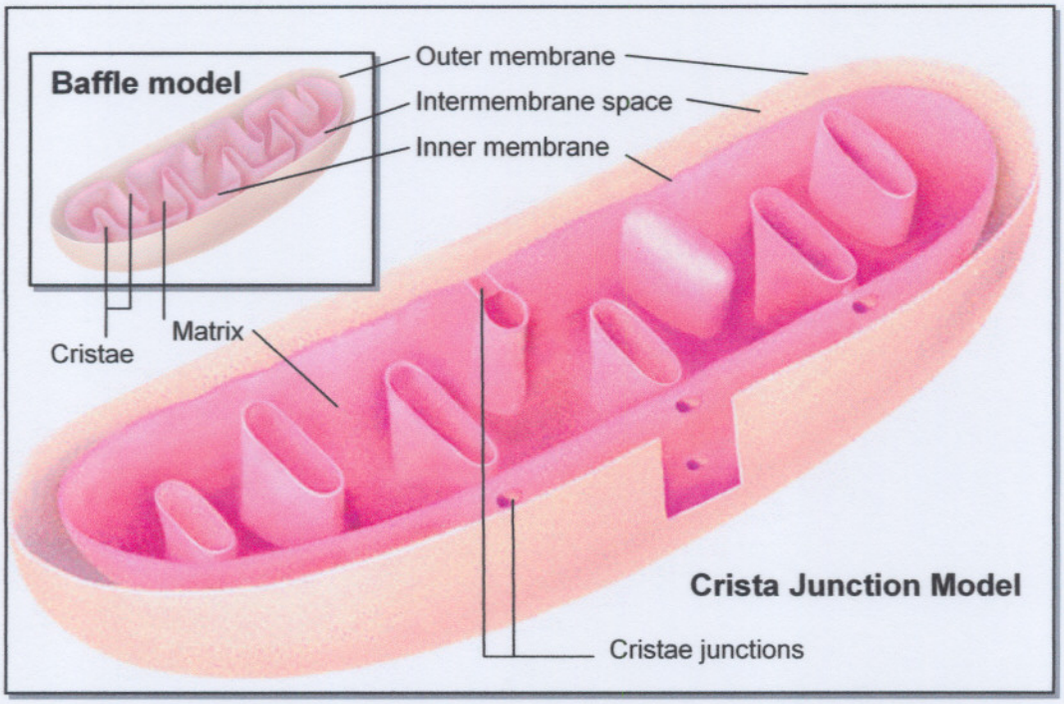

Fig. 2.1. Two models of mitochondrial membrane structures. The well-known "baffle" model originated with Palade in the 1950s. It shows large openings connecting the intracristal space to the membrane space. The Crista junction model, which shows narrow tubular openings (crista junctions) connecting the spaces. Most cristae have more than one crista junction, and can be located on opposite sides if the crista extends completely across the matrix (used with permission from of Perkins & Frey, 2000).

In this "septa-like" model, the inner membrane is adjacent to the outer membrane and it frequently gets in contact with the outer membrane. The second membrane domain is produced by the inner membrane that invaginates to form cristae (tubular or lamellar structures) through narrow, tubular openings, called crista junctions or *pediculi crista* (Perkins *et al.*, 1997; Scheffler, 2001a; Scheffler, 2001b).

It is thought ATP phosphorylation rates could be influenced by these cristae junctions, due to the fact that this phosphorylation depends on diffusion of ions and substrates through the inner membrane (Frey & Mannella, 2000). It is also

thought that the inner membrane can alter in shape in response to environmental conditions. (Hackenbrock, 1966).

The outer mitochondrial membrane contains porin that forms non-specific pores, causing the semi-permeable nature of the outer membrane. The inner membrane is much richer in proteins than the outer membrane and is freely permeable only to O_2, CO_2 and H_2O. The proteins mediating electron transport and oxidative phosphorylation are bound to this inner membrane, as are the numerous transport proteins that control the passage of metabolites such as ATP, ADP, pyruvate, Ca^{2+} and phosphate. The matrix consists of a gel-like substance of less than 50 % water, high concentrations of the soluble enzymes of oxidative metabolism such as citric acid cycle enzymes, substrates, nucleotide co-factors and inorganic ions. The mitochondrial genetic machinery, i.e. DNA and RNA utilised in the transcription of several mitochondrial proteins are also contained in the matrix (Voet & Voet, 1995).

2.1.3. Mitochondrial biochemistry

Mitochondria are the site at which amino-acid metabolism, fatty acid oxidation, and most importantly, oxidative phosphorylation occurs. This results in the production of ATP, the form of energy used by cells. Mitochondria are also involved in apoptosis or regulated cell death, which is caused by various types of environmental stress (Carelli *et al.*, 2004). Figure 2.2 gives a representation of a combination of these pathways.

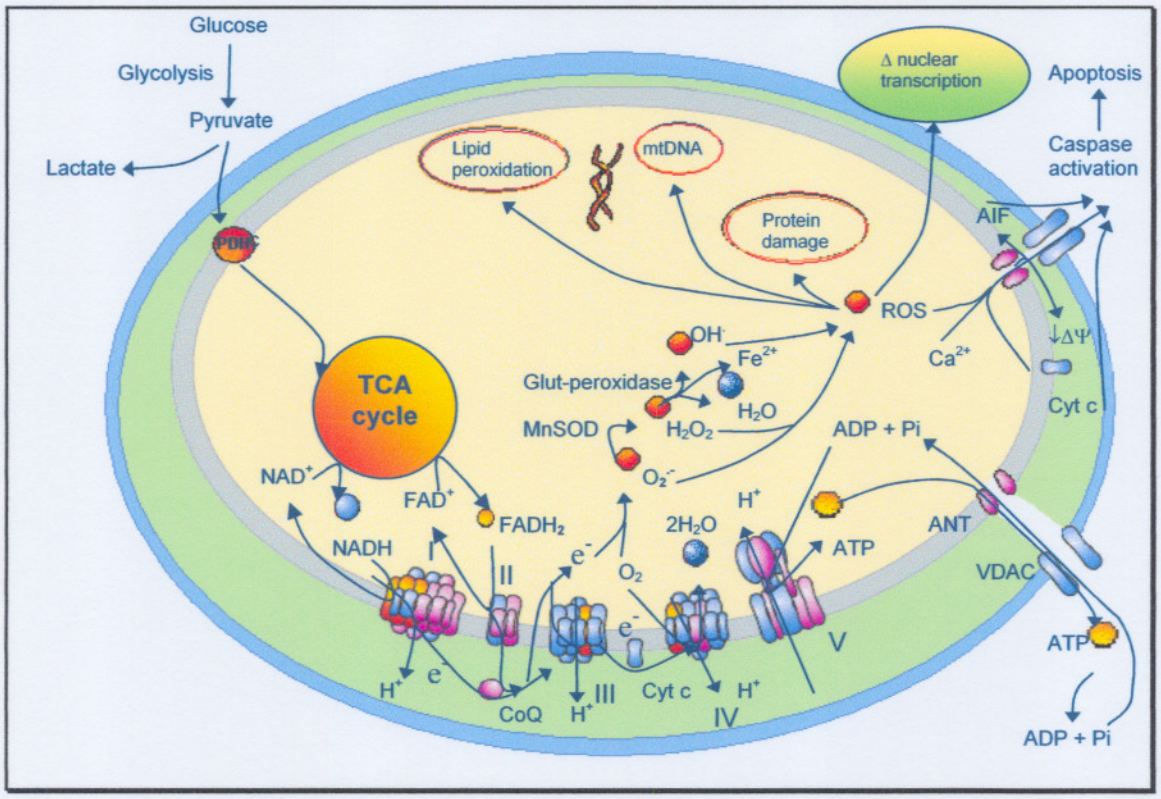

Figure 2.2. Simplified schematic representation of the mitochondrial metabolism. It shows the outer mitochondrial membrane (blue), the intermembrane space (green), inner membrane (grey) and the matrix (yellow). Pyruvate is produced from glucose during glycolysis, which enters the mitochondria via the pyruvate dehydrogenase complex (PDH_c). It generates acetyl-CoA which enters the Krebs cycle (TCA cycle). It then combines with oxaloacetate and follows a series of enzymatic reactions, leading to the production of NADH and $FADH_2$ from NAD^+ and FAD^+. This provides electrons (e^-) to complex I (NADH:ubiquinone oxidoreductase) and complex II (succinate ubiquinone oxidoreductase) respectively. The electrons are then passed onto complex III (ubiquinol: cytochrome c oxidoreductase) and complex IV (cytochrome c oxidase) that passes the electrons onto the final acceptor oxygen (O_2) to produce water (H_2O). The electrochemical gradient ($\Delta\psi$) generated in the process is utilised to produce ATP from ADP and P_i through the action of complex V (ATP synthase). ATP can then be transported into the cytosol via ANT (adenine nucleotide translocater) and VDAC (voltage dependant anion channel). With a complex I deficiency the electrons are passed directly from complex I onto O_2. This leads to the formation of superoxide ($O_2^{\cdot-}$) which can be converted to hydrogen peroxide (H_2O_2) through the action of manganese superoxide dismutase (MnSOD). H_2O_2 can then be converted to hydroxyl radicals ($OH^{\cdot}$) via the Fenton reaction, or to water via glutathione peroxidase. These reactive oxygen species (ROS) can lead to damaging effects such as lipid peroxidation, protein oxidation and mitochondrial DNA (mtDNA) damage, and could also influence both mitochondrial and nuclear transcription processes, which could finally lead to apoptosis or programmed cell death (adapted from Wallace, 1999).

2.1.4. Oxidative phosphorylation

Mitochondria produce most of the energy in animal cells in the form of ATP by a process called oxidative phosphorylation. This is also known as the chemiosmotic theory and was first proposed by Mitchell in 1961 in response to work done by Keilin on the respiratory chain of aerobic energy metabolism.

The main substrates for this process are oxidised from glucose and fatty acids, through processes such as glycolysis and β-oxidation (Ruitenbeek *et al.*, 1996). The products then enter the Krebs cycle in order to produce electrons in the form of reduced equivalents, i.e. NADH (nicotinamide adenine dinucleotide) from NAD^+ and $FADH_2$ (flavin adenine dinucleotide) from FAD^+ (Mitchell, 1961; Mitchell, 1979). These electrons are passed onto a series of respiratory enzyme complexes (I, II, III and IV), located in the inner mitochondrial membrane, which catalyze sequentially organized redox reactions with standard redox potentials (E^0) ranging from ± 0.320 to + 0.380 V (Liu *et al.*, 2002). NADH:ubiquinone oxidoreductase (complex I), the first complex of the respiratory chain, transfers electrons from NADH to Coenzyme Q (CoQ, ubiquinone), thereby generating ubiquinol ($coQH_2$), which then shuttles two electrons to complex III (ubiquinol:ferricytochrome *c* oxidoreductase, or *cytochrome* bc_1 *complex*). Ubiquinol is also produced by complex II (succinate:ubiquinone oxidoreductase), which, in a pathway parallel to but not including complex I, transfers electrons from $FADH_2$ to the highly hydrophobic CoQ. Other sources that transfer electrons to CoQ to generate ubiquinol are glycerol-3-phosphate dehydrogenase and the electron transfer flavoprotein (ETF) (Munnich & Rustin, 2001). Complex III then shuttles two electrons from $CoQH_2$ to cytochrome *c* (cyt *c*), a low molecular weight hemoprotein, which in turn transports the electrons to complex IV (ferricytochrome:oxygen oxidoreductase or *cytochrome c oxidase*, COX). Complex IV, the terminal component of the respiratory chain, then transfers the electrons to oxygen (E^0 = + 0.815 V), the final electron acceptor, to produce water (Munnich *et al.*, 1996; Liu *et al.*, 2002; Carelli *et al.*, 2004).

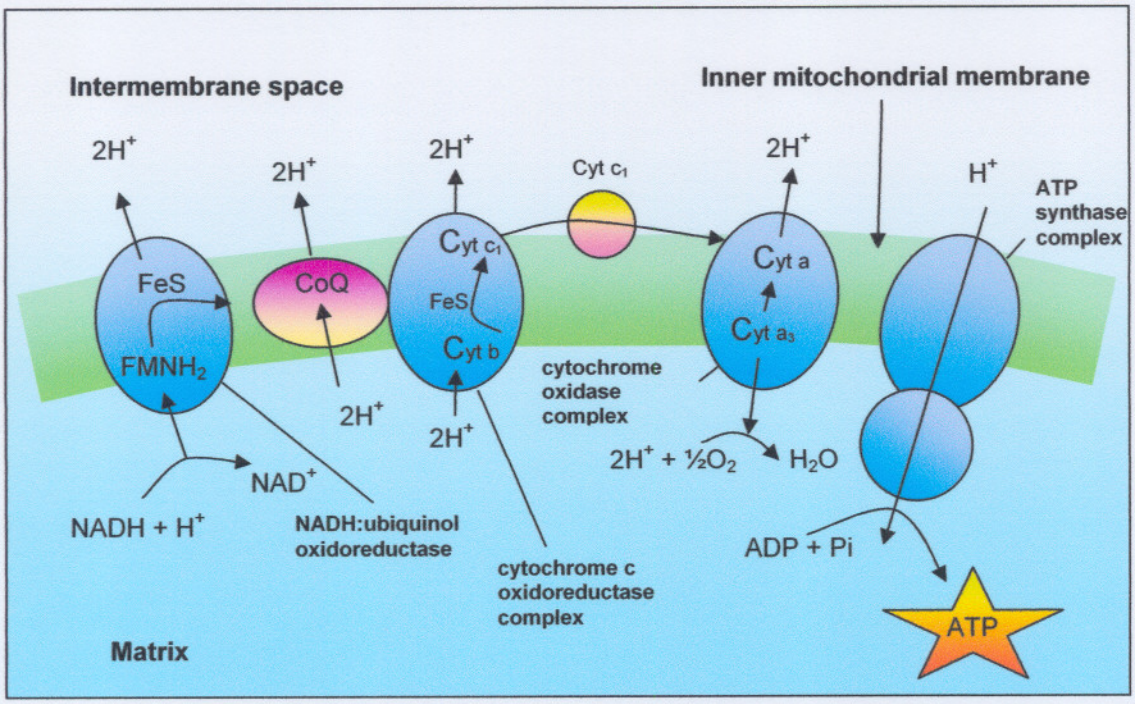

Figure 2.3. Schematic representation of the process of oxidative phosphorylation. The figure shows the process of oxidative phosphorylation in and around the inner mitochondrial membrane. The reduced equivalents produced by the TCA cycle in the form of NADH are passed onto Coenzyme Q by the action of complex I (NADH:ubiquinone oxidoreductase), which contains flavin mononucleotide (FMN) and seven iron-sulphur clusters (FeS). In this process two protons are released into the inner membrane space. Complex II (succinate ubiquinone oxidoreductase) carries the reduced equivalents in the form of $FADH_2$ also to Coenzyme Q. The electrons are then passed onto cytochrome c by complex III (ubiquinol: cytochrome c oxidoreductase), resulting in the pumping of four protons over the inner membrane. Complex IV (cytochrome c oxidase) then passes the electrons onto the final acceptor, O_2, to produce H_2O and also carries two protons into the innermembrane space. This electrochemical gradient is then utilised to produce ATP from ADP and inorganic phosphate (Pi) through the action of complex V (F_1F_0-ATP synthase) that allows the flow of the protons back into the mitochondrial matrix (adapted from Wallace, 1999; Munnich & Rustin, 2001).

The energy released by each of these electron transfers is used to pump protons across the membrane: two via complex I, two times two via complex III and two via complex IV (Wallace, 1999; Munnich & Rustin, 2001; Nicholls & Ferguson, 2002). The resulting electrochemical gradient ($\Delta\psi$) enables complex V (F_1F_0-ATP synthase), to form the energy carrier ATP from ADP and inorganic phosphate (Pi), by the reverse flow of the protons back into the matrix through

this complex (Munnich *et al.*, 1996). This process of oxidative phosphorylation is depicted in Figures 2.2 and 2.3.

The ATP synthesized in the mitochondrial matrix is then transported across the inner mitochondrial membrane, accompanied with the import of cytosolic ADP via the adenine nucleotide translocator (ANT) and through the outer membrane via VDAC (Voltage dependant anion channel) also called porin (Wallace, 1999; Carelli *et al.*, 2004).

2.1.5. Mitochondrial genome

A large number of mtDNA molecules exist in a healthy cell due to the hundreds of mitochondria in an individual cell, each containing 2–10 copies of mtDNA (Bogenhagen & Clayton, 1974; Pulkes & Hanna, 2001). Although the vast majority of the proteins of the mitochondria (almost a thousand) are encoded by nuclear genes (nDNA), 13 structural proteins are encoded by mtDNA that are indispensable for oxidative phosphorylation (Pulkes & Hanna, 2001).

The human mtDNA is a double-stranded, intronless, circular molecule of 16 569 base pairs as represented in Figure 2.4 (Anderson *et al.*, 1981). Mammalian mtDNA is compact with only ~1 kb of noncoding sequence (the D- or displacement loop) where replication and/or transcription of the mtDNA is initiated from (Bogenhagen *et al.*, 1984; Chinnery *et al.*, 2000). It contains 37 genes coding for two rRNAs (ribosomal RNA), 22 tRNAs and 13 structural polypeptides (Anderson *et al.*, 1981). These tRNAs and rRNAs are essential for intramitochondrial protein synthesis, whilst the structural proteins are essential for oxidative phosphorylation (Scheffler, 2001b).

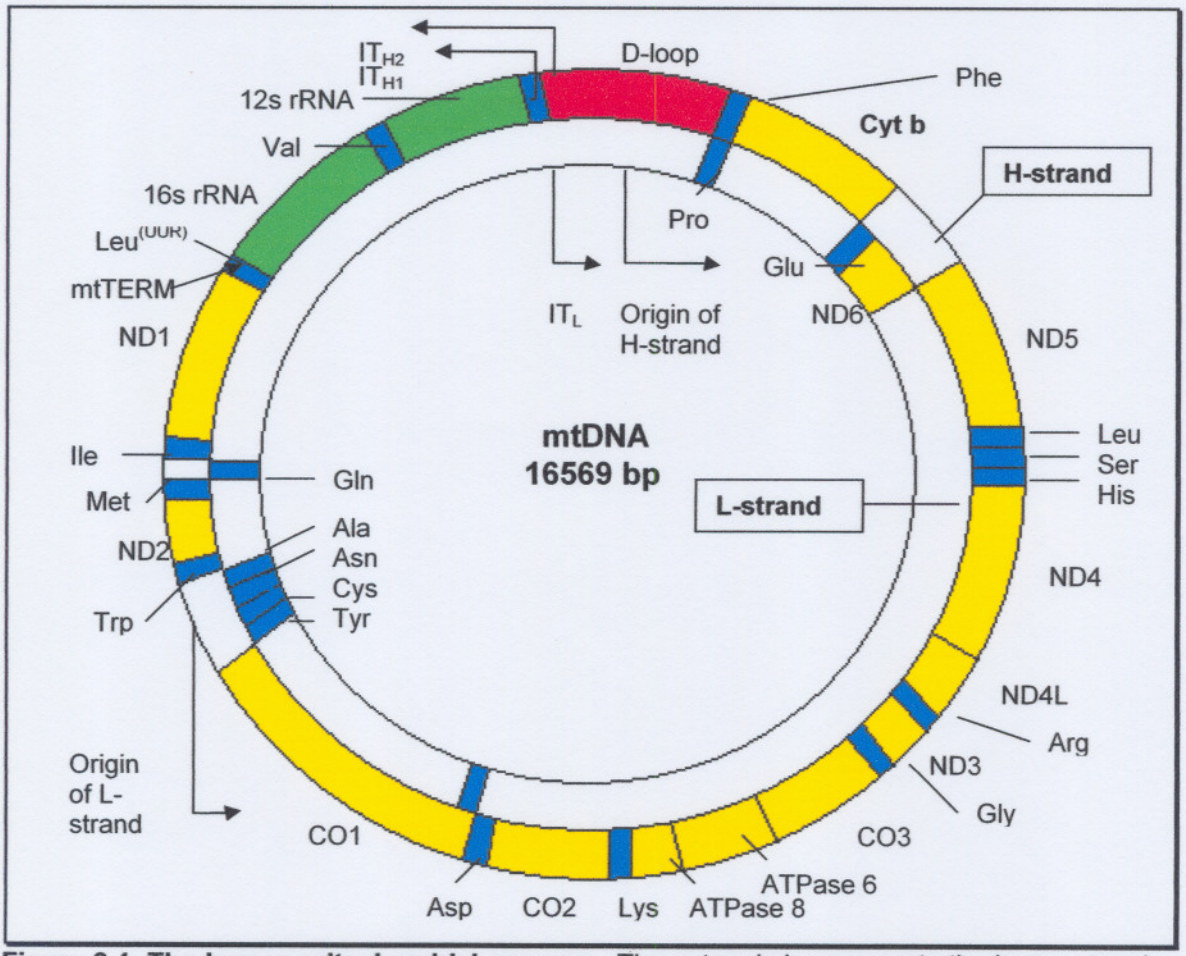

Figure 2.4. The human mitochondrial genome. The outer circle represents the heavy strand (H-strand) and the inner circle the light strand (L-strand). The D-loop (displacement loop) is indicated in red. The tRNA's are indicated in blue, and the amino acids are identified by their abbreviations. Ala = alanine, Arg = arginine , Asn = asparagine, Asp = aspartic acid, Cys = cysteine, Gln = glutamine, Glu = glutamic acid, Gly = glycine, His = histidine, Ile = isoleucine, Leu = leucine with anticodon CUN, Leu $^{(UUR)}$ = leucine with anticodon UUR, Lys = lysine, Met = methionine, Phe = phenylalanine, Pro = proline, Ser = serine, Trp = tryptophan, Tyr = tyrosine, Val = valine. The various mtDNA-encoded complex subunits are indicated in yellow. For complex I these are ND1, 2, 3, 4, 4L, 5 and 6 (NADH:ubiquinone oxidoreductase subunits 1-6). The complex III subunit is cyt b (cytochrome b), and the three complex IV sub-units are CO 1, 2 and 3 (cytochrome c oxidase 1 – 3). The complex V genes are ATPase 6 and 8 (ATP synthase sub-units 6 and 8). The rRNAs are indicated in green. 16S rRNA = 16 Svedberg units ribosomal RNA, 12S rRNA = 12 Svedberg units ribosomal RNA. O_H = heavy strand origin or replication, O_L = light strand origin of replication, IT_{H1} and IT_{H2} = heavy strand initiation of transcription sites 1 and 2, IT_L = light stand initiation of transcription site. mtTERM = binding site for the mitochondrial transcription terminator (adapted from Taanman, 1999; Wallace, 1999; Wallace & Lott, 2004).

The 13 structural proteins encoded by mammalian mtDNAs include seven subunits (ND1, 2, 3, 4, 4L, 5, 6) for NADH-ubiquinone oxidoreductase (complex I), one subunit (cytochrome b) for ubiquinone-cytochrome *c* oxidoreductase (complex III), three subunits (COX1, 2, 3) for cytochrome oxidase (complex IV), and two subunits (ATPase6 and ATPase8), which are part of the membrane-bound portion (F_0) of the enzyme, ATP synthase otherwise known as complex V (Scheffler, 2001b).

Diseases caused by mitochondrial dysfunction may therefore be due to nDNA defects and thus follow the Mendelian genetic rules, or they may be due to mutations that occur in the mtDNA, due to the following characteristics of mtDNA (Wallace, 1999; Triepels *et al.*, 2001b; Carelli *et al.*, 2004; DiMauro, 2004a).

1) Human mitochondria, and therefore mtDNA, are primarily maternally inherited. This is due to the fact that, as a rule, all mtDNA are derived from the oocyte. The only part of the sperm cell containing mitochondria does not penetrate the ovum during fertilization. A mother harbouring a mtDNA mutation will therefore transmit the mutant mtDNA to her offspring (Pulkes & Hanna, 2001);

2) Some deleterious mutations of mtDNA usually affect some, but not all mtDNA copies within a cell or tissue. This mixture of wild-type and mutant mtDNA is called heteroplasmy and stands in contrast to identical mtDNA sequences which is known as homoplasmy. For many of these mutations, a relation between the percentage of heteroplasmy and phenotype exists such as either MELAS (mitochondrial encephalomyelopathy with lactic acidosis and stroke-like episodes) or MERRF (myoclonus epilepsy with ragged red fibres), whereas other mutations such as LHON (Leber's hereditary optic neuropathy), lack such correlations (Chinnery *et al.*, 2000; Pulkes & Hanna, 2001). Section 2.2.2 describes these diseases in more detail;

3) Various studies have indicated that mtDNA mutations exhibit a threshold effect. That means, a certain proportion of mutant mtDNA is required before there is a reduction in respiratory chain activity and/or clinical symptoms are expressed. The exact threshold seems to vary between different mtDNA

mutations, different types of tissue, nuclear background etc. For some mutations it seems that even 100% mutant mtDNA is not always sufficient to produce a disease phenotype (Pulkes & Hanna, 2001; Scheffler, 2001a).

4) The tissue distribution of mutant DNA is another important factor in phenotype expression. During cell division, different proportions of mutant mtDNA is arbitrarily distributed to daughter cells (mitotic segregation). The proportion of mutant mtDNAs in daughter cells may shift and the phenotype may change accordingly (Wallace, 1999; Pulkes & Hanna, 2001).

2.2. COMPLEX I

2.2.1. Biochemistry and structure of complex I

NADH:ubiquinone oxidoreductase (complex I) is a complicated, membrane-bound assembled enzyme with a characteristic L-shape. It catalyses the first step and is also the largest multi-protein enzyme complex of the mitochondrial electron transfer chain (Grigorieff, 1998; Triepels *et al.*, 2001a). The oxidation of NADH provides two electrons for the reduction of ubiquinone to ubiquinol. They are transferred from NADH to the primary electron acceptor, a non-covalently bound flavin mononucleotide (FMN), and then via a series of iron–sulphur clusters to ubiquinone. In mitochondria, the transfer of two electrons is coupled to the translocation of four protons across the inner membrane, contributing to the proton motive force (ψ). Ubiquinone is then reduced from ubiquinol by complex III (Hirst *et al.*, 2003).

Complex I consist of 46 subunits, with a combined molecular mass of 980 kDa, assuming that complex I contain one copy of each subunit. Seven of them, the 'ND-subunits' (ND1-6 and ND4L), are encoded by the mitochondrial genome and the rest (39) are nuclear gene products that are imported from the cytoplasm into the organelle (Grigorieff, 1999; Triepels *et al.*, 2001a; Hirst *et al.*, 2003). The ND subunits and seven of the nuclear encoded subunits contain all the known redox

co-factors and substrate binding sites of the enzyme. They bind a FMN at the active site for NADH oxidation, eight iron–sulphur clusters and ubiquinone molecules. Other subunits have less clearly defined roles and are peripheral. They may stabilise of the complex, are important for its assembly, or for reactions unrelated to the NADH:ubiquinone oxidoreductase activity of the complex (Hirst *et al.*, 2003).

Three sub-complexes , Iα, Iβ and Iλ, constitute membrane-bound and -unbound domains of complex I. Subunits of sub-complex Iλ are largely hydrophilic and constitutes the globular arm that protrudes into the mitochondrial matrix. It includes the seven core subunits which are known to bind the FMN and ligate all of the iron–sulphur clusters. Sub-complex Iβ is the most hydrophobic of the three sub-complexes and it constitutes a major part of the membrane arm of complex I (Triepels *et al.*, 2001a; Hirst *et al.*, 2003). Figure 2.5 gives the structural overview of complex I.

Three fractions can be separated from complex I with chaotropic agents. They are known as the flavoprotein (FP), iron–protein (IP) and hydrophobic-protein (HP) fractions. Both the FP and the IP fractions represent the peripheral arm, whereas the HP fraction represents the water-insoluble aggregate of the inner-membrane arm of the complex. FP is a well-defined and catalytically active sub-complex, containing the active-site FMN, the NADH binding site, one [4Fe–4S] and one [2Fe–2S]. Except for seven other subunits contained in the IP fraction, the remaining proteins are all thought to be part of the HP fraction (Triepels *et al.*, 2001a; Hirst *et al.*, 2003). The three fractions in complex I are depicted in Figure 2.5.

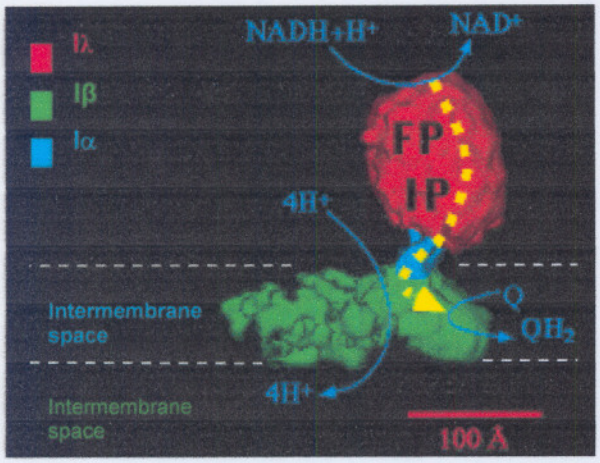

Figure 2.5. Structure of complex I (NADH:ubiquinone oxidoreductase). The reduced equivalents from NADH (in the mitochondrial matrix), generated through the TCA cycle, are passed onto Coenzyme Q by complex I (located in the inner mitochondrial membrane). In this process, four protons are carried over the inner membrane into the inter-membrane space. The three sub-complexes Iα, Iβ and Iλ are discussed in the text, as are the three fractions FP (flavoprotein), IP (iron-protein) and HP (hydrophobic-protein). The model presented here are with permission from Grigorief (1998).

2.2.2. Complex I deficiency and its consequences

2.2.2.1. Clinical presentations

The first mitochondrial 'disorder' was described by Roland Luft in the early 1960s when accumulation of mitochondria was observed in patients with exercise intolerance. Studies have shown that deficiencies of the respiratory chain have a prevalence of at least one in 8500 and are therefore considered a very common form of metabolic disorder (Chinnery, 2002). Of these oxidative phosphorylation diseases, complex I deficiency is significantly more frequent. (Triepels *et al.*, 2001b).

Human complex I deficiency can present with a wide variety of biochemical and symptomatic phenotypes, but appears to be primarily an autosomal recessive disease, suggesting that nuclear mutations predominates (Triepels *et al.*, 2001b). The most affected tissues are generally those with a high energy demand, i.e. brain (neuropathies), cardiac muscle (cardiomyopathies), skeletal muscle (myopathies) and eyes. Often, more than one of these are affected and other tissues can be affected as well (Scheffler, 2001a). In addition, various degrees of

severity and age of onset are observed. Hence the phenotypical expression ranges from fatal infantile lactic acidosis to adult onset exercise intolerance or optic neuropathy (Munnich *et al.*, 1996).

Many of the problems that revolve around the diagnosis of complex I defects stem from the fact that complex I is a huge multi-enzyme complex of bi-genomic origin. In summary, all the cellular processes of expression, targeting, mitochondrial import of nuclear-encoded proteins, as well as the correct assembly of the sub-units, represent potential contributions to complex I deficiency (Triepels *et al.*, 2001b). Gene products are derived from both nuclear and mitochondrial genomes, even though mtDNA mutations cause only 5–10 % of complex I deficiency (Robinson, 1998; Triepels *et al.*, 2001b). Mutations can also be structural (present in both nuclear and mitochondrial DNA, affecting any of the sub-units), or non-structural (impairing mitochondrial protein synthesis), such as those located in mitochondrial tRNA genes (Triepels *et al.*, 2001b; DiMauro, 2004a).

Table 2.1. Clinical presentation of some common mutations related to Complex I deficiency

Type of mutation	Phenotype
mtDNA encoded structural genes	Bilateral striatal necrosis, MELAS, LHON, Myopathy, Exercise intolerance, Long QT syndrome, dystonia, Parkinsonism, Leigh's syndrome.
nDNA encoded structural genes	Cardiomyopathy, encephalomyopathy, Leigh-like or Leigh's syndrome, Leukodystrophy, myoclonic epilepsy.
tRNAs	MELAS, Isolated myopathy, Lactic acidosis, MERRF.

MELAS = mitochondrial encephalomyopathy, lactic acidosis and stroke-like episodes; LHON = Leber's hereditary optic neuropathy; MERRF = myoclonus epilepsy with ragged red fibres (Adapted from Pulkes & Hanna, 2001; Triepels *et al.*, 2001b; DiMauro 2004a).

Table 2.1 shows some of the clinical manifestations of complex I deficiency, of which four major syndromes, (LHON, Leigh's syndrome, MELAS and MERRF) are discussed below.

LHON presents with rapid loss of central vision in one eye (unilateral visual loss) in young males. The condition is usually painless and associated with fading of colours (dyschromatopsia) in the one eye, followed by similar involvement of the other eye (bilateral optic atrophy), within days, months, or rarely years (Carelli *et al.*, 2004; DiMauro, 2004a).

Leigh's syndrome is a devastating encephalopathy in infancy or childhood characterized pathologically by symmetrical areas of necrosis involving midbrain, basal ganglia, thalamus, pons and optic nerves. This disease is also the most common phenotype (up to 50 %) associated with isolated complex I deficiency (Triepels *et al.*, 2001b).

Mutations in the mtDNA encoded tRNA species for leucine and lysine also leads to complex I (and other complex) deficiencies. Mutations in the $tRNA^{Leu(UUR)}$ produce major complex I defects in the muscle of affected patients because of the high titre of leucines encoded in the ND subunits of complex I. These deficiencies are classified as ragged red fibre diseases due to the 'red' colouring of these fibres with Gomori trichrome stain. This includes amongst others MELAS and MERRF (Robinson, 1998; Triepels *et al.*, 2001b). MELAS usually presents in children or young adults. Symptoms include recurrent vomiting, migraine-like headache and stroke-like episodes causing cortical blindness, hemiparesis, or hemianopia. MERRF can be characterised by myoclonus, seizures, mitochondrial myopathy and cerebellar ataxia. Dementia and hearing loss can also appear (DiMauro, 2004a).

The above mentioned phenotypes can also manifest with other complex deficiencies, e.g. the $tRNA^{Leu(UUR)}$ mutations which may also affect the assembly of other complexes, as all the complexes contain leucine-residues. A complex I deficiency in association with another complex deficiency is therefore commonly found (Triepels *et al.*, 2001b).

Modern therapy for complex I deficiencies remains largely symptomatic and does not significantly alter the course of the deficiency. Treatment includes avoidance of drugs and procedures known to have a detrimental effect (such as sodium valproate, barbiturates, tetracyclines and cloramphenicol), prevention of oxygen radical damage (ascorbate administration) and dietary recommendations such as high lipid-low carbohydrate diet (Ruitenbeek *et al.*, 1996; Munnich *et al.*, 1996). Succinate and riboflavin supplementation can also be considered as succinate enters the respiratory chain via complex II and riboflavin is the precursor of the flavin moiety in complex I (Ruitenbeek *et al.*, 1996; Munnich *et al.*, 1996). In cases of acute exacerbation of lactic acidosis, bicarbonate could relieve the symptoms (Ruitenbeek *et al.*, 1996). However, the effectiveness of all of these supplementations cannot be guaranteed, and in the majority of cases modern therapeutic intervention has failed (Triepels *et al*, 2001b). This underlines the importance of ongoing investigations into possible remedies of complex I deficiencies.

2.2.2.2. Reactive oxygen species

The mitochondrial electron transport chain has been recognised as one of the major cellular generators of ROS, which include superoxide ($O_2^{\cdot-}$), hydrogen peroxide (H_2O_2) and the hydroxyl free radical or $OH^{\cdot}$ (Loschen *et al.*, 1971; Loschen *et al.*, 1974). Under normal physiological conditions, ROS are produced by leakage of electrons from the chain and produce subtle or transient changes in the cellular redox state.

When the electron transport chain is inhibited as with a complex I deficiency, the electrons accumulate at this point (Piccolo *et al.*, 1991; Ide *et al.*, 1999; Wallace 1999; Raha & Robins, 2000). They can be donated to molecular oxygen (O_2) to form superoxide, which is quickly dismutated by the mitochondrial superoxide dismutase (Mn-SOD) to H_2O_2 (Loschen *et al.*, 1971; Loschen *et al.*, 1974). Subsequently, H_2O_2 can then be converted to H_2O by glutathione peroxidase (GPx). Alternatively, H_2O_2 can also be converted to the highly reactive hydroxyl

radical ($OH^{\cdot}$) by the Fenton reaction in the presence of reduced transition metals such as Fe^{2+} (Wallace, 1999). Furthermore, $O_2^{\cdot-}$ may react directly with nitric oxide ($NO^{\cdot}$) to produce peroxynitrite ($ONOO^{\cdot}$) (Carelli *et al.*, 2004).

Excess ROS reacts with and modifies all classes of cellular macromolecules and critical cellular targets, causing various types of damage due to its tremendous reactivity (Dalton *et al.*, 1999). This excessive ROS production from the respiratory chain causes even further local damage to the Fe–S centre of complexes I, II and III, as well as to tricarboxylic acid cycle (TCA) enzymes, such as aconitase. Moreover, the highly reactive peroxynitrite can permanently damage tyrosine residues of nearby proteins, such as MnSOD, through thiol-nitrosylation. Furthermore, unlike nuclear DNA, mtDNA is not coated by protective histones. It is tethered to the inner mitochondrial membrane and therefore in close proximity to the respiratory chain and hence the oxygen free radicals. This contributes to a high rate of mtDNA mutations. Lipid peroxidation, caused by these free radicals, may also damage the mitochondrial and cellular membranes (Carelli *et al.*, 2004). Constant ROS production can therefore result in extensive oxidative damage to mitochondrial and cellular proteins, lipids and nucleic acids, thus magnifying the consequences of the already present complex I deficiency (Robinson, 1998; Wallace, 1999).

2.2.2.3. Apoptosis and the mitochondrial permeability transition pore

Apoptosis (also known as regulated cell death) is tightly regulated through multiple independent signalling pathways, of which at least three general mechanisms have been proposed (Perkins & Frey, 2000; Nicholls & Ferguson, 2002; Carelli *et al.*, 2004). Firstly, protein activators of a family of proteases called caspases are released, including cytochrome *c*. Secondly, electron transport and ATP production is disturbed. Finally, there is a change in redox. Opening of the mitochondrial permeability transition pore (mtPTP), shown in Figure 2.6, and the accompanying apoptosis can be initiated by the mitochondrion's excessive uptake of Ca^{2+}, increased exposure to ROS, a

decrease in $\Delta\psi$ or a decline in energetic capacity, and therefore also by a deficiency in complex I. However, there exists controversy among researchers whether mtPTP is a central, determining and irreversible event in apoptosis, or whether it is a secondary consequence later in the pathway (Scheffler, 2001b).

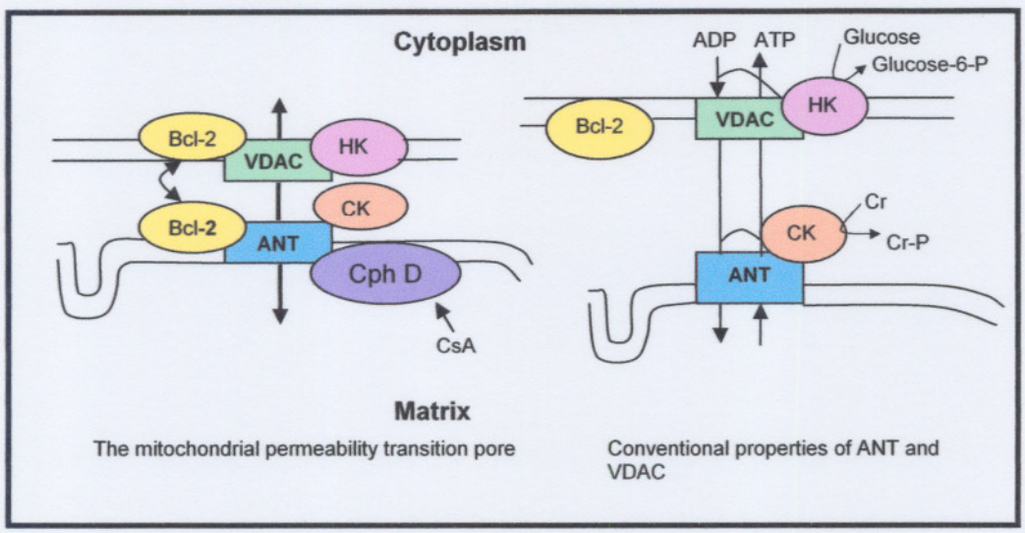

Figure 2.6. Components of the mitochondrial permeability transition pore. The components of the mtPTP during oxidative conditions and during normal homeostasis are shown. On the left, the adenine-nucleotide translocator (ANT) and the voltage-dependent anion channel (VDAC) are proposed to be specialized components of the permeability-transition pore, which is a large-conductance channel that promotes chemical equilibration between the mitochondrial matrix and the cytoplasm. Other proteins proposed to be involved in the mtPTP include hexokinase (HK), creatine kinase (CK), cyclophilin D (Cph D), cyclosporine A (CsA) and the pro-apoptotic Bcl-2 family members such as Bax. On the right, the more established role of the VDAC and ANT in adenine-nucleotide transport and the more conventional function of HK in the phosphorylation of glucose to glucose-6-P and CK in the phosphorylation of creatine (Cr) to creatine phosphate (Cr-P) is shown (adapted from van der Heiden & Thompson, 1999).

Under non-pathological conditions this mtPTP 'mega pore' permits solutes of less than ~1500 Da to cross the mitochondrial inner membrane (Scheffler, 2001a). VDAC, together with ANT, pro-apoptotic Bcl-2 family members such as Bax and cyclophilin D are thought to come together at the mitochondrial inner and outer membrane contact point to create the mtPTP (Scheffler, 2001a). These voltage-sensitive sites are in equilibrium with the oxidation-reduction potential of the intracellular glutathione (GSH) pool and with the pyridine nucleotide pool (NAD +

NADP):(NADH + NADPH) (Dalton *et al.*, 1999). Operationally, mtPTP is defined as a sudden breakdown of the $\Delta\psi$ and dissipation of proton and ion gradients (Scheffler, 2001a; Kristián, 2004). High levels of inorganic phosphate (P_i), depletion of mitochondrial glutathione and alkaline pH also favour mtPTP pore opening (Kristián, 2004). Alternatively, adenine nucleotides (particularly ATP and ADP), magnesium ions, and low pH will decrease the probability of the mtPTP pore opening.

The mitochondrial inner membrane space contains a number of cell death-promoting factors including cyt *c*, apoptosis-inducing factor (AIF, a flavoprotein), and latent forms of specialised proteases called caspases that activate apoptosis (Frey & Mannella, 2000). Caspases exist as inactive precursors in non-apoptotic cells and are activated by proteolytic cleavage (Nicholls & Ferguson, 2002). They selectively cleave proteins on the C-side of Asp-residues. Opening of the mtPTP causes the collapse of $\Delta\psi$ and release of the death-promoting factors (AIF and cyt *c*) and actives Apaf-1, which is an apoptosis-inducing factor. Together, these components are driven by ATP hydrolysis to form an apoptosome which is capable of aggregating procaspase-9 and allows the proteases monomers to cross-activate each other by proteolysis. Activated caspase-9 can activate additional caspase-9 molecules, as well as caspases 3 and 7, which in turn activate caspases 2, 6, 8 and 10 (Nicholls and Ferguson, 2002). The activated caspase-9 then initiates the proteolytic degradation of cellular proteins and DNA, leading to cell death (van der Heiden & Thompson, 1999; Wallace, 1999; Perkins & Frey, 2000; Carelli *et al.*, 2004).

2.2.3. Inhibitors of Complex I

A structurally diverse group of inhibitors has been identified for complex I. Based on kinetic analyses and the behaviour of these inhibitors in competition with ubiquinone they have been grouped into two classes: firstly piericidin A, aurachins A and B, annonin VI, thiangazole, and phenalamid A2 inhibit in a partially competitive manner, whilst rotenone, phenoxan, aureothin, and others

inhibit noncompetitively. All inhibit the transfer of electrons from the high potential iron–sulphur cluster (N-2) to ubiquinone (Scheffler, 2001b).

2.2.3.1. Rotenone

Rotenone (Figure 2.7) is a common insecticide that strongly inhibits the electron transport of complex I and is the classical major inhibitor of complex I activity utilised in research (Esposti, 1998). Six rotenoid esters (in the family of isoflavonoids) occur naturally and are isolated from the plant *Derris eliptica* which is found in south-east Asia or from the plant *Lonchocarpus utilis* which is native to South America (Isenberg & Klaunig, 2000). Of these, rotenone is the most potent. Tribes in certain parts of the world pulp the roots of trees along river banks to release rotenone into the water to paralyse fish and make them easy prey. Because rotenone is extremely lipophilic, it crosses biological membranes easily and independent of transporters, getting to the brain swiftly (Greenamyre *et al.*, 2003). Rotenone inhibition is also markedly time-dependent and binds specifically and irreversible to complex I with high affinity (Esposti, 1998; Isenberg & Klaunig, 2000; Greenamyre *et al.*, 2003). The ND1 subunit has been shown to be the binding site for both rotenone and ubiquinone analogues, even though rotenone binds non-competitively. It was found that the ND4 subunit could also be involved in rotenone binding (Esposti, 1998; Robinson, 1998; Lambert & Brand, 2004).

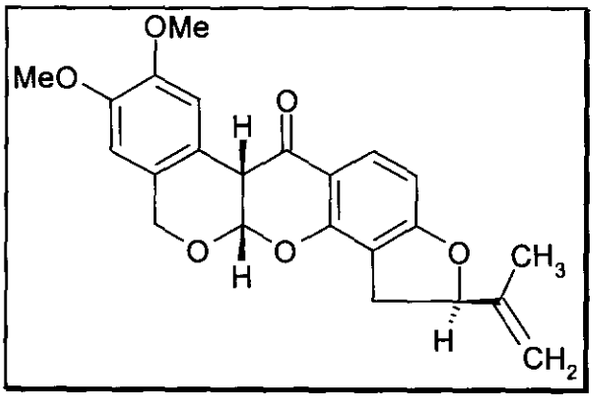

Figure 2.7. Chemical structure of rotenone. Me = Methyl group.

2.3. METALLOTHIONEINS

2.3.1. General properties of metallothioneins

MTs belong to a superfamily of intracellular metal-binding proteins, present in virtually all living organisms. MTs were first characterised by Margoshes and Vallee in 1957 (Kägi & Vallee, 1960). Their unique structural characteristics give rise to their potent metal-binding and redox capabilities which are important in almost all biochemical processes (Coyle *et al.*, 2002). Figure 2.8 shows the structure of rat MT-2A. The following are seen as features of MT:

1. High content of heavy metals (typically 4-12 atoms/molecule), predominantly Zinc (Zn), Copper (Cu) or Cadmium (Cd), bound exclusively by clusters of thiolate bonds;
2. highly conserved high cysteine content (typically 23-33 %) and lack of aromatic and hydrophobic amino acid residues;
3. low molecular weight (± 6 600 Da);
4. Demonstrated structural or functional homology amongst mammalian MTs (Kägi *et al.*, 1974; Hamer, 1986; Coyle *et al.*, 2002).

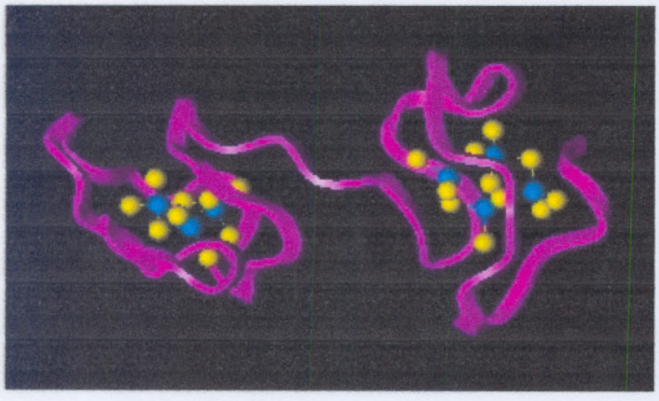

Figure 2.8. Structure of rat MT-2A. MT consists of two separate tetra-coordinated metal-sulphur clusters surrounded by a polypeptide chain (purple). All cysteine residues (yellow) are involved in the binding of metal ions (blue) (With permission from Binz & Kägi, 2001).

MTs are ubiquitously expressed in eukaryotes, even though the different isoforms may be distributed in various ratios in individual tissues (the highest concentration of MT in the body is found in the liver, kidney, intestine and

pancreas) and have differing rates of degradation (Ghoshal & Samson, 2001; Coyle *et al.*, 2002; Haq *et al.*, 2003).

The number and position of the cysteine residues are highly conserved and form cys-x-cys, cys-x-y-cys and cys-cys sequences, where x and y are non-cysteine amino acids. There are no free thiol groups and no intramolecular disulphide bonds. Instead, the cysteine residues are co-ordinated to heavy metals such as Zn or Cd in a tetrahedral arrangement (or trigonal for Cu^{+}) (Ghoshal & Samson, 2001). The extensive metal-thiolate bonds account for the high stability of these molecules, whereas the metal-free apo-thioneins are unstable *in vivo* and are rapidly degraded. The metal ions bonded to MT molecules are thermodynamically stable, however, they are kinetically labile and are exchanged or donated, in the presence of GSH, to other metalloproteins (Ghoshal & Samson, 2001). The binding affinity varies between metals, with Cu^{+} having the greatest stability constant, followed by Cd and then Zn. The strength of binding can therefore vary by as much as six orders of magnitude depending on the ion (Hamer, 1986; Coyle *et al.*, 2002). MT can incorporate up to 7 divalent metal atoms or 12 monovalent atoms per molecule. Divalent ions bound by MT include zinc (Zn^{2+}), cadmium (Cd^{2+}), mercury (Hg^{2+}), lead (Pb^{2+}), nickel (Ni^{2+}), cobalt (Co^{2+}) and Ag^{2+} (Kägi & Vallee, 1961; Karin *et al.*, 1980; Hamer, 1986; Ghoshal & Samson, 2001). MTs can also bind monovalent and trivalent metal ions, such as platinum (Pt^{+}), silver (Ag^{+}), copper (Cu^{+}), antimony (Sb^{3+}), and bismuth (Bi^{3+}), even though MT exists primarily in Zn-form or as mixed-metal proteins *in vivo* (Ghoshal & Samson, 2001; Coyle *et al.*, 2002).

Mammalian MTs are single-chain polypeptides of 61 to 68 amino acid residues. They consist of two sub-units: the more stable α-domain or C-terminal, (extending from amino acid 31 to 61) which contains 11 cysteines binding 4 divalent metal ions; and the more reactive β-domain or N-terminal, (extending form amino acid 1 to 30), which contains 9 cysteines binding only 3 divalent metal ions. The amino acid sequences of these domains are shown in Figure 2.9. The tertiary structure of MT is dynamic, and Zn and Cd exchange rapidly within the β-domain, more slowly in the α-domain and may also exchange with other

ions bound to intracellular ligands (Coyle *et al.*, 2002). The amino acid sequence and two globular metal-binding domains, α- and β-, are conserved among all four isoforms of MT (Ghoshal & Samson, 2001).

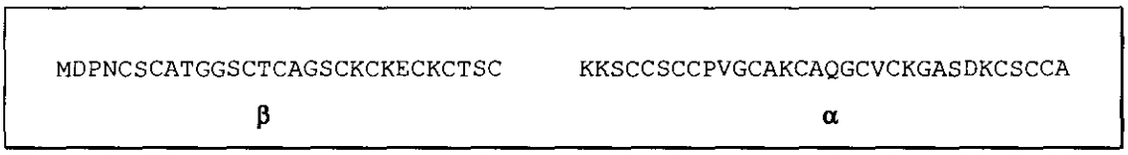

Figure 2.9. The consensus amino acid sequence for the α- and β-domains. (Modified from Hamer, 1986).

The rate of degradation of MT is determined by the identity of the metal atom bound to the protein. The half-lives for Cd-, Zn- and Cu-MT in liver have been estimated at 80, 20 and 17 hours respectively, though it varies among animal species. In hepatocytes, MT has been found to be degraded in both lysosomal and non-lysosomal compartments, with cathepsin B the most important protease that degrades apo-MT (metal-free thionein). Cu- and Zn-MT appear to be degraded differently. Zn is rapidly released from the protein and therefore able to participate in cellular function and to induce further MT synthesis. Due to the greater affinity of thionein for copper, Cu-MT is oxidised to form insoluble polymers that accumulate in the lysosome, presumably in a non-toxic form and are eventually secreted in bile (Coyle *et al.*, 2002).

2.3.2. Classification of metallothioneins

Due to a lack of one known enzymatic function, MTs have traditionally been classified according to their structural features as mentioned in Section 2.3.1 (Hamer, 1986).

Metallothioneins are currently classified as a family consisting of 16 genes in a cluster of about 82 kb (Vallee, 1995; Coyle *et al.*, 2002). In humans, at least 10 of the MT genes which cluster within the q13 region on chromosome 16 (Karin *et al.*, 1984), are functional, and these encode multiple isoforms of hMT-1

(designated by the letters A, B, C, D, E, F, G, H and X) and one isoform of hMT-2A (Stennard *et al.*, 1994). Single genes also code for hMT-3 and -4. The non-functional MTs include MT-1I, -J, -K and -L. Genes for the different MT isoforms are arranged in tandem head-to-tail fashion in the chromosome with a cluster of 13 closely-linked MT-1 genes on the chromosome (Quiafe *et al.*, 1994; Ghoshal & Samson, 2001).

Metallothionein-like 5 (MTL-5, encoding tesmin protein) has been reported by Haq and co-workers (2003) to reside on chromosome 11q13. It acts as a marker of early male germ cell differentiation. Fairly recently, hMT-M and hMT-E genes of unknown locations have also been described (Haq *et al.*, 2003).

Five human pseudogenes have also been reported to exist. These are ψMT-2B, ψMT-1C and ψMT-1D, ψMT-1G and ψMT-1H (not shown in Figure 2.10) (Hamer, 1986). The criteria that have been used to distinguish functional from non-functional genes include:

1) Conformity of the amino acid sequence with the structure of known functional MTs, position and number of cysteine residues and absence of aromatic amino acids,
2) Conservation of the three exon/two intron structure of mammalian MT genes, and
3) Absence of in-frame termination codons. (Stennard *et al.*, 1994)

In summary, mammalian MTs display many of the characteristics of a multigene family. This includes the presence of introns, the chromosomal linkage of functional and non-processed pseudogenes, and processed pseudogenes throughout the genome. (Hamer, 1986)

Although the general physico-chemical properties of MT isoforms are similar, there is some specialisation of biological function and differential expression in specific tissue/organ systems in the four major isoforms. The most widely expressed isoforms in the body are MT-1 and -2, which are rapidly induced,

particularly the liver, by a wide range of metals, drugs and inflammatory mediators. (Coyle *et al.*, 2002) MT-2A also appears to be expressed more in human tissues than MT-1A. Heguy *et al.* (1986) also reported that hMT-1B expression is either very low or absent in, amongst others, HeLa cell cultures, even though MT-1A is expressed in these cells. This is probably due to methylation keeping the gene in a non-active state (Heguy *et al.*, 1986). MT-3 is expressed predominantly in the brain, primarily in glutaminergic neurons, although low expression has been reported in the tongue, stomach, pancreas, intestines, heart, kidney and reproductive tissues. MT-IV is expressed exclusively in the squamous epithelial cells in skin, tongue and intestinal lining, and appears to play an important role in the differentiation of these tissues (Quiafe *et al.*, 1994; Ghoshal & Samson, 2001; Coyle *et al.*, 2002).

2.3.3. Functions of metallothioneins

In view of MTs ubiquity and tissue dependent expression it may not be possible to prove a single 'primary' function. Constitutive MT may play a background role in certain homeostatic mechanisms, whereas highly induced MT levels are adaptive to various environmental stresses (Coyle *et al.*, 2002). Although the primary MT function is controversial, evidence suggests that MTs have a protective effect with exposure to heavy metals (sequestrating toxic metals such as Cd and Hg, or physiologically important metals that are chemically disruptive in an ionised form, such as Cu and Zn). A role in metal homeostasis or detoxification is strongly suggested by the ability of MT to both bind to and be induced by heavy metal ions. It also has a protective effect against inflammation, infection and low Zn nutrition (Stennard *et al.*, 1994; Jacob *et al.*, 1999; Coyle *et al.*, 2002). Other possibilities include control of the intracellular redox potential, activated oxygen detoxification (scavenging of ROS) and sulphur metabolism. While MTs do not appear to be essential for life, it does provide a survival advantage in these situations (Coyle *et al.*, 2002).

Metallothioneins are the single most abundant group of intracellular zinc-binding proteins in eukaryotic cells and mammalian zinc-MT can reactivate various zinc-dependent enzymes, including carbonic anhydrase, aldolase and alkaline phosphatase (Haq *et al.*, 2003). Of the more than 300 enzymes in which Zn is a structural and/or catalytic element, their actions include membrane stabilisation, participation in apo-enzyme synthesis by influencing DNA stability, as well as being an integral part of DNA-binding protein (Zn-finger) motifs (Hamer, 1986; Jacob *et al.*, 1999; Coyle *et al.*, 2002). MT reaches maximal levels in cells at the G1/S transition, a period during which cells are preparing for DNA synthesis. Zinc is also required at this G1/S boundary. This has led to the suggestion that MT might regulate the supply of zinc for DNA and protein synthesis (DNA- and RNA polymerases and transcription factors) and repair enzymes needed during the S phase (Rossman *et al.*, 1997; Ghoshal & Samson, 2001). Further evidence showed the expression of MTs both in the cytoplasm and nucleus of rapidly proliferating cells. It has been proposed that this nuclear retention of MTs might protect DNA from oxidative damage or regulate Zn supply to crucial enzymes and transcription factors involved in cell division (Coyle *et al.*, 2002).

A number of investigators have suggested that a major role of MT is to protect against electrophilic agents such as free radicals and reactive metabolites (Thornalley & Vašák, 1985; Satoh *et al.*, 1988; Bauman *et al.*, 1991; Andrews, 2000; Ghoshal & Samson, 2001; Coyle *et al.*, 2002). Kägi and co-workers already proposed in 1974 that MT might play a role in maintaining oxidation-reduction potential and in transport, possibly similar to that of glutathione. In fact, MT can protect DNA with an 800-fold higher molar efficiency compared to glutathione due to its extremely high scavenging ability of $OH^{\cdot}$ radicals (Thornalley & Vašák, 1985; Abel & de Ruiter, 1989). However, Thomas and his co-workers proposed in 1986 that the antioxidant function of Zn-metallothionein may be predominantly due to the metal ions having antioxidant properties, by interacting with cell membranes and interfering with lipid peroxidation. Their suggestion is based on the following: Firstly, Zn release is dependent on the redox status of the cell. Under oxidative conditions, the released Zn could prevent lipid peroxidation. Simultaneously, the free thiol groups of the MTs

scavenge the $O_2^{\cdot-}$ and H_2O_2, but particularly $OH^{\cdot}$ very efficiently. Finally, glutathione could then reduce the disulfide bonds in the oxidized MTs, making metallothionein an expendable ROS scavenger. Upon release, Zn(II) might also act as a compensatory messenger of oxidative stress by stimulating further MT expression (Thomas *et al.*, 1986; Bauman *et al.*, 1991; Kling & Olsson, 2000; Andrews, 2000; Ghoshal & Samson, 2001; Coyle *et al.*, 2002). Since the thiol groups of metallothioneins are bound by different metals, such as Zn, Cd, and Cu, it has been proposed that MTs antioxidant properties are dependent on which metals are bound to it. (Kling & Olsson, 2000) The presence of MT not only in the cytoplasm, but also in the nuclei during the G1/S phase of the cell cycle, shows that it does not only play a protective role in the cytoplasm, but also protects DNA from oxidative damage (Ghoshal & Samson, 2001). Investigations carried out by Kondoh and co-workers (2001) suggested that MTs particularly play a major role in protection against oxidative stress induced in mitochondria. Seeing that complex I deficiencies produce an increase in ROS, it was hypothesized that MTs may have a protective response to ROS-mediated damage in complex I deficient cell lines (van der Westhuizen *et al.*, 2003).

2.3.4. Induction of metallothionein transcription and oxidative stress

MT is generally considered a "housekeeping" protein because it is expressed in many different tissues and cell types (Cherian *et al.*, 2003). Nevertheless, there are substantial quantitative variations in levels of MT expression upon various stimuli. Whilst MT-1 and MT-2 isoforms are considered to be ubiquitously expressed as well as inducible, MT-3 and MT-4 subforms are only expressed in certain neurons and epithelial cells respectively and usually are not induced by the same stimuli as MT-1 and MT-2 (Haq *et al.*, 2003).

Some of the metals that bind and induce MT-1 and MT-2 expression in mammalian cells include Zn, Cd, Hg, Cu and Bi. Other inducers of MTs are Ni and Co (Haq *et al.*, 2003). Except for heavy metal induction, MT gene transcription is also induced by bacterial endotoxins, alkylating agents, X-

irradiation, alcohols, glucagon, catecholamine, glucocorticoid hormones, interferon and also rapidly by stress conditions where ROS is produced (Sato *et al.*, 1995). At more complex levels, MT expression can be altered by changes in gene structure, such as amplification and methylation, and by cellular differentiation and development (Hamer, 1986; Andrews, 2000).

This heavy metal- and oxidative stress induction process occurs via six common *cis*-acting elements, called metal responsive elements (MREs), which are located in the proximal promoter of these genes and can be *trans*-activated by transcription factors such as the six zinc-finger MTF-1 (metal-responsive element-binding transcription factor 1). The various non-identical MRE copies (MREa-g) consist of multiple copies of 13-15 imperfect repeats in either orientation and contain the consensus sequence CTC**TGCRCBC**XGCCC, where R is a purine, B is any base other than A, X represents G/C and bold-face residues are absolutely required for heavy metal response (Ghoshal & Samson, 2001).

Of the several transcription factors involved in MT-expression, MTF-1 is indispensable for the constitutive and induced expression of MT-1 and MT-2 genes (Ghoshal & Samson, 2001). MTF-1 has more than one activation domain and probably binds to the immediate promoter spanning the MREs and probably interacts with the components of RNA polymerase II transcription machinery in the presence of Zn (Ghoshal & Samson, 2001). Seeing that the binding of MTF-1 to MRE requires Zn to occupy zinc fingers, it is the only metal ion that can directly activate MTF-1 by means of allosteric interaction (Haq *et al.*, 2003). The mechanism(s) of activation of MTF-1 by means of other metals are still unknown (Ghoshal & Samson, 2001). The free zinc present under oxidative conditions can consequently serve as a second messenger to activate the DNA-binding activity of MTF-1 (Andrews, 2000; Van der Westhuizen *et al.*, 2003). Because MTs cannot themselves bind to DNA or activate transcription, they depend on regulation of Zn and binding thereof to MTF-1. This is probably true for other Zn regulators as well. This would then result in a multiple factor signal transduction system (Haq *et. al.*, 2003).

A common feature of MTs is that *cis*-acting elements of MTs are activated by agents against which they protect, which includes various free radical generators. In mitochondrial respiratory chain deficiencies, induction of MT transcription is also ROS-related (Haq *et. al.*, 2003; van der Westhuizen *et al.*, 2003). The MLTF (adenomajor late transcription factor)/ARE (antioxidant response element) *cis* element activates both basal and induced expression of MT genes and is a complex element comprising an overlapping E-box motif and an ARE (TGACnnnGC). The ARE, discovered by Andrews (2000), is an oxidative stress response and cadmium response element in the MT-I promoter. The ARE (also called electrophile response element) also mediates induction of glutathione *S*-transferase γ-subunit and the quinone reductase genes in response to H_2O_2. It was also found that mice can survive without MT, but not without GSH. It could therefore be assumed that the combined antioxidant capacity of both of these proteins would cover a vast number of oxidative stressors (Andrews, 2000; Ghoshal & Samson, 2001; Haq *et al.*, 2003).

Studies concerning the induction of all six MREs as well as MLTF/ARE after heavy metal or ROS induction implicates involvement of the same transcription factor(s) in MT expression, probably by distinct signalling mechanisms (Ghoshal & Samson, 2001). The ARE site of the MT-1 promoter was occupied only in specific oxidative situations, (such as H_2O_2 treatment, but not with *t*-BHQ (*tert*-butyl hydroquinone)), which suggests that specific signal transduction cascades may mediate response to different forms of oxidative stress (Andrews, 2000). The hybrid MLTF/ARE, together with MREs are thus responsible for the response of MT genes to ROS as can be seen in Figure 2.10 (Ghoshal & Samson, 2001; Haq *et. al.*, 2003).

The majority of studies show that MT expression is regulated on the transcription level, however, some evidence show that post-translational modifications could also be involved. Until present, the nature of such modifications remains unknown (Haq *et al.*, 2003).

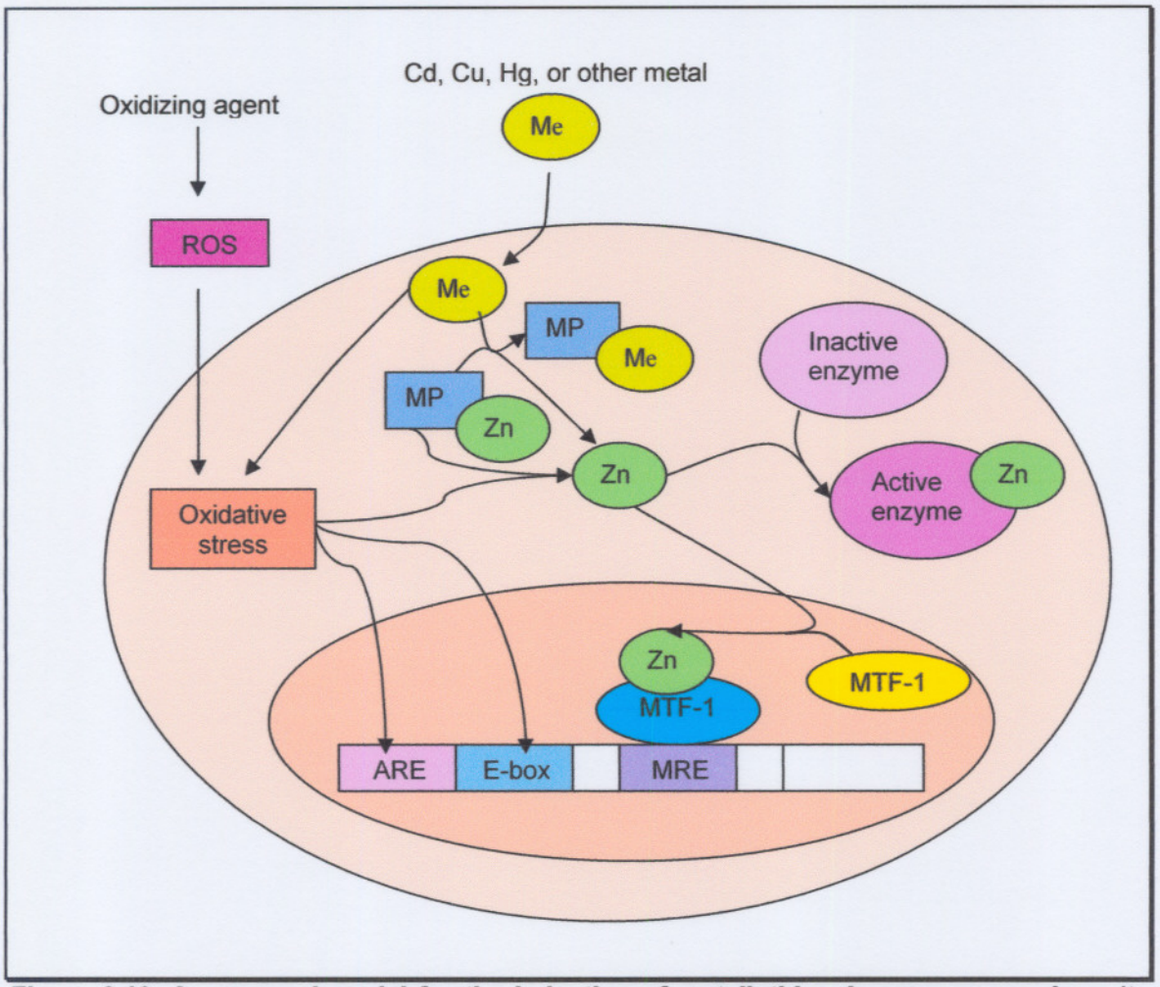

Figure 2.10. A proposed model for the induction of metallothionein gene expression. It shows a schematic representation of a cell (beige), containing a nucleus (orange), in which the metal-responsive gene is located. MP = Metallo-regulatory protein which is hypothesized to mediate the intracellular zinc availability in response to the entry of metal ions. Metallothionein may, under certain circumstances, act as the MP to control the zinc availability to enzymes and transcription factors. ARE = antioxidant response element, E-box = *cis*-element in DNA associating with MLTF (adenomajor late transcription factor, or upstream stimulatory factor (USF)). MTF-1 = the metal-responsive element-binding transcription factor 1. MRE = metal responsive element. Oxidative stress is postulated to enhance the dissociation of Zn from metallothionein, and thereby inducing MT gene expression (Adapted from Haq *et. al.*, 2003).

2.4. PROBLEM STATEMENT, HYPOTHESIS, AIMS AND STRATEGY

2.4.1. Problem statement, hypothesis and aims

Due to the prevalence of complex I deficiencies in respiratory chain diseases and the quite frequent occurrence of related diseases, more and more investigations into various agents presumably having protective effects against these diseases and their consequences are currently conducted. The increased production of ROS due to complex I deficiencies is a widely accepted event (see Section 2.2.2.2), and has been shown to lead to various other severe consequences, including DNA, lipid and protein damage. The increased levels of metallothioneins under oxidative conditions have also been widely accepted (Section 2.3.3) and the protective role of the metallothioneins in the cytoplasm and nucleus against these reactive oxygen species is also acknowledged, either by way of scavenging ROS or increasing free zinc levels leading to other protective effects. Recent evidence has also suggested that MTs are induced in mitochondrial diseases and a related study to the one described here focused on this aspect (Olivier, 2004). All of the above indications lead to the question whether or not metallothioneins also have a protective capacity in complex I deficient cells.

After careful consideration of the above mentioned facts, *the hypothesis of this study was formulated, namely that the overexpression of metallothioneins has a protective effect in cells with a complex I deficiency.*

The aim of this study is therefore to investigate the putative protective role of metallothioneins in a complex I deficient cell line, and specifically whether this protection relates to ROS and ROS-induced consequences such as apoptosis. A further aim of this study is to establish whether different isoforms would lead to different levels of protection in this complex I deficient cell line.

2.4.2. Strategy and experimental design

In order to study the role of metallothioneins during conditions of oxidative stress, various researchers have utilised knock-out or knock-down models of MT expression. These studies have shown that although metallothioneins pose a survival advantage, they are not essential for life during these oxidative conditions. In the past it has proven difficult and at times impossible to interpret the results of knock-out experiments of genes for proteins of unknown function and to predict the phenotype of transgenic animals in other instances (Vallee, 1995). Another alternative would be to utilise temporary inhibitors that would lead to low expression levels. Instead, we chose to create an MT over-expression model by utilising stable transfections to investigate the function of two different isoforms of MTs in the presence of a complex I deficiency. This would lead to long term use and would be relatively less expensive.

In short the following approach was considered for this study: Firstly, to construct suitable expression vectors containing MT-1B- and MT-2-encoding sequences, respectively, and to transfect a human cell line with these plasmid vectors. Secondly, to evaluate the transfected cell lines for gene presence and expression of the respective MT isoforms. Thirdly, several relevant biochemical aspects of these modified cell lines could be investigated and compared when a complex I deficiency was induced by rotenone.

The choice of metallothioneins suitable for the study was done based on the fact that MT-1 and MT-2 are ubiquitously expressed proteins and rapidly induced by oxidative stress, in contrast to MT-3 and MT-4. The cell line chosen for this work is HeLa cells, as many metallothionein studies have been conducted in these cells in the past. They are also adequate for the transfections required in the study and have excellent growth capabilities. Importantly, MT-1B also has very low expression levels in HeLa cells in contrast to MT-2A (Section 2.3.2). There would therefore be low background levels in the MT-1B overexpressed cell line, ensuring the results would only indicate the effect of the introduced MT-1B expression.

Several important requirements had to be met in choosing an appropriate expression vector for this specific study. The final choice fell on the pIRESneo2 vector (BD Biosciences Clontech), in view of the fulfilled requirements listed below (1 and 2) and some additional valuable characteristics (3 to 5):

1) Firstly, it contains a multiple cloning site (MCS) housing a selection of 16 unique restriction sites, utilising various common restriction endonuclease enzymes also found in the two metallothionein cDNA sequences that had to be cloned.
2) Secondly, it contains both an ampicillin resistance (ß-lactamase) gene for transformed prokaryotic cell selection and a neomycin phosphotransferase gene giving rise to resistance in transfected eukaryotic cells cultured in the presence of G418 (neomycin).
3) It produces a high copy number when transformed and replicated in the available *E.coli* DH10B strain commonly used in our laboratory.
4) It also contains the human cytomegalovirus (CMV) major immediate early promoter which ensures constant expression of the MTs. This is in contrast to inducible promoters which express the gene of interest only in the presence of an inducer. Many inducers for expression vectors, such as dexamethasone, also induce MT expression.
5) Last, but not least, the pIRESneo2 vector contains the internal ribosome entry site (IRES) of the encephalomyocarditis virus (ECMV), which permits the translation of two open reading frames from one messenger RNA. The expression cassette of pIRESneo2 therefore contains both the MCS and the neomycin phosphotransferase genes. Hence, after selection with a high concentration of G418, nearly all surviving clones will stably express similar high levels of the gene of interest, providing the opportunity to, if suitable, use the pool of transfected cells surviving selection instead of extensively isolating and characterizing clones after transfections.

The strategy for this study is summarized in Figure 2.11. This figure also indicates which sections correlates with the subsequent chapters to follow in this

dissertation. Chapter 3 describes the cloning and characterization of MT-expression vectors, after which the expression of MTs (Chapter 4) and biochemical analyses (Chapter 5) are described. The final discussions and conclusions follow in Chapter 6.

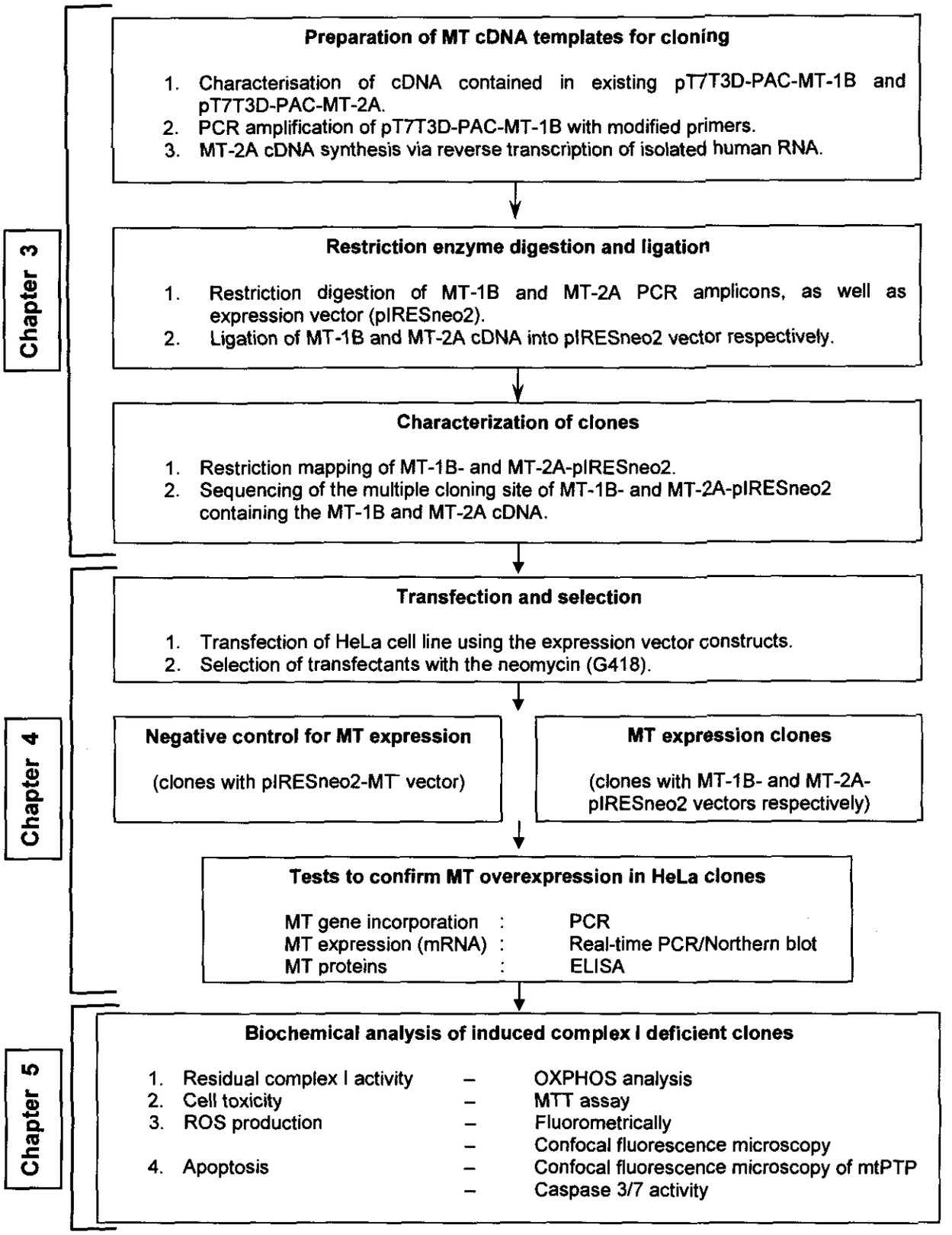

Figure 2.11. Strategy for metallothionein cloning and functional study.

CHAPTER THREE

CONSTRUCTION OF MT-1B- AND MT-2A- EXPRESSION VECTORS

3.1. MATERIALS AND METHODS

3.1.1. INTRODUCTION

As was described in Chapter 2, the strategy to investigate the functional properties of metallothioneins included the overexpression of MTs in HeLa cells by transfecting the cells with MT-containing expression plasmids. The MT-1B and MT-2A cDNAs were originally obtained from an intermediary recombinant construct of vector pT7T3D-PAC, which was supplied by van der Westhuizen *et al.* (2003). However, the final MT-2A cDNA was obtained by reverse transcribing RNA followed by high fidelity PCR amplification and cloning. The MT-1B and MT-2A amplicons were separately ligated into the pIRESneo2 vector, which was transfected into the HeLa cells as discussed in Chapter 4. Figures 3.1 and 3.2 summarise the steps and components for the cloning of MT-1B and MT-2A, respectively.

The protocols followed in this study were performed according to the specifications included with the respective kits utilised, or according to published protocols as indicated. Modifications to these protocols are indicated throughout.

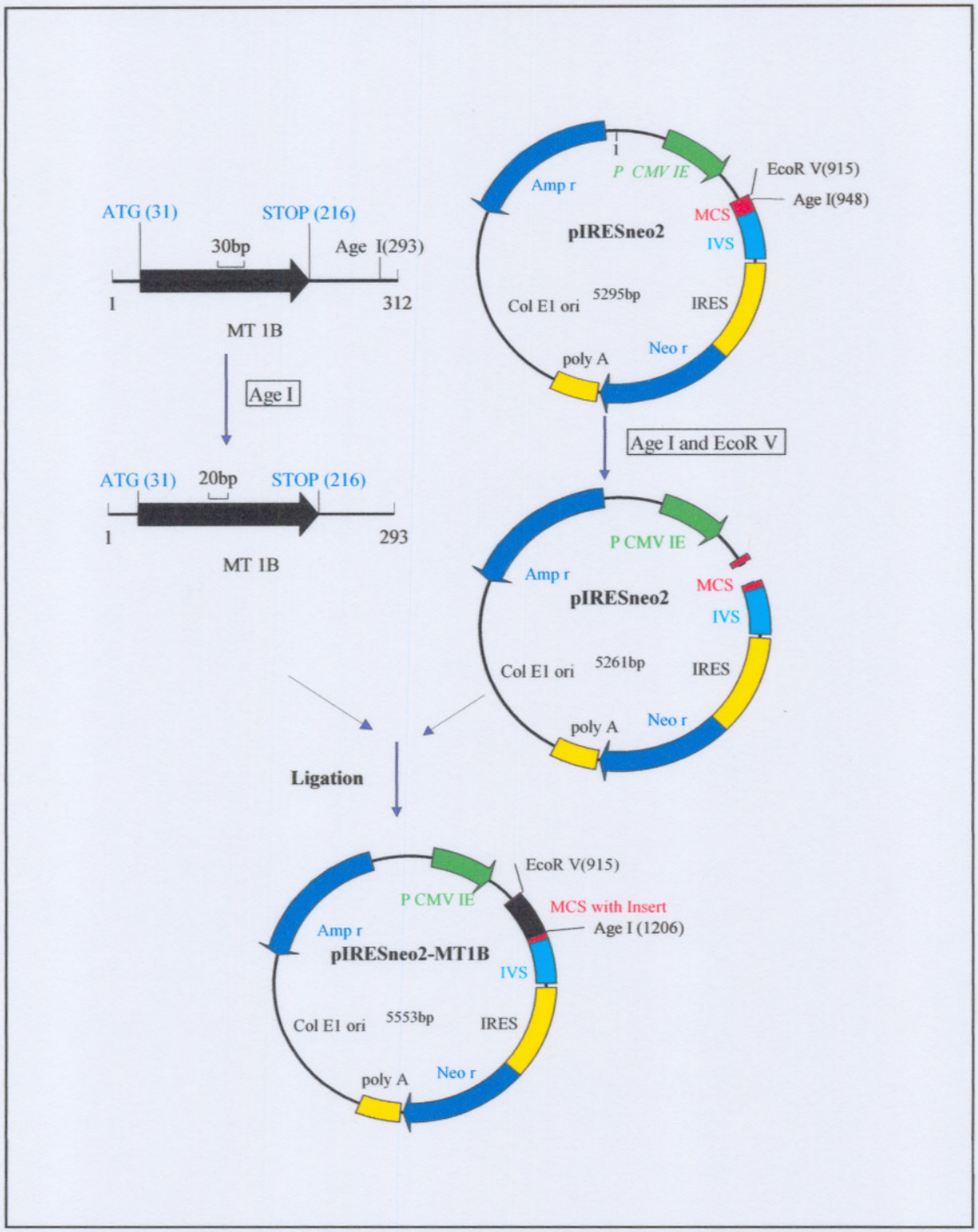

Figure 3.1. The steps and components for the cloning of the MT-1B cDNA obtained from a pT7T3D-PAC-MT1B plasmid. Key enzyme sites (*Eco*R V and *Age* I) are indicated in the multiple cloning site (MCS). These were utilised for ligation into the expression vector as indicated. Amp^r = ampicillin resistance (β-lactamase) gene. P CMV IE = Human cytomegalovirus (CMV) major immediate early promoter. IVS = synthetic intron. IRES = attenuated internal ribosome entry site from encephalomyocarditis virus. Neo^r = Neomycin phosphotransferase coding sequence. PolyA = fragment containing bovine growth hormone poly-A signal. Col E1 ori = *E.coli* replication origin.

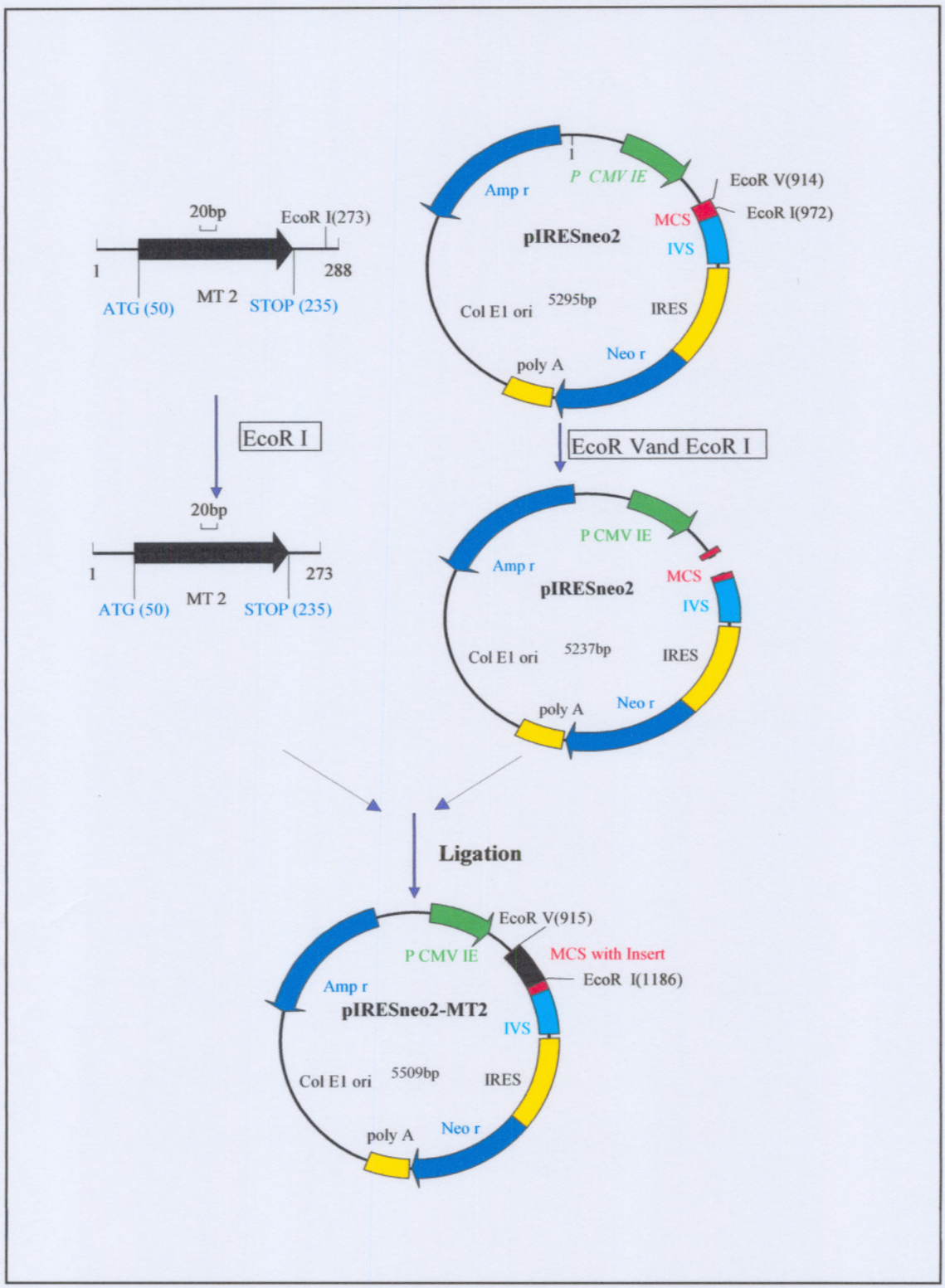

Figure 3.2. The steps and components for the cloning of the MT-2A cDNA obtained from human muscle. Key enzyme sites (*Eco*R V and *Eco*R I) are indicated in the multiple cloning site (MCS). These were utilised for ligation into the expression vector as indicated.

3.1.2. PREPARATION OF MT cDNA FRAGMENTS FOR CLONING

3.1.2.1. Design of primers for PCR and cloning

In order to design the appropriate primers for amplification it was necessary to take into consideration some critical parameters. The first was that the primer had to be approximately 18–24 bp in length, with a GC content of 45 – 55 %. Primer sequences were also verified for primer-dimer formation and self-complementarity. In addition, oligonucleotide primer pairs were designed so that they have similar melting temperatures (Chen *et al.*, 2003). These parameters were evaluated with the software program DNAMAN (version 4.13, Lynnon BioSoft, Quebec, Canada).

The calculated temperature, at which a primer set for a specific reaction is utilised, is known as the calculated mean melting temperature (T_m). The supplier of all the primer sequences (Inqaba Biotechnical Industries (Pty) Ltd) provided a calculated T_m-value. A software program called Oligonucleotide Properties Calculator software (OLIGONUCLEOTIDE PROPERTIES CALCULATOR, 2003) was also utilised to determine the T_m of each primer set through nearest neighbour and thermodynamic calculations by using the values published by Sugimoto *et al.* (1996). Another equation, used most often, is that of Thein and Wallace (1986) as presented in Equation 3.1, where the adenine/thymine (A+T) and guanine/cytosine (G+C) content is used to determine the T_m value and does not include complex thermodynamic parameters. An average T_m value determined by all of these methods was utilised.

Equation 3.1: Calculation of the primer melting temperature

$$T_m = 2(A+T) + 4(G+C)$$

T_m = calculated melting temperature, A + T = adenine and thymine content of primer sequence and G + C = guanine and cytosine content of primer sequence. Adapted from Thein and Wallace (1986).

However, in general, PCR conditions used for amplification are optimised from a temperature 2 °C below that of the T_m-value. This estimated annealing temperature (T_a) of the primer set can serve as a starting point from where the experimental annealing temperature can be increased or decreased to achieve optimal amplification. Table 3.1 summarises the primers and annealing temperatures used for primer pairs in this study. The equation for the calculation of T_a is presented in Equation 3.2.

Table 3.1: Sequences of PCR primers utilised for cloning

Primer	Primer sequence (5′ – 3′)	T_m (°C)	T_a (°C)	Size (b)
F: Universal-fwd	ctactactactactgcaaggcgattaagttgggtaac	62	**64**	37
R: Universal-rev	atcatcatcatcgtgagcggataacaatttcacacag gaaacagc	67	**64**	45
F: MT1B-fwd	cctaggaactccaggctagc	64	**60**	20
R: MT1B-rev	aaagaatgtagcaaaccggtc	60	**60**	21
F: MT2-fwd	gcgaacccgcgtgcaaccggtccc	79	**57**	24
R: MT2-rev2	caggtttgtggaa**t**tcgcgt	60	**57**	20
R: MT2-rev	caggtttgtggaagtcgcgt	62	**57**	20
F: T7	taatacgactcactatagg	52	**60**	19
R: pIRES-3′	gccctagatgcatgctcg	58	**60**	18

T_m indicate average calculated melting temperature in °C according to OLIGONUCLEOTIDE PROPERTIES CALCULATOR (2003), Inqaba Biotechnical Industries (suppliers) and Thein and Wallace (1986). The experimental annealing temperature in °C for each set of forward (F) and reverse primers (R) is indicated as T_a. The first primer set was utilised in sequencing of intermediary vectors, the second sets for cloning and the last set for sequencing of recombinant plasmids pIRESneo2-MT-1B and pIRESneo2-MT-2A. Size = primer size in bp. The point mutation introduced in MT2-rev2 in order to create the appropriate restriction site is indicated in bold text.

Equation 3.2: Calculation of estimated annealing temperature of primer sets

$$T_a = \text{Mean } T_m - 2°C$$

T_a = experimental annealing temperature of primer set in °C and Mean T_m = the mean melting temperature of the primer set in °C.

3.1.2.2. Amplification of MT-1B from pT7T3D-PAC intermediary vectors

The regions of interest in the respective plasmids were amplified using PCR (polymerase chain reaction), an enzymatic amplification reaction of a specific DNA-region. The amplification of the fragments was performed in a Thermo Hybaid® [1] Multiblock System 0.2 G thermocycler. Standard PCR reaction mixtures with 1.5 mM $MgCl_2$ were utilised except when otherwise indicated. *Pfu* polymerase (Promega®[2]) was utilised as suggested by the manufacturer. The enzyme has 3′→ 5′ exonuclease proofreading activity that ensures high fidelity amplification needed for accurate cloning and produces blunt ends for further cloning procedures. The PCR conditions are listed in Table 3.2 except when indicated otherwise.

To amplify the MT-1B cDNA coding region from the intermediary vector for ligation into the pIRESneo2 expression vector, the MT1B-fwd and MT1B-rev primers listed in Table 3.1 were used. The positions of the annealing sites of the primers as well as the coding region of MT-1B cDNA are indicated in Figure 3.3. The sequence amplified is therefore theoretically 312 bp in length. The cycling parameters for denaturation, annealing and extension are shown in Table 3.2.

The amplification of the MT-1B and MT-2 products were observed by separating these products via agarose gel electrophoresis (Maniatis *et al.*, 1982). A 1 or 2 % (w/v) agarose gel was used depending on the size of the fragments to be separated. Various DNA ladders were utilised to estimate the size of DNA

[1] Thermo Hybaid® is a registered trademark of Hybaid Limited, Ashford, Middlesex, United Kingdom.
[2] Promega® is a registered trademark of Promega Corporation, Madison, WI, U.S.A.

fragments. A 50 bp GeneRuler™[1] DNA ladder (Fermentas) was utilised for the estimation of the sizes of the smaller fragments. The second ladder, a 50 bp Step Ladder (Sigma-Aldrich) was utilised for determination of longer fragments. A loading buffer containing bromophenol blue (BDH) was used. The voltage applied varied according to the size of the gel, with an average of 10 $V.cm^{-1}$ for mini and midi gels. The fragments were visualised using a UV fluorescence trans-illuminator at 254 nm with the use of ethidium bromide (Amresco). The results were photographed with a Polaroid camera.

#	Sequence and translation
	Nhe I
1	gcctgccctg acttctcata tcttgcctag gaactccagg **cttgt**cttgg ctccaaat**gg**
1	M
	*Bam*H I
61	**atcc**caactg ctcctgcacc acaggtggct cctgtgcctg cgccggctcc tgcaagtgca
20	D P N C S C T T G G S C A C A G S C K C
121	aagagtgcaa atgtacctcc tgcaagaagt gctgctgctc ttgctgcccc gtgggctgtg
40	K E C K C T S C K K C C C S C C P V G C
181	ccaagtgtgc ccagggctgt gtctgcaaag gctcatcaga gaagtgccgc tgctgtgcct
60	A K C A Q G C V C K G S S E K C R C C A
241	gatgttggga gagccctgct cccagacata aatagagcaa ccagtactaa cctggatttt
80	*
	Pin AI
301	ttttttaac taccct**gacc ggt**ttgctac attctttttt ctattcaata tgtgaaagac
361	aataaaacac ttttgacttg aaaaaaaaaa aaaaaaaaaa aaaa

Figure 3.3. cDNA and amino acid sequence of Homo sapiens MT-1B cDNA. The position of the MT-1B forward primer is indicated by the underlined text (xxx) and the position of the MT-1B reverse primer is indicated by double underlined text (yyy). The MT-1B cDNA (GenBank accession number NM_005947) coding sequence is indicated in blue and the restriction sites utilised are indicated in bold text (Adapted from NCBI, 2004). # indicates nucleotide or amino acid number.

[1] GeneRuler™ is a trademark of Fermentas, Vilnius, Lithuania.

Table 3.2: PCR conditions for amplification of MT-1B and MT-2A from intermediary and expression vectors

PCR step	# of cycles	Action	Temperature (°C)	Duration (min)
1	1	Denaturation	94	5:00
2	30	Denaturation	94	0:30
		Annealing	x	0:30
		Extension	72	0:30
3	1	Extension	72	5:00
4	1	Cooling	4	Hold

= number of cycles,

x = 64 °C for the amplification of MT-1B and MT-2A from the intermediary vector, 60 °C for the amplification of MT-1B, 57 °C for the amplification of MT-2A and 60 °C for the amplification of MT-1B and MT-2A from pIRESneo2.

3.1.2.3. Preparation of MT-2A cDNA from human muscle

DNA sequencing data showed that the sequence of MT-2A was not completely conserved in the intermediary vector (pT7T3D-PAC-MT-2A) supplied by van der Westhuizen et al. (2003), and the cDNA therefore had to be prepared via an alternative way. To achieve this, total RNA was extracted from a human muscle *vastus laterals* biopsy sample and the cDNA for MT-2A was synthesized using this RNA sample. Written consent was obtained before using the sample for cDNA synthesis.

Total RNA was extracted from the human muscle using the QuickPrep™[1] total RNA extraction kit (Amersham Biosciences), according to the manufacturer's specifications for tissue. This kit is based on a procedure that combines the disruptive and protective properties of guanidinium thiocyanate with selective

[1] QuikPrep™ is a trademark of Amersham Biosciences UK Limited, Buckinghamshire, United Kingdom.

precipitation and isopycnic centrifugation using lithium chloride and caesium trifluoroacetate (CsTFA).

The concentration of the total isolated RNA was estimated by measuring the absorbance at 260 nm using ultraviolet (UV) spectrophotometry with a Uvikon XS double beam spectrophotometer (BIO-TEK Instruments). For RNA, which is single stranded, the concentration was calculated using Equation 3.3 (Maniatis *et al.*, 1982). An estimation of the purity of the DNA sample is provided by the ratio between the readings at 260 nm and 280 nm (OD_{260}/OD_{280}). Values of approximately 1.8 were considered sufficiently pure RNA preparations with little contamination of protein. To estimate the integrity of RNA samples a small volume of each sample was analysed via agarose gel electrophoresis (Section 3.1.2.2). The approximate intensities of the 28S and 18S rRNA bands, visible tRNA patches lower on the gel as well as the lack of high molecular weight DNA was used as an indication of relatively good quality RNA samples suitable for cDNA synthesis.

Equation 3.3: Calculation of the total RNA concentration from the absorbance at 260 nm

$$[RNA] \text{ in } \mu g.\mu l^{-1} = (A_{260} - A_{320}) \times 40 \text{ ng}.\mu l^{-1} \times \text{dilution factor} / 1000$$

[RNA] = RNA concentration and A_{260} = absorbance of samples at 260 nm. A_{320} = absorbance of samples at 320 nm, used as a background reference. Adapted from Maniatis *et al.* (1982).

To synthesise the cDNA copy of an RNA-template, it was first necessary to synthesise the first cDNA strand, with a reverse transcriptase enzyme such as M-MLV RT (Moloney Murine Leukemia Virus Reverse Transcriptase, Promega®). A reaction mixture containing approximately 2 µg total human RNA and 20 pmoles of the MT-2rev primer (see Table 3.1) was subjected to reverse transcription with M-MLV RT as described by the supplier. Subsequent PCR amplification ensured the generation of the second complementary strand, which was evaluated by means of agarose gel electrophoresis.

#	Sequence
	Pin AI
1	Agtcccagcg aacccgcgtg caaccggtcc cgactctagc cgcctcttca gcacgccatg
1	M
	*Bam*H I
61	gatccaact gctcctgcgc cgccggtgac tcctgcacct gcgccggttc ctgcaaatgc
20	D P N C S C A A G D S C T C A G S C K C
121	aaagagtgca aatgcacttc gtgcaagaaa agctgctgct cctgctgccc tgtgggctgt
40	K E C K C T S C K K S C C S C C P V G C
181	gccaagtgtg cccaaggctg catctgcaaa ggggcgtcgg acaagtgcag ctgctgcgcc
60	A K C A Q G C I C K G A S D K C S C C A
	*Eco*R I
241	tgatgctggg acagccccgc tcccagatgt aaagaacgcg agttccacaa acctggattt
80	*
301	tttatgtaca accctgaccg tgaccgtttg ctatattcct ttttctatga aataatgtga
361	atgataataa aa

Figure 3.4. cDNA and amino acid sequence of Homo sapiens MT-2A cDNA. The position of the MT-2A forward primer is indicated by the underlined text (xxx) and the position of the MT-2A reverse primer is indicated by double underlined text (yyy). The MT-2A cDNA (GenBank accession number NM_005953) coding sequence is indicated in blue, and the restriction sites utilised are indicated in bold text. Note the original nucleotide which was modified in the MT2-rev2 primer to facilitate restriction enzyme digestion (original nucleotide highlighted in yellow), also shown in Table 3.1 to create the restriction site for *Eco*R I (Adapted from NCBI, 2004). # indicates nucleotide and amino acid number.

Table 3.3: PCR conditions for amplification of MT-2A cDNA

PCR step	# of cycles	Action	Temperature (°C)	Duration (min)
1	1	Initial denaturation	94	5:00
2	40	Denaturation	94	1:00
		Annealing	57 (with each cycle increasing with 0.1°C)	1:00
		Extension	72	0:40
3	1	Final extension	72	10:00
4	1	Cooling	4	Hold

= number of cycles.

To amplify the MT-2A cDNA, the MT2-fwd and MT2-rev2 primers listed in Table 3.1 were utilised. The amplification created restriction site introduced in the MT2-rev2 primer facilitates the presence of a *Eco*R I restriction site. Theoreticaly, the fragment length after amplification should be 288 bp. For this amplification, *Pfu* polymerase was again utilised instead of Taq DNA polymerase. In the sequence presented in Figure 3.4 the position of the annealing sites of the primers as well as the coding region are indicated. Table 3.3 shows the specific PCR conditions for this amplification procedure.

3.1.3. LIGATION OF MT cDNAS INTO pIRESneo2 EXPRESSION VECTOR

3.1.3.1. Restriction endonuclease cleavage

In order to ligate MT-1B cDNA into the pIRESneo2 vector, the MT-1B amplicon was cut close to the 3′ end (nucleotide 318 in Figure 3.3) with the restriction enzyme *Pin* AI (an isoschizomer of *Age* I, Roche Products (Pty) Ltd) to produce a 3'-overhang, according to the manufacturer's specifications. It was also necessary to cleave the pIRESneo2 vector (Southern Cross Biotechnology (Pty) Ltd) with *Pin* AI on the 3′-side to ensure the ligation of the 3′-end of the MT1B amplicon into the vector. The vector was also cut with *Eco*R V (Promega®), which is a blunt-end forming restriction enzyme. This allowed the 5′-end of the MT-1B fragment to be inserted as produced by *Pfu* polymerase during the amplification mentioned in Section 3.1.2.2 (thus from nucleotide 26 to 318 in Figure 3.3). Figure 3.1 shows the restriction map and Figures 3.5 and 3.6 shows the positions of the restriction sites within the vector.

To facilitate the ligation of the MT-2A cDNA sequence into the pIRESneo2 vector, the MT-2A amplicon was cut close to the 3′ side of the sequence (nucleotide 280 in Figure 3.4) with *Eco*R I (3′-overhang, Promega®) according to the enzyme manufacturer's specifications. Again, it was necessary to cut the pIRESneo2

enzyme sites utilised in restriction mapping (Section 3.1.6) is shown in bold text. The MCS is indicated in yellow highlighted text (Adapted from NCBI, 2004). # indicates nucleotide number.

3.1.4. PREPARATION OF COMPETENT *E.COLI* DH10B CELLS AND TRANSFORMATION WITH THE PLASMIDS

To study the function of the metallothionein genes (MT-1B and MT-2A), the intermediary and expression vectors containing the MT-1B and MT-2A cDNAs were transferred into bacterial cells. These plasmids can attain a high copy number during bacterial growth and thus ensure a sufficient stock of plasmid DNA for experimentation. This process is called transformation of the bacterial cells (Freshney, 2000). Selection of transformed cells is ensured by addition of ampicillin to the medium. The ampicillin resistance gene present in a plasmid codes for β-lactamase, which cleaves the β-lactam ring of the antibiotic, rendering the antibiotic inactive (Atlas, 1997).

To ensure competent cells, an overnight culture of *E.coli* DH10B was prepared by inoculating 5 ml Luria broth (LB, 10 g Tryptone (Biolab), 5 g NaCl (BDH), 5 g yeast extract (Biolab), up to 1 litre with MilliQ®[1] water, autoclaved) with 3 µl of the culture and incubating at 37 °C. LB (250 ml) was inoculated with 5 ml of the overnight culture and incubated at 37 °C whilst shaking for approximately 2 hours. The culture was put on ice for 10 minutes to keep the cells in the logarithmic growth phase. All further steps were performed at 4 °C. The culture was centrifuged for 15 minutes at 1.9 x g to pellet the bacteria and suspended in 0.5 ml sterile transforming buffer [60 mM $CaCl_2$ (Merck), 10 mM Tris®[2]-HCl (Roche Products (Pty) Ltd), pH 8.0 and 15% glycerol (Sigma-Aldrich)]. Another 9.5 ml transforming buffer was added and the suspension left on ice for 25 minutes, after which it was centrifuged for 15 minutes at 1.9 x g. The supernatant was decanted and the cells carefully suspended in 3 ml transforming buffer, aliquoted to 200 µl volumes and stored at -70 °C (Maniatis *et al.*, 1982).

For transformations, an aliquot of the *E.coli* DH10B competent culture was thawed on ice, and 5 µl of the appropriate ligation mix (obtained in Section

[1] MilliQ® is a registered trademark of Millipore Corporation, Billerica, MA, U.S.A. It refers to water treated with a Milli-Q® Ultrapure Water Purification System as per manufacturer's instructions.
[2] Tris® is a registered trademark of the United States Biochemical Corporation, Cleveland, OH, U.S.A.

3.1.3.2) added to 100 µl of this culture. It was left on ice for 25 minutes to allow the adsorption of the DNA onto the cell membranes. It was transferred to a preheated water bath (42 °C) for 1 to 2 minutes and immediately placed on ice afterwards for approximately 2 minutes. LB (400 µl) was added and incubated at 37 °C for 30 minutes, whilst shaking, to allow the cells to recover and start expressing β-lactamase. 100 µl of the culture was spread onto an agar plate (LB and 100 $\mu g.ml^{-1}$ ampicillin (Boehringer Mannheim GmbH) and incubated overnight at 37 °C (Maniatis *et al.*, 1982). 3 ml of LB, containing 100 $\mu g.ml^{-1}$ ampicillin was inoculated with single colonies from the plate and incubated overnight at 37 °C whilst shaking. A freshly diluted culture was made by inoculating 30 ml LB (with 150 $\mu g.ml^{-1}$ ampicillin) with 1 ml of the overnight culture and incubated for 2 hours at 37 °C. Aliquots of the transformed cells were prepared by adding 150 µl 100% glycerol to 850 µl of the cell culture and storing it at -70 °C (Maniatis *et al.*, 1982).

3.1.5. ISOLATION OF PLASMID DNA

To isolate the plasmid DNA from the bacterial cells, both the NucleoBond®[1] Plasmid Purification kit (Macherey-Nagel) and the QIAGEN®[2] Plasmid Midi Kit (QIAGEN®) was utilised according to the manufacturer's indications. The concentration of the isolated DNA was estimated by measuring the absorbance/optical density at a wavelength of 260 nm by ultraviolet (UV) spectrophotometry with a Uvikon XS double beam spectrophotometer (BIO-TEK Instruments). The DNA concentrations were calculated using Equation 3.4 (Maniatis *et al.*, 1982). An estimation of the purity of the DNA sample is provided by the ratio of the readings at 260 nm and 280 nm (OD_{260}/OD_{280}). Values of approximately 1.8 were considered sufficiently pure DNA preparations with little contamination of protein (Maniatis *et.al.*, 1982). To estimate the integrity of DNA samples a small volume of each sample was analysed via agarose gel electrophoresis (Maniatis *et al.*, 1982).

[1] NucleoBond® is a registered trademark of Macherey-Nagel GmbH, Dueren Germany.
[2] QIAGEN® is a registered trademark of QIAGEN, Clifton Hill, Victoria, Australia.

Equation 3.4: Calculation of the total DNA concentration from the absorbance at 260 nm

$$[\text{ds-DNA}] \text{ in } \mu g.\mu l^{-1} = (A_{260} - A_{320}) \times 50 \text{ ng}.\mu l^{-1} \times \text{dilution factor} / 1000$$

[DNA] = DNA concentration and A_{260} = absorbance of samples at 260 nm (Adapted from Maniatis *et al.*, 1982).

3.1.6. RESTRICTION ANALYSES OF INTERMEDIARY AND EXPRESSION VECTORS

The treatment of a DNA molecule with a restriction endonuclease produces a series of precisely defined DNA fragments that can be separated according to size by agarose gel electrophoresis as described in Section 3.1.2.2 (Voet and Voet, 1995).

To determine whether or not the pT7T3D-PAC-MT-1B and pT7T3D-PAC-MT-2A recombinant plasmids contained the fragments of correct lengths they were treated with two combinations of restriction enzymes according to the manufacturer's specifications. The first combination included *Eco*R I (Promega®) and *Bam*H I (3´-overhang, Promega®). The expected size for the MT-1B fragment was 353 bp and for the MT-2A fragment 320 bp. The second combination included *Hind* III (3´-overhang, Promega®) and *Eco*R I. The expected size of the MT-1B fragment was 439 bp and the MT-2A fragment 407 bp. The recognition sites of *Bam*H I in the MT-1B and MT-2A cDNA coding regions are indicated in Figures 3.3 and 3.4. Figure 3.6 shows the positions of the *Hind* III and *Eco*R I restriction sites in the pT7T3D-PAC vector.

To determine whether the ligations of MT-1B and MT-2A into pIRESneo2 were successful, these vectors were cleaved with *Hind* III and *Bam*H I according to the manufacturer's specifications. According to the number and sizes of the fragments produced, it could be ascertained whether the inserts were correctly ligated. Figure 3.7 shows the restriction map of the digested vectors and Table

3.4 shows the theoretical expected fragment lengths produced from the restriction mapping. The restriction sites of *Bam*H I in the MT-1B and MT-2A cDNA sequences can be seen in Figures 3.3 and 3.4. Figure 3.5 shows the recognition sites of *Hind* III in the pIRESneo2 vector.

#	Sequence
1	cccattcgcc attcaggctg cgcaactgtt gggaagggcg atcggtgcgg gcctcttcgc
61	tattacgcca gctggcgaaa gggggatgtg ctgcaaggcg attaagttgg gtaacgccag
121	ggttttccca gtcacgacgt tgtaaaacga cggccagtgc caagctaaaa ttaaccctca
	Hind III *Pac I*
181	ctaaagggaa t**aagctt**gcg gccgc**ttaat taaagatc**ga cggatccccg actacgtagt
	*Eco*R I
241	cggtcgtgcc **gaattc**ttgg cctcgagggc caaattccct atagtgagtc gtattaaatt
301	cgtaatcatg gtcatagctg tttcctgtgt gaaattgtta tccgctcaca attccacaca
361	acatacgagc cggaagcata aagtgtaaag cctggggtgc ctaatgagtg agctaactca
421	cattaattgc gt...

Figure 3.6. Sequence of the cloning site within the intermediary vector pT7T3D-PAC. The position of the Universal forward primer is indicated by the underlined text (xxx) and the position of the Universal reverse primer is indicated by double underlined text (yyy).The restriction enzyme sites located in the multiple cloning site, *Pac* I and *EcoR* I, where the MT-1B and MT-2 sequences respectively were cloned into, are shown in bold text. The restriction site of *Hind* III (see section 3.1.5) is also shown in bold text (Adapted from Biology and Biotechnology Research Program, 2004). # indicates nucleotide number.

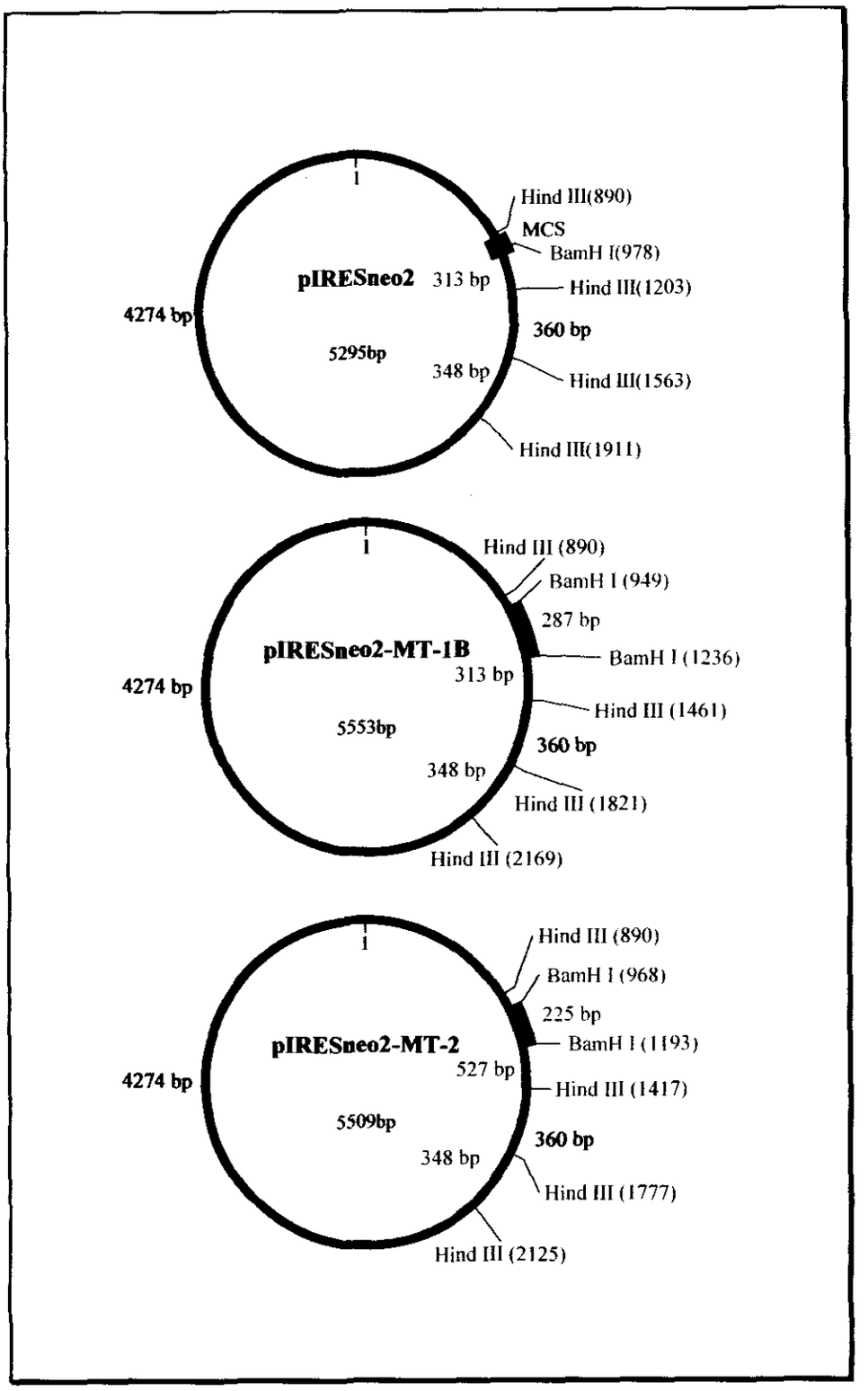

Figure 3.7. Restriction analysis maps of pIRESneo2, pIRESneo2-MT-1B and pIRESneo2-MT-2A with *Bam*H I and *Hin*d III. The positions of the restriction sites are indicated in brackets and the theoretical fragment lengths are indicated between the restriction sites.

Table 3.4: Theoretical fragment lengths produced from restriction mapping analyses with *Bam*H I and *Hind* III

	pIRESneo2		pIRESneo2-MT-1B		pIRESneo2-2A	
Enzyme	Site	**Length (bp)**	Site	**Length (bp)**	Site	**Length (bp)**
***Bam*H I**	978	**5295**	949	**5265**	968	**5285**
			1236	**287**	1193	**225**
***Hind* III**	890	**4274**	890	**4274**	890	**4274**
	1203	**373**	1461	**570**	1417	**527**
	1563	**360**	1821	**360**	1777	**360**
	1911	**348**	2169	**348**	2125	**348**

Site = restriction sites indicating the nucleotide position where the various restriction enzymes cleave the vectors. Length = the theoretical fragment lengths in bp visible via agarose gel electrophoresis after cleavage.

3.1.7. SEQUENCING OF INTERMEDIARY AND EXPRESSION VECTORS

A modernised version of the chain termination or dideoxy sequencing, first described by Sanger *et al.* in 1977, that incorporates fluorophores, was used to determine the sequence of DNA. With the use of capillary electrophoresis, the different fluorophores can be detected because of their different emission spectra, with the smallest fragments being detected first. For all the DNA concentration determinations carried out to be used for sequencing, an Eppendorf®[1] BioPhotometer was used.

The Universal primers (Universal-fwd and Universal-rev) utilised for the amplification of MT-1B and MT-2A cDNAs from the intermediary vector, pT7T3D-PAC are listed in Table 3.1. The theoretical fragment length of MT1B should be 461 bp and for MT-2A 317 bp. In the sequence presented in Figure 3.6 the position of the annealing sites of the primers as well as the restriction enzyme

[1] Eppendorf® is a registered trademark of Eppendorf AG, Hamburg, Germany.

site in which the MT coding regions were ligated into, are indicated. The cycling parameters for denaturation, annealing and extension are shown in Table 3.2.

To amplify the MT-1B and MT-2A containing regions from the pIRESneo2 vector, for sequencing purposes, the T7 and pIRES-3′ primers listed in Table 3.1 were utilised. The theoretical fragment length of the pIRESneo2-MT-1B amplicon is 740 bp and for the pIRESneo2-MT-2A fragment 693 bp. In the sequence presented in Figure 3.5 the positions of the annealing sites of the primers are indicated. For this specific primer set, the amplification of MT-1B was optimised at 60 °C with 1.8 mM $MgCl_2$. For MT-2A, an annealing temperature of 62 °C was chosen, together with a $MgCl_2$ concentration of 2 mM[1]. The rest of the cycling parameters for denaturation, annealing and extension are shown in Table 3.2. The amplified products were visualised with agarose gel electrophoresis as described in Section 3.1.2.2.

The QIAquick®[2] PCR purification kit (QIAGEN®) was used to purify the PCR products before sequencing and the ABI Prism®[3] Big Dye™[4] Terminator version 3.0 Ready Reaction Cycle Sequencing Kit (ABI) was utilised according to the manufacturers' specifications.

The various PCR products were sequenced using both forward and reverse primers (as for the previously mentioned PCR reactions) in separate PCR and sequencing reactions, to ensure that sequencing results were trustworthy at close proximity to the primer annealing sites. The cycle sequencing of the PCR products were performed according to the program outlined in Table 3.5. The four steps were repeated for 25 cycles.

Following the thermal cycle sequencing, the products were purified from unincorporated dye terminators, enzymes and primers, as these would interfere

[1] Optimisation of PCR conditions was done in collaboration with T. Semete and DNAbiotec (Pty) Ltd., Pretoria, South Africa.
[2] QIAquick® is a registered trademark of QIAGEN Pty. Ltd., Clifton Hill, Victoria, Australia.
[3] ABI Prism® is a registered trademark of Applera Corporation, Foster City, CA, U.S.A.
[4] Big Dye™ is a trademark of Applera Corporation, Foster City, CA, U.S.A.

with the base identification during electrophoresis. This purification consisted of a precipitation reaction where 62.5 µl 99.8 % EtOH, 3 µl 3M NaOAc (pH 4.6), 14.5 µl ddH_20 and 10 µl of the sequence reaction mix were vortexed and centrifuged at 13 000 x g for 20 min at 4°C. The supernatant was immediately discarded and 250 µl of 70% EtOH was added to wash the pellet, after which the centrifugation was repeated for 10 minutes. The supernatant was discarded again, and the pellet was air-dried at room temperature for approximately 35 min.

The precipitated samples were sent to Inqaba Biotechnical Industries (Pty) Ltd to be analysed. The pellet was resuspended in 6 µl Hi-Di™[1] deionised formamide and 3 µl was injected into a SpectruMedix™[2] (SCE2410) Genetic Analyser for capillary detection. The dye/base relationships and the colours of the BigDye™ terminators v3.0 as they appear on the gel image of the instrument used are presented in Table 3.6. The sequences received from Inqaba Biotechnical Industries (Pty) Ltd were then studied and aligned, utilising the BioEdit[3] Sequence Alignment editor version 5.0.9.1 (2001). The processed sequences were then analysed using the nucleotide-nucleotide Basic Local Alignment Search Tool (BLAST) from NCBI.

[1] Hi-Di™ is a trademark of Applera Corporation, Foster City, CA, U.S.A.
[2] SpectruMedix™ is a trademark of SpectruMedix LLC., State College, PA, U.S.A.
[3] BioEdit is a licensed program from Tom Hall, North Carolina State University, 2001.

Table 3.5: Conditions for cycle sequencing

Cycle step	Action	Temperature (°C)	Duration (min)
1	Rapid Thermal ramp (1 °C.s^{-1}) to	96	
	Denaturation	96	0:10
2	Rapid Thermal ramp to	50	
	Annealing	50	0:05
3	Rapid Thermal ramp to	60	
	Elongation	60	4:00
4	Rapid Thermal ramp to	4	Hold

The four steps were repeated for 25 cycles. Adapted from the ABI Prism® Big Dye™ Terminator version 3.0 Ready Reaction Cycle Sequencing Kit protocol.

Table 3.6: Colours of the bases detected on a SpectruMedix TM (SCE2410) Genetic Analyser

DNA base	Terminator	Colour of peak on the instrument
G	V3 Dye 1	Black
A	V3 Dye 2	Green
T	V3 Dye 3	Red
C	V3 Dye 4	Blue

A=adenine, C=cytosine, G=guanine and T= thymine.

3.2. RESULTS AND DISCUSSION

The optimisation of the different experimental protocols will not be discussed, as most of the various protocols were followed exactly according to manufacturer's specifications. PCR conditions were briefly optimised in only a few cases and quickly discussed below as this is not the primary focus of the study. The most critical results generated during the cloning of the correct pIRESneo2-MT-1B and pIRESneo2-MT-2A expression plasmids are shown and discussed below.

3.2.1. OPTIMISATION OF PCR CONDITIONS

Optimisation of PCR conditions only included annealing temperatures, with $MgCl_2$ kept at 1.5 mM, unless stated otherwise. The criteria for choosing an optimal annealing temperature was that only one DNA fragment of correct size was observed and that the visual amount of the fragment was the highest in the particular set of optimisation reactions. For the following primer sets the optimal annealing temperatures were as follows: MT-1B-fwd/MT-1B-rev, 60 °C; MT2A-fwd/MT2A-rev, 57 °C; Universal-fwd/Universal-rev, 64 °C; T7/pIRES-3′ for MT-1B, 60 °C (1.8 mM $MgCl_2$); T7/pIRES-3′ for MT-2A, 62 °C (2 mM $MgCl_2$).

3.2.2. PREPARATION OF MT-1B- AND MT-2A-CDNA FRAGMENTS FOR CLONING

In order to produce the pIRESneo2-MT-1B and -MT-2A expression vectors, the MT-1B cDNA sequence was amplified from the intermediary vector, pT7T3D-PAC-MT-1B and the MT-2 cDNA sequence was generated via reverse transcription from a human muscle biopsy mRNA. In Section 3.2.2.1 the results obtained with restriction analyses of the intermediary vectors is presented and discussed and Section 3.2.2.2 examines the sequencing results of these vectors.

3.2.2.1. Confirming the presence of the intact MT-1B and MT-2A human cDNA sequence from the intermediary vectors with restriction analyses

Figure 3.8 shows a photographic representation of the restriction digestion of pT7T3D-PAC-MT-1B and pT7T3D-PAC-MT-2A as visualised with agarose gel electrophoresis. From the restriction digestion of the pT7T3D-PAC-MT-1B plasmid the expected 439 bp fragment after treatment with *Eco*R I and *Hin*d III was detected. However, instead of showing the expected 353 bp fragment after treatment with *Eco*R I and *Bam*H I, it showed a fragment of 67 bp in length (indicated by the arrow). This fragment corresponds to a reverse insert orientation in the vector. Figure 3.9 a) and b) depicts a schematic representation of the fragment lengths visualised, when such a reverse insert orientation would occur.

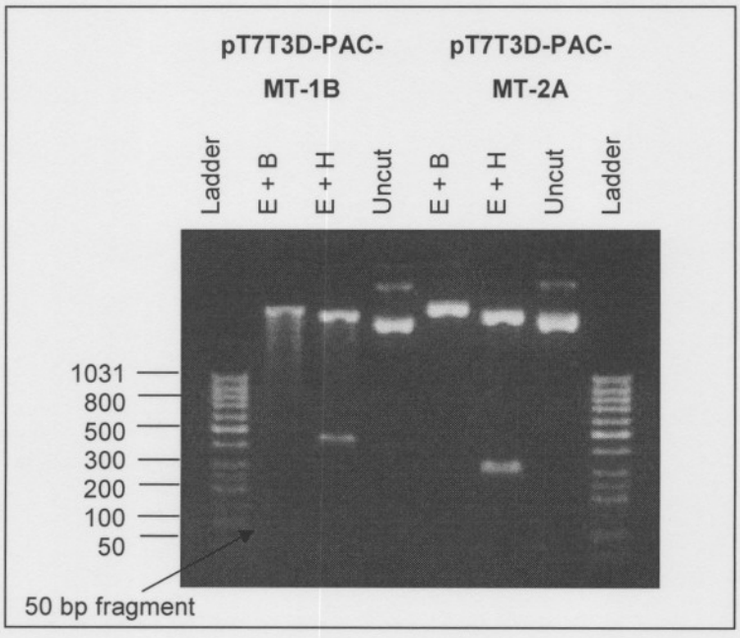

Figure 3.8. Restriction endonuclease products for pT7T3D-PAC-MT-1B and pT7T3D-PAC-MT-2A . 2% Agarose gel electrophoresed at 80 V for approximately 30 – 45 min in 1 x TAE buffer. Ladder = 50 bp Step ladder (Sigma-Aldrich). E + B = Restriction digestion set consisting of *Eco*R I and *Bam*H I. E + H = Restriction digestion set consisting of *Eco*R I and *Hin*d III. Both pT7T3D-PAC-MT-1B and pT7T3D-PAC-MT-2A were analysed with both of these restriction digestion sets. The 67 bp fragment (position indicated by the arrow) produced after restriction analysis of pT7T3D-PAC-MT-1B with *Eco*R I and *Bam*H I is not visible on the photograph. At the time it was taken the fragment was faint but visible.

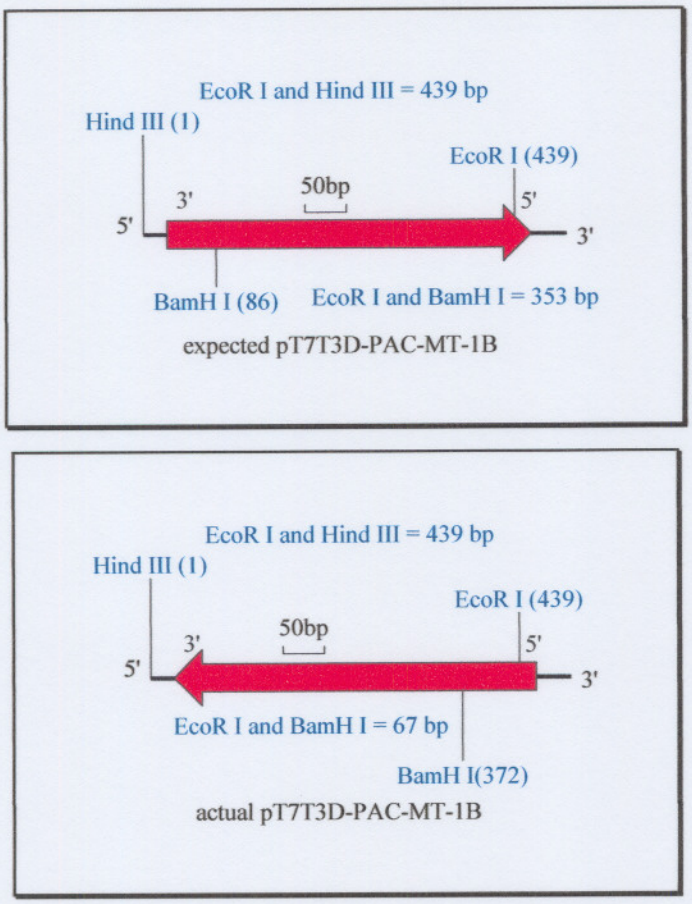

Figure 3.9. Schematic representation of positions of restriction enzyme sites (*Eco*R I, *Bam*H I and *Hin*d III) in a) expected forward and b) reverse insert orientation of the MT-1B cDNA sequence in the intermediary vector pT7T3D-PAC-MT-1B.

The restriction endonuclease cleavage of the pT7T3D-PAC-MT-2A plasmid produced a fragment size of approximately 300-350 bp, in contrast to the expected fragment length of 407 bp after treatment with *Eco*R I and *Hin*d III. It also did not produce the expected 320 bp fragment after cleavage with *Eco*R I and *Bam*H I. The likelihood of this insert to contain the correct cDNA sequence was therefore very small. Even so, this plasmid was still sequenced.

3.2.2.2. Confirming the presence of the intact MT-1B and MT-2A human cDNA sequence from the intermediary vectors with sequencing

The pT7T3D-PAC-MT-1B and pT7T3D-PAC-MT-2A plasmids were then amplified with the Universal-fwd and Universal-rev primers, and sequenced utilising both primers[1]. Figure A.1 shows an example of a typical sequence electropherogram. Figure A.2 (Appendix A) shows the final sequencing result, in the 3′-5′ direction, for MT-1B. The sequence of the human MT-1B cDNA obtained from NCBI (Genbank accession number NM_005947) corresponds exactly to the MT-1B insert in the pT7T3D-PAC-MT-1B plasmid, even though it is present in the reverse orientation. This however, did not affect the sequential cloning strategy. After sequencing, the MT-1B cDNA region was amplified from the pT7T3D-PAC-MT-1B vector with the MT-1B fwd and MT-1B rev primers, to be utilised in the rest of the cloning procedure. Figure 3.10 shows the photographic representation of this PCR amplification.

However, as expected, the pT7T3D-PAC-MT-2A plasmid only contained a few base pairs of the MT-2A cDNA (data not shown). It was previously reported by Halgren *et al.* (2001) and also by van der Westhuizen *et al.* (2003) that some of the clones, which were commercially obtained from the IMAGE Consortium cDNA clone collection, had a high error rate with only 62.2 % of 1189 bacterial stock cultures tested being uncontaminated and containing cDNA inserts that had significant sequence identity to published data for the ordered clones. This prompted us to synthesize the MT-2A cDNA from human muscle.

3.2.2.3. Synthesis of MT-2A cDNA from human muscle RNA

At first, lymphocytes isolated from EDTA blood samples was utilised for the RNA isolation required for cDNA synthesis of the MT-2A cDNA. Both the cell culture and tissue methods proposed by the manufacturer (QuickPrep™ total RNA

[1] Sequencing analyses was done in collaboration with Dr. B. Semete.

extraction kit (Amersham Biosciences)) were assessed. However, not enough total RNA could be isolated from the samples. Total RNA from a human muscle biopsy was subsequently used.

Agarose gel electrophoresis visualisation of the PCR amplification of the MT-2A cDNA synthesis is depicted in Figure 3.10. It yielded a fragment of approximately 250-300 bp, which corresponds to the expected 287 bp MT-2A cDNA fragment. This fragment was therefore utilised in the subsequent cloning procedure.

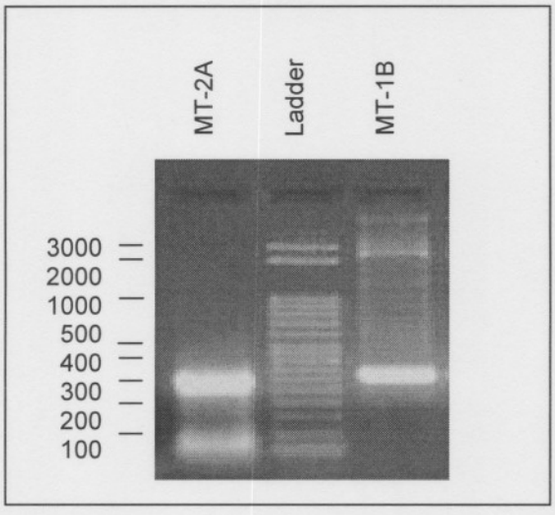

Figure 3.10. PCR products of MT-2A and MT-1B cDNA with specific primers. 2% Agarose gel electrophoresed at 80 V for approximately 30 – 45 min in 1 x TAE buffer. Ladder = 50 bp Step Ladder (Sigma-Aldrich). The left lane indicates the MT-2A cDNA (amplified with MT2-fwd and MT2-rev2) with a fragment size of approximately 287 bp. The right lane indicates the PCR product of the MT-1B cDNA after amplification with the MT-1B-fwd and MT-1B-rev primers, as needed for restriction digestion. It has a fragment length of approximately 311 bp.

3.2.3. ASSESSMENT OF LIGATION

The MT-1B fragment was amplified from the intermediary vector with the use of the MT-1B-fwd and MT-1B-rev primers in order to introduce some restriction cleavage sites. Specific point mutations were therefore introduced in the MT-1B-fwd, MT-2-fwd and MT-2rev2 primers utilised in the amplification of these sequences (see Section 3.1.2.1). Originally, the MT-1B insert was to be cut with

Nhe I on the 5′-end, and with *Pin* AI on the 3′-end of the amplified fragment. After optimisation of the restriction cleavage it was decided to use blunt-end ligation of the 5′-end with the expression vector, pIRESneo2 after restriction with *Eco*R V. Due to the mutations being nearby the 3′-end of the MT-1B-fwd primer annealing would therefore not be optimal, leading to incorrect or no amplification. MT-2A was to be cleaved with *Pin* AI on the 5′-end and *Eco*R I on the 3′-end of the fragment. Again, it was decided to rather use blunt-end ligation between the 5′-end of the MT-2A amplified fragment and the 3′-end of the vector due to the expensive nature of the enzyme. The cloning strategy for MT-1B and MT-2A cDNA into pIRESneo2 is presented in Figures 3.1 and 3.2.

Two of the clones (3 and 9) produced by transformation with the pIRESneo2-MT-2A plasmid were analysed further in order to select the most appropriate clone for transfections. Three of the transformants of pIRESneo2-MT-1B (clones 1, 3 and 5) were also analysed further for selection of a correct clone for transfections.

3.2.3.1. Confirming successful ligation with restriction analyses

Ligation of MT-1B and MT-2A into the expression vectors were analysed via restriction mapping with *Bam*H I and *Hin*d III in order to produce the theoretical fragment lengths as listed in Table 3.4.

Figure 3.11 depicts the photographic representation of the restriction analyses of the MT-2A clones 3 and 9, as visualised with agarose gel electrophoresis. The correct insertion of MT-2A was to generate fragments of 5265 and 225 bp in length after *Bam*H I treatment. For restriction analysis with *Hin*d III, it was used to generate fragments of 4274, 527, 360 and 348 bp in length. Clone 3 showed the fragment of approximately 250 bp with *Bam*H I restriction. For the *Hin*d III analysis it also showed the expected fragment lengths. Both of these restriction analyses on pIRESneo2-MT-2A clone 3 indicate that this clone was a good candidate for successful cloning, hence it was sequenced. On the other hand,

clone 9 did not show the expected fragment lengths after *Bam*H I restriction. The restriction analysis with *Hin*d III, however, showed approximately the right sized fragments. It was therefore very likely that this sequence did not contain the correct insert (coding region), or that the restriction site was lost or mutated during cloning, which would imply that the coding region also contained some mutations. Even so, both of these clones were sequenced.

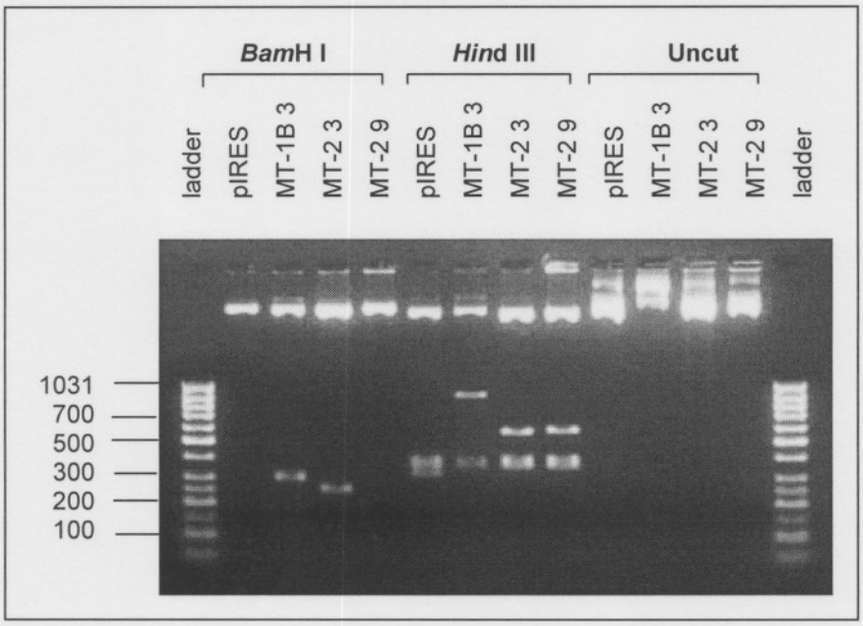

Figure 3.11. Restriction cleavage of pIRESneo2-MT-1B Clone 3 and pIRESneo2-MT-2A Clones 3 and 9. A 2% Agarose gel was electrophoresed at 80 V for approximately 30 – 45 min in 1 x TAE buffer. The first lane on the left and the last on the right contain DNA ladders (50 bp from Fermentas). pIRES = pIRESneo2. MT-1B 3 = pIRESneo2-MT-1B clone 3. MT-2 3 = pIRESneo2-MT-2A clone 3. MT-2 9 = pIRESneo2-MT-2A clone 9. *Bam*H I indicate vectors cleaved with *Bam*H I, and *Hin*d III indicate vectors cut with *Hin*d III. Uncut refers to the controls in which the vectors were not cleaved with any enzymes.

The restriction analysis of pIRESneo2-MT-1B clone 3, as visualised with agarose gel electrophoresis is indicated in Figure 3.11. The correct insertion of MT-1B was to produce fragments of 5285 and 287 bp in length after *Bam*H I treatment, and restriction with *Hin*d III was to produce fragments of 4274, 570, 360 and 348 bp in length if the MT-1B fragment. However, even though a fragment of roughly 300 bp was present after *Bam*H I restriction of clone 3, the restriction with *Hin*d III had unexpected results. In addition to the correct fragments of approximately

4000 bp and two fragments of 300-400 bp for the *Hin*d III restriction, it showed a 900 bp band, in contrast to the expected 570 bp fragment. This would indicate a possible double insertion of the MT-1B fragment. This double insertion would then not be evident with *Bam*H I restriction, as this would also produce a fragment of 348 bp in length, therefore appearing as one fragment on the agarose gel after electrophoresis. As a result of the possibility of this double insert, which could influence protein synthesis in transfected cells, two other clones were also examined.

Figure 3.12 (a, b) shows the agarose gel after electrophoresis of the MT-1B clone 1 restricted with *Bam*H I. Both clones 1 and 5 showed the expected 300 bp fragment with *Bam*H I restriction. Clone 5 did not show any *Hin*d III digestion (Data not shown), unlike clone 1 which showed the expected fragment lengths, as mentioned above. Clone 1 would therefore be likely to contain the correct cDNA insert and was sequenced together with clone 3.

a)

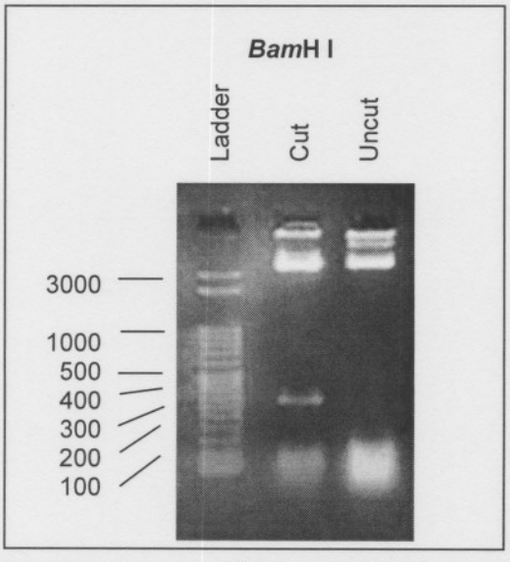

Figure 3.12. a) Restriction cleavage of pIRESneo2-MT-1B Clone 1 with *Bam*H I. A 2% garose gel was electrophoresed at 80 V for approximately 30 – 45 min in 1 x TAE buffer. The left lane contains a 50 bp Step Ladder from Sigma-Aldrich. Cut = pIRESneo2-MT-1B clone 1 cleaved with *Bam*H I. Uncut = pIRESneo2-MT-1B clone 1.

b)

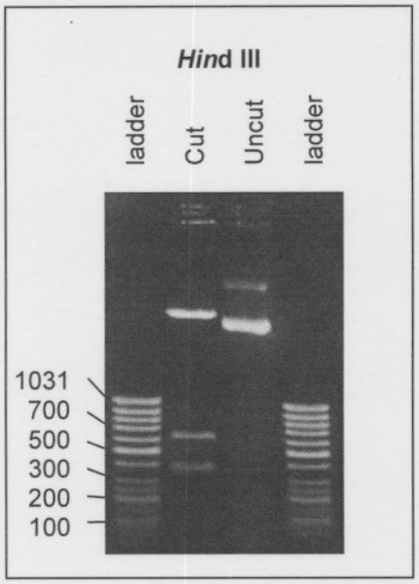

Figure 3.12. b) Restriction cleavage of pIRESneo2-MT-1B clone 1 with *Hind* III. 2% Agarose gel electrophoresed at 80 V for approximately 30 – 45 min in 1 x TAE buffer. Ladder = 50 bp DNA ladder from Fermentas. Cut = pIRESneo2-MT-1B clone 1 cleaved with *Hind* III. Uncut = pIRESneo2-MT-1B clone 1.

3.2.3.2. Confirming successful ligation with sequencing

Figure A.3 shows the sequencing result of pIRESneo2-MT-1B clone 3[1], using the primer set T7/pIRES-3´. It confirmed the double insertion of the correct MT-1B cDNA sequence ligated into the vector according to NCBI (Genbank accession number NM_005947). This double insertion could possibly lead to a non-functional protein and could also lead to inaccurate transcription by forming a much longer mRNA sequence and could therefore not be utilised in the functional studies of MT-1B.

The sequencing result of pIRESneo2-MT-1B clone 1, as depicted in Figure A.4 (Figure A.5 shows the sequence analysis comparison from NCBI) showed the correct insert ligated into the vector according to NCBI (Genbank accession

[1] Sequencing analysis after ligation was done by Dr. B. Semete.

number NM_005947). Even though parts of the reverse primer (MT-1B-rev), which were cleaved with *Pin* AI for ligation purposes, were also inserted on either side of the insert, the expression of MT-1B would not be affected. This evidence, together with the restriction analysis, showed pIRESneo2-MT-1B clone 1 to be ideal for further transfections and functional studies of MT-1B.

The sequencing result of pIRESneo2-MT-2A clone 3 as presented in Figure A.6 (Figure A.7 shows the sequence analysis comparison from NCBI), showed the correct insertion of the MT-2A cDNA sequence after ligation into the vector according to NCBI (Genbank accession number NM_005953). Even though parts of the reverse primer (MT-2-rev) which was cleaved with *Eco*R I for ligation purposes were also inserted on the 3′-end of the insert, this would not affect the expression of MT-2A. The sequencing result of pIRESneo2-MT-2A clone 9 (data not shown) did not show any correlation to the MT-2A sequence as indicated by NCBI (Genbank accession number NM_005953). It only showed correlation to the pIRESneo2 vector on either side of an insert. The sequencing result, together with the restriction analysis for MT-2A clone 3, rendered this clone to be sufficient for further transfections and functional studies of MT-2A.

3.3. SUMMARY

In this chapter the characterisation of the two intermediary vectors, pT7T3D-PAC-MT-1B and -MT-2A, was described. MT-1B cDNA was amplified from its intermediary vector, whilst the MT-2A cDNA was synthesised from human muscle total RNA. These two cDNA sequences were then digested and ligated into the expression vector pIRESneo2, respectively. The resultant clones were characterised with restriction mapping and sequencing. Accordingly, it was decided to use pIRESneo2-MT-1B Clone 1 and pIRESneo2-MT-2A Clone 3 for subsequent transfections and functional analyses.

CHAPTER FOUR

TRANSFECTION OF HeLa CELLS WITH EXPRESSION PLASMIDS CONTAINING MT-1B AND MT-2A AND CONFIRMATION OF METALLOTHIONEIN OVEREXPRESSION

4.1. MATERIALS AND METHODS

The expression plasmids created as described in Chapter 3 were utilised for the transfection of HeLa cells in order to create cells over-expressing respectively MT-1B and MT-2A. To verify the over-expression of the metallothioneins, the gene presence, mRNA expression and protein levels in the various pools of MT clones were analysed.

The protocols followed in this study were performed according to the specifications included with the respective kits utilised or according to published protocols. Modifications to these protocols are indicated throughout.

4.1.1. TRANSFECTION OF HELA CELLS AND SELECTION OF TRANSFECTANTS

To facilitate the functional study of individual genes, the plasmids containing the sequences of interest (MT-1B and MT-2A) were transferred into the eukaryotic host HeLA cells. A variety of transfection techniques exist. These techniques include calcium phosphate transfection, lipofection, electroporation and retroviral infection, each suitable for different cellular systems and different molecules (DNA, RNA, oligonucleotides, proteins). Transfections can be either transient (short term and used shortly after transfection with the use of reporter gene assays) or stable as in this case. Stable transfections utilise plasmid DNA containing a selectable marker, such as *neo*^{r} that confers resistance to G418

(geneticin, an analogue of neomycin). Geneticin interferes with the function of 80S ribosomes and blocks protein synthesis in normal eukaryotic cells. The transfected cells are then selected by continuous exposure to the selection agent, and resistant clones can be isolated (Freshney, 2000).

4.1.1.1. Transfection and selection

For this study the X-tremeGENE™[1] Q2 transfection reagent (Roche) was utilised. This transfection reagent, supplied as a dried lipid film, was specifically designed and optimised for transfection of and high-level protein expression in HeLa cells, which ordinarily are difficult to transfect. It also shows much lower cellular toxicity in comparison to other transfection reagents, which provides an advantage when investigating issues such as apoptosis. HeLa cells (National Repository for Biological Materials of the National Cancer Association of South Africa[2], NRBM No. 0001, Origin/No. of passage ATCC) were transfected with the three plasmids, pIRESneo2, pIRESneo2-MT-1B and pIRESneo2-MT-2A respectively. Each transfection procedure for the individual plasmids was carried out in duplicate, together with duplicate control wells. Transfections were performed according to the manufacturer's instructions.

Following a 24 hour incubation period after transfections, the selection procedure was started, by replacing the normal media (without G418) with the selection media [1000 $\mu g.ml^{-1}$ G418 (Geneticin, Sigma-Aldrich) in DMEM media, 5% (v/v) FBS and 1% (v/v) P/S]. The selection media was replaced every second day with freshly prepared media to ensure the efficiency of the antibiotic. This selection procedure was carried out until all the control cells were dead or showed 100% mortality, which occurred after approximately 13 days.

[1] X-tremeGENE™ is a trademark of a member of Roche Diagnostics Corporation, Indianapolis, IN, U.S.A.
[2] The National Repository for Biological materials of the National Cancer Association of South Africa is in association with Highveld Biological, JHB, South Africa.

To prepare a "pool of clones" (transfected cells where individual clones (foci) are not separated but still combined) for each of the three expression vectors, one well of each transfected cell lines was trypsinised and transferred to a 25 cm^3 flask. This allowed the combined clones for the functional analysis to grow. This trypsination was done during the selection process to keep the cells from adhering too tightly to the bottom of the well, as prolonged growth significantly hinders trypsination. The selection procedure was continued after which standard culturing procedures, as discussed in Section 4.1.1.2, was utilised.

The other well of each duplicate set was utilised for selection of individual clones, using two different methods. The first is a method previously developed by van der Westhuizen and Pretorius (2002). This technique (scraping) allows much quicker isolation than other methods utilised, such as dilution cloning, in which clones are selected from single cells. After 10 - 13 days (only after all control cells have died) the transfected cells can be viewed as macroscopic cell colonies (foci) approximately 2 mm in diameter. Round stainless steel bars (3 mm in diameter, 240 mm long) with spoon-shaped sharpened tips (5 x 3 mm) were used to scrape the adherent cells from the bottom of the well. The cells were then trypsinised and suspended in culture medium. For each of the clones needed (pIRESneo2, pIRESneo2-MT-1B and pRESneo2-MT-2A), at least six single clones were scraped and cultured further using standard culturing procedures as discussed in Section 4.1.1.2. Subcultures were confluent in a 6-well plate after two to three weeks.

The second method of individual clone isolation was that of dilution cloning adapted from Freshney (2000). Cells were seeded in such a way that theoretically each well of a 96-well plate contained one cell. When 60 – 90% confluency was reached in wells indeed containing colonies, the cells were trypsinised to a 6-well plate and finally a 25 cm^2 flask. Subcultures took several weeks to reach confluency in a 6-well plate.

4.1.1.2. Standard culturing procedures

In general cells were grown at 37 °C with 5 % CO_2 in a humidified HERA cell incubator (Kendro Laboratory Products[1]). The normal HeLa cells were cultured in Dulbecco's Modified Eagle's Medium (DMEM, with 4.5 $g.L^{-1}$ glucose and 0.110 $g.L^{-1}$ sodium pyruvate with L-Glutamine, Highveld Biological (PTY) LTD, South Africa) containing 5% (v/v) FBS (Fetal bovine serum, GIBCO™[2], E.U approved origin) and 1% (v/v) penicillin/streptomycin antibiotic solution (GIBCO™, 5 000 units/ml penicillin G sodium and 5 000 µg/ml streptomycin sulphate in 0.85 % saline). After selection, transfected cells were cultured in a selection media consisting of normal medium (as described above) and 200 $\mu g.ml^{-1}$ Geneticin (Sigma-Aldrich). Cells were cultured in 25 cm^2 and 75 cm^2 flasks containing 4 or 8 ml media respectively. When cells were 90-100 % confluent, they were trypsinised for analyses or culturing purposes. This procedure started with removing the media and washing the cells twice with 1 x volume 1 x PBS [without calcium or magnesium, BioWhittaker™[3]]. For cells grown in 24- or 6-well plates 3-5 drops trypsin (10 x dilution of 0.5% trypsin, 5.3 mM EDTA.4Na, GIBCO™) was added to each well. For cells grown in a 25 or 75 cm^2 flask, respectively 1 ml or 2 ml trypsin was added, after which it was incubated at 37 °C for 3-5 minutes. The cells were shaken loose by tapping the flasks on the benchtop. For the well plates, a pipette was utilised to gently loosen the cells. All procedures were carried out aseptically.

To harvest cells for analyses, a confluent 25 cm^2 flask containing the desired cells was trypsinised as described before. Subsequently, 4 ml 1 x PBS was added to remove the cells from the flask and transferred to a 10 ml conical tube. After centrifugation at 400 x g and 25 °C for 2 minutes, the supernatant was discarded. An additional 4 ml of PBS was added to the flask to remove residual cells, which was also transferred to the tube. The centrifugation was repeated

[1] Kendro Laboratory Products, GmbH, Hanau, Germany.
[2] GIBCO™ is a trademark of Invitrogen Corporation, Grand Island, New York, U.S.A.
[3] BioWhittaker™ is a trademark of Cambrex Bio Science Inc, Walkersville, MD, U.S.S.

and again the supernatant discarded. DNA was immediately isolated from the sample as described in Section 4.1.2.2.

4.1.2. CONFIRMATION OF METALLOTHIONEIN cDNA PRESENCE IN TRANSFECTED CELLS

To confirm the presence of the MT-1B and MT-2A cDNA in the transfected cells, the T7 and pIRES-3' vector-specific primers were utilised to amplify these cDNA sequences from the genomic DNA isolated from the various clone-pools. The use of Southern blots was attempted, however, these attempts were not as successful, probably due to the probe not producing a strong enough signal (see Appendix B that describes the use of Northern blots).

The DNA was isolated from the cell pellet collected as described in Section 4.1.1.2, based on the principle of phenol extraction and ethanol precipitation. The concentration of the DNA was estimated by measuring the optical density at a wavelength of 260 nm with an Uvikon XS Double beam spectrophotometer (BIO-TEK Instruments) as discussed in Section 3.1.5.

The cell pellet was suspended in 500 µl preheated lysis buffer [10 mM Tris®-HCl (Roche), pH 7.4, 10 mM EDTA (Sigma-Aldrich) and 0.5 % (w/v) SDS (sodium dodecylsulfate, Boehringer Mannheim GmbH) and incubated on ice for 10 minutes. RNase [1 $mg.ml^{-1}$ freshly prepared in water, Boehringer Mannheim GmbH] was added to a final concentration of 50 µg. The mixture was incubated at 37 °C for 1 hour. Subsequently, 50 µg proteinase K (1 $mg.ml^{-1}$ freshly prepared in water, Roche) was added and incubated overnight at 50 °C. The sample was transferred to micro-centrifuge tubes and 1 x volume of a 1:1 phenol: chloroform [phenol (Riedel-de-Haën), chloroform (HOLPRO Analytic Division, Midrand, South Africa)] mixture was added. The mixture was shaken and centrifuged at 15 700 x g and 4 °C for 10 minutes. The upper phase was carefully transferred to a new tube and 1 x volume chloroform added. The mixture was again mixed by inversion and centrifuged at 15 700 x g and 4 °C for

5 minutes. The upper phase was collected and $^{1}/_{10}$ x volume 5 M NaOAc (Merck) solution was added together with 2 x volumes of ice-cold EtOH (LABCHEM). The sample was precipitated at -20 °C for at least 1 hour and then centrifuged at 15 7000 x g and 4 °C for 5 minutes. The supernatant was discarded and the pellet washed with the addition of 1 ml 70 % EtOH. The centrifugation step was repeated and the pellet air dried. The DNA was then dissolved in 100 µl MilliQ water.

The amplification of the MT-1B and MT-2A sequences from the transfected cells were carried out with the vector-specific T7 and pIRES3' primers as indicated in Table 3.1 and 3.2, with the annealing temperature for the amplification of the gDNA at 56°C. The expected fragment length of the pIRESneo2-MT-1B amplicon is approximately 740 bp, and that of the pIRESneo2-MT-2A amplicon approximately 700 bp. The theoretical fragment length of the amplicon from pIRESneo2 base vector is 468 bp whereas no PCR fragment should be produced from DNA isolated from untransfected HeLa cells.

4.1.3. CONFIRMATION OF METALLOTHIONEIN mRNA EXPRESSION

The expression levels of MT-1B and MT-2A mRNA in the various clones were quantified using Real-time PCR.

The use of fluorescence-based kinetic real-time-PCR procedures significantly simplifies the reproducible relative quantification of mRNAs. The successful detection of low-abundance mRNA with real-time PCR ensures much greater sensitivity compared to Northern Blotting (Bustin, 2000) and also proved to be less time consuming. The fluorescent dye SYBR Green® I binds to all double-stranded DNA and on binding emits a fluorescent signal with an excitation and emission maxima at 494 nm and 521 nm, respectively. During denaturation however, the dye dissociates and fluorescence measurements are therefore performed during the extension step of every PCR cycle. Thus, signal intensity

increases with increasing cycle number due to the accumulation of the PCR product. Relative quantification allows gene expression levels to be calculated by determining the ratio between the amount of a target gene and one or more endogenous reference genes, such as GAPDH and β-2-microglobulin housekeeping genes which was utilized in this study (see Appendix C). This ratio is then compared between different samples (Bustin, 2000; Pfaffl *et al.*, 2002). To evaluate the relative expression levels of MT-1B and MT-2A respectively, real-time PCR was carried out with MT-1B and MT-2A specific primer sets as listed in Table 4.1.

Cells were harvested as discussed in Section 4.1.1.2. The total RNA was immediately isolated from the cell pellet, using the QIAzol™ [1] lysis reagent (QIAGEN®, Cat. No. 79306) according to the manufacturer's instructions. The concentration of the total isolated RNA was estimated by measuring the absorbance/optical density at a wavelength of 260 nm with a Uvikon XS Double beam spectrophotometer (BIO-TEK Instruments) as described in Section 3.1.2.3.

cDNA was prepared from the total RNA with the use of M-MLV RT. A reaction mixture containing 3 µg total RNA and 0.5 µg random primers (Promega) was subjected to reverse transcription with 200 U M-MLV RT as described by the supplier.

The real-time PCR reaction mixture contained the following in a final volume of 20 µl: 10 µl iQ™ [2] SYBR Green® [3] I Supermix (Bio-Rad), 20 pmoles each of the forward and reverse primers (as indicated in Table 4.2), 1 µl cDNA (75 ng) and 8 µl RNase-free water in thin wall tubes (Bio-Rad). Table 4.2 shows the PCR protocol. Real-time PCR was carried out with the iCycler iQ™ [4] (Bio-Rad) and iCycler iQ Real-time Detection System Software, version 3.0 (Bio-Rad) was used to analyse the results.

---

[1] QIAzol® is a registered trademark of QIAGEN, Clifton Hill, Victoria, Australia.
[2] iQ™ is a trademark of BIO-RAD Laboratories, Inc, Hercules, CA, U.S.A.
[3] SYBR Green® is a registered trademark of Molecular Probes, Inc, Eugene, OR, U.S.A..
[4] iQ™ is a trademark of BIO-RAD, Hercules, CA, U.S.A.

Table 4.1: Sequence for PCR primers utilised in real-time PCR

Target gene	Primer (5′ – 3′)	Primer sequence	Size (bp)
GAPDH	GAPDH-fwd	gaaggtgaaggtcggagtc	226
	GAPDH-rev	gaagatggtgatgggatttc	
β2-MG	Beta2-MG-fwd	agcgtactccaaagattcaggtt	306
	Beta2-MG-rev	atgatgctgcttacatgtctcgat	
MT-1B	F:MT1B-RTfwd	gaactccaggcttgtcttgg	187
	F:MT1B-RTrev	gatgagcctttgcagacaca	
MT-2A	F: MT2-RTfwd	tcctgcaaatgcaaagagtg	187
	R: MT2-rev	caggtttgtggaagtcgcgt	

GAPDH = Glyceraldehyde-3-phosphate dehydrogenase. β-2-MG = β-2-microglobulin.
F = forward primer and R = reverse primer. Size = Amplicon size. All primers supplied by Inqaba Biotechnical Industries. GAPDH and β-2-MG primer sequences from Radonic *et al.* (2004) and MT-1B and MT-2A primers generated by Primer3 software.

Table 4.2: Real-time PCR conditions

Cycle	# cycles	Action	Step	Temperature (°C)	Duration (min)
1	1	Denaturation		95	3:00
2	40	Data collection and real-time analysis	1	95	0:20
			2	60	0:10
			3	72	0:10
			4	82	0:05
3	1	Extension and denaturation	1	72	5:00
			2	95	1:00
4	1			55	1:00
5	80	Melting curve program		55-95	0:05
6	1	Cooling		4	Hold

Cycles repeated 30 times. Cycle 5 (melting curve program) had a heating rate of 0.5 °C per 5 seconds.

Equation 4.1: Calculation of relative expression of MT-1B and MT-2A

$$SD_{Ct} = \sqrt{\frac{sum(x-mn)^2}{n-1}} \quad \ldots(1)$$

$$E = 10^{(-1/S)} - 1 \quad \ldots(2)$$

$$Q = E^{\Delta Ct} \quad \ldots(3)$$

$$Q = E^{(minCT - sampleCt)} \quad \ldots(4)$$

$$SD_Q = E^{\Delta Ct}.\ln E.SD_{sampleCt} \quad \ldots(5)$$

$$NF_n = \sqrt[n]{Q_{HG1}xQ_{HG2}x...xQ_{HGn}} \quad \ldots(6)$$

$$SD_{NFn} = \sqrt[n]{\left(\frac{SD_{QHG1}}{n.Q_{HG1}}\right)^2 + ... + \left(\frac{SD_{QHGn}}{n.Q_{HGn}}\right)^2} \quad \ldots(7)$$

$$NE = \frac{Q}{NF} \quad \ldots(8)$$

$$SD_{NEn} = NE_n.\sqrt{\left(\frac{SD_{NFn}}{NF_n}\right)^2 + \left(\frac{SD_{Qn}}{Q_n}\right)^2} \quad \ldots(9)$$

SD = Standard deviation. Ct = cycle threshold. E = amplification efficiency (2 = 100 %). S = slope of standard curve of ΔCt against log ng total RNA utilised. ΔCt = lowest Ct value minus Ct value of sample. Q = relative quantity. Ln E = natural logarithm of the amplification efficiency. NF = normalization factor based on number (n) of housekeeping genes. n = number of housekeeping genes utilised. NE = Normalized expression of target genes (MT-1B and MT-2A). HG = Housekeeping gene (Vandesompele *et al.*, 2002, Pfaffl *et al.*, 2002).

The fluorescence measured in each cycle was automatically used to calculate a cycle threshold (Ct) value, which is the number of PCR cycles after which the fluorescence signal exceeds the detection threshold value for that sample. This threshold is set to the log linear range of the amplification curve and kept constant for data analysis throughout the study. PCR efficiency (E) for each primer set was calculated by a serial dilutions method using REST software tool

(Pfaffl *et al.*, 2002)[1]. The relative expression quantities (Q) for each sample and each primer set were calculated by the comparative Ct method and gene expression was analysed using GeNorm software tool (Vandesompele *et al.*, 2002). Two housekeeping genes (GAPDH and β-2-microglobulin) were utilised for MT-2A and MT-1B expression normalization and normalization factors for each experimental set were calculated with the GeNorm software tool (see Appendix C). The equations utilised are shown in Equation 4.1.

4.1.4. CONFIRMATION OF METALLOTHIONEIN PROTEINS

In order to determine the metallothionein protein levels in the various clones a competitive solid phase ELISA assay, adapted from Butcher *et al.* (2003) was utilised[2].

4.1.4.1. Protein determination

The determination of the total protein present in the samples collected for the ELISA assay, as well as for other assays discussed in Chapter 5, was utilised to enable the comparative analyses between different samples or enzyme activities, based on the amount of total protein present in the various samples. Under alkaline conditions Cu^{2+} forms a complex with the peptide bonds of proteins and in turn is reduced to Cu^{+}. This cuprous ion together with the R groups of tyrosine, tryptophan and cystein residues then react with bicinchoninic acid (BCA), first producing an unstable product which is slowly reduced to molybdenum/tungsten blue. BCA is a highly specific chromogenic reagent with an absorbance maximum at 560 nm directly proportional to protein concentration (Smith *et al.*, 1985; Stosckeck, 1990). The assay was performed essentially as described before (Smith *et al.*, 1985) using BCA (Sigma-Aldrich), Copper (II) sulphate (pentahydrate, 4 % (w/v), Sigma-Aldrich), and protein standard (bovine serum albumin, Sigma).

[1] Amplification efficiency was executed in collaboration with O.Levanets.
[2] ELISA assay was performed in collaboration with Y. Olivier (2004).

4.1.4.2. ELISA assay

Cells were harvested as described in Section 4.1.1.2 and the pellet dissolved in 500 µl 1 % Tween 20™[1] (Merck) in PBS. The samples were stored at -70 °C until needed.

In a 96-well microtiter plate (Maxisorb NUNC-Immunoplates, NUNC), 100 µl coating buffer [4 $\mu g.ml^{-1}$ metallothionein (Sigma-Aldrich) in 0.1 M $NaHCO_3$ (F.C. Scientific c.c.), pH 9.6] was incubated overnight at 4 °C. Simultaneously, 60 µl 1:1000 diluted primary antibody (Rabbit polyclonal antibody to metallothionein, Biogenesis, in 1 % Tween 20™ in PBS), was added to each standard (160 µl of 0 – 200 $\mu g.ml^{-1}$ metallothionein). To each sample (250 $\mu g.180\mu l^{-1}$) 180 µl primary antibody was added. These standards and samples were incubated overnight at 4 °C. The plate was washed with 3 x 200 µl washing buffer [0.05 % Tween 20™ in PBS]. It was blocked with 200 µl blocking buffer [0.3 % BSA, Roche, and 0.05 % Tween 20™ in PBS] for 2 hours at room temperature with gentle shaking to prevent non-specific binding. It was then again washed with 3 x 200 µl washing buffer. Then, 100 µl of the samples and standards were added to the appropriate wells and incubated for 60 minutes at room temperature with gentle shaking. The plate was washed with 5 x 200 µl washing buffer. The addition of 100 µl detection antibody [1:5000, horseradish peroxidase - conjugated Goat anti Rabbit IgG (Zymed) in blocking buffer] and incubation for 60 minutes at room temperature with gentle shaking followed. It was again washed five times more with 200 µl washing buffer. The detection followed by the addition of 100 µl TMB substrate (Immuno Pure 3,5,3',5'-tetramethylbenzidine substrate kit, Pierce). The reaction was terminated by the addition of 100 µl 1 M HCl (Bio-Zone Chemicals, Van Riebeeck Park, RSA), which produced a yellow colour of which the absorbance was determined at 460 nm with a Uvikon XS Double beam spectrophotometer (BIO-TEK Instruments).

[1] Tween is a trademark of ICI Americas, Inc., Wilmington, D.E., U.S.A.

4.1.5. STATISTICAL ANALYSES OF RESULTS

All results were analysed with Statistica version 6[1] software. The results of the MT mRNA expression and protein levels are presented in table format, indicating the means and median respectively of the results obtained for the particular experimental parameter. The results presented in Chapter 5, regarding the functional properties of MTs, are presented in graphical format, with tables listed in the various Appendixes. Results are again indicated by the means of the results obtained for each measurement with the number of measurements indicated as *n*. The standard deviations of these values are indicated by SD. To determine whether a certain parameter showed a normal distribution the Shapiro-Wilk W test was performed. If the W statistic is significant ($p<0.05$), then the hypothesis that the respective distribution is normal should be rejected. The Shapiro-Wilk W test is the preferred test of normality because of its good power properties as compared to a wide range of alternative tests. If the distribution of the results were found to be normal, the Student t-test with independent variables was performed to ascertain the SD and *p* values. If results were found not to be distributed normally, the non-parametric comparisons of the mean ranks for multiple independent samples were performed. Statistical significance ($p<0.05$) for all the data sets are indicated throughout, as determined with one of the two above mentioned methods. Data was also analysed to identify any outliers. Outliers were regarded as atypical, infrequent observations or data points which do not appear to follow the characteristic distribution of the rest of the data and were therefore discarded.

[1] STATISTICA version 6 (2003) is a licensed program from StatSoft, Inc., Tulsa, OK, U.S.A.

4.2. RESULTS AND DISCUSSION

4.2.1. CONFIRMATION OF METALLOTHIONEIN cDNA PRESENCE IN TRANSFECTED CELLS

PCR amplification of the isolated genomic DNA with the plasmid-specific primers confirmed the presence of the MT-1B and MT-2A cDNAs (Figure 4.1 a) and b)) as determined by specific PCR product sizes. Genomic DNA from non-transfected HeLa control cells did not show any amplification and amplification of DNA isolated from pIRESneo2-transfected cells showed an expected fragment length of approximately 500 bp (theoretically 468 bp). The pIRESneo2-MT-1B clones showed a fragment between 700 and 800 bp in length (expected size 740 bp). The pIRESneo2-MT-2A clones also showed a fragment of 693 bp in length as expected (Section 3.1.7). The PCR therefore confirmed the presence of the MT-1B and MT-2A cDNAs in plasmid form in the pIRESneo2-MT-1B and pIRESneo2-MT-2A transfected cells. Southern blot analyses would have been useful to confirm whether the transfected plasmids have remained un-incorporated in the cell or have been incorporated into the nuclear DNA of clones. Unpublished observation from gels prepared for Southern blots, however, revealed patterns similar to uncut, supercoiled plasmid DNA in DNA isolated from clones. It is therefore expected that at least some of the transfected plasmids remain in an un-incorporated form in the clones.

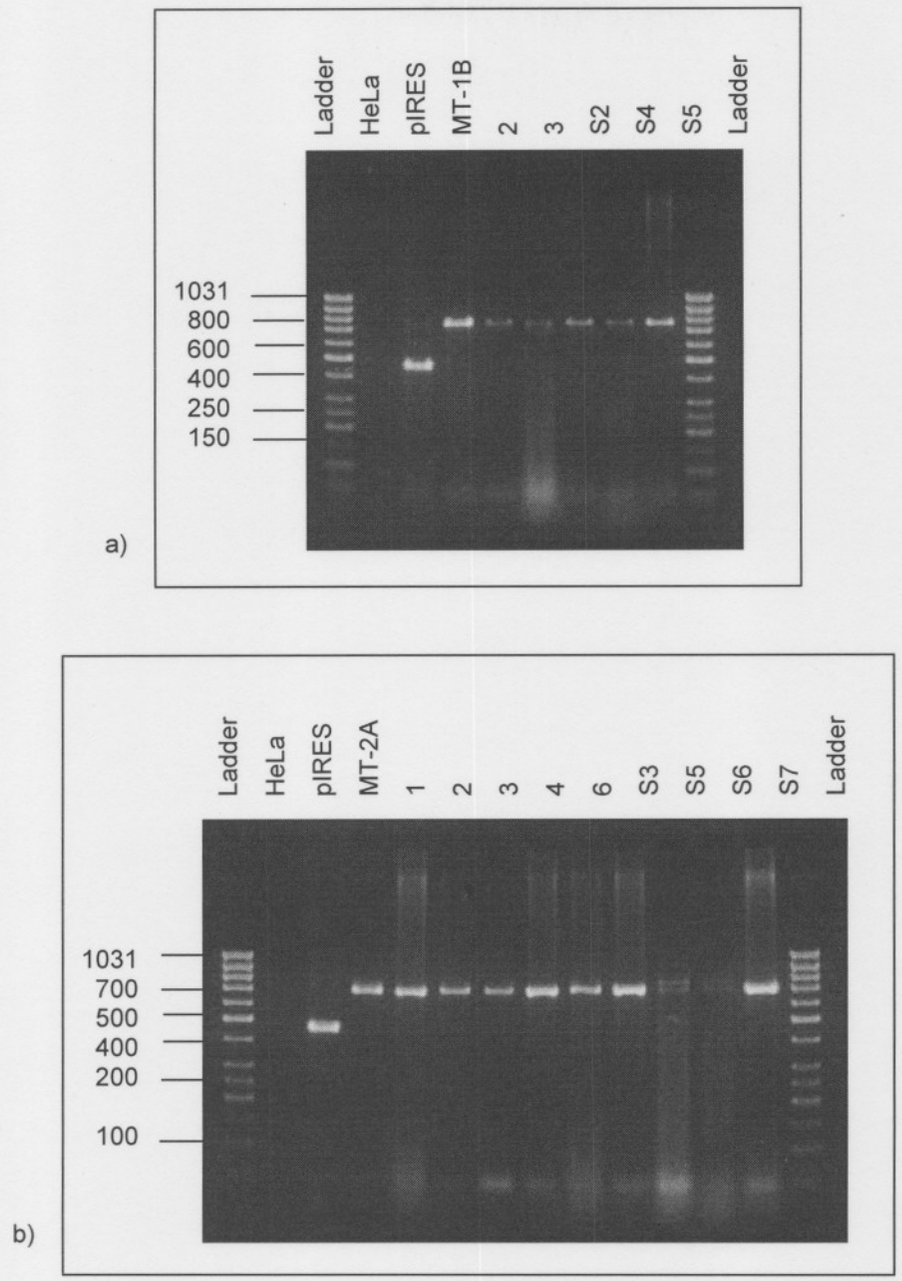

Figure 4.1. PCR products of pIRESneo2-MT-1B (a) and pIRESneo2-MT-2A (b) transfected clone pool gDNA amplified with the primer set T7/pIRES3´. Two 2% gel electrophoresed at 80 V for approximately 45 min in 1 x TAE buffer are shown. Ladder = O'GeneRuler™ 50 bp DNA ladder (Fermentas). HeLa indicates amplification products of HeLa cell gDNA. pIRES indicates gDNA of pIRESneo2 transfected cells. MT-1B and MT-2A respectively indicate the amplification products of gDNA isolated from pIRESneo2-MT-1B and -MT-2A transfected clone pools. PCR products of pIRESneo2-MT-1B (a) and pIRESneo2-MT-2A (b) transfected individual clones. Clone pools are indicated by arbitrary numbers, whilst single clones are indicated as S2, S3, etc.

4.2.2. CONFIRMATION OF METALLOTHIONEIN mRNA EXPRESSION

4.2.2.1. Northern Blotting

The first method for evaluating MT expression levels was Northern blot. The protocol is discussed in Appendix B.1. Figure B.1 shows the Northern blot result for MT-1B expression with the MT-1B specific probe. The normal expression levels of MT-1B showed a very weak signal in all of the samples (HeLa control cells, pIRESneo2, pIRESneo2-MT-1B and pIRESneo2-MT-2A). The pIRESneo2-MT-1B pool also shows the introduced MT-1B overexpression, visible as a bigger sized band (bicistronic RNA) with a much stronger signal. As can be seen in the figure the quality of the blots was very poor and even decreasing with time. Rehybridisation of the blots with MT-2A-specific probe was unsuccessful. The reason for these problems can vary from washing conditions being too stringent to a lack of sensitivity or fluorescent activity of the probes. In light of the very sensitive and accurate real-time expression analysis of the clones (discussed hereafter) and the time spent to standardise this technique, it was decided not to use northern blots for further analyses. As mentioned previously, the problems unfortunately also prohibited the use of Southern blots to determine the cDNA presence of the MTs in the clones, as it would also rely on the same detection and exposure principles.

4.2.2.2. Real-time PCR

Figure B.2 depicts an example of real-time PCR results, obtained as Ct values. The Ct values for pIRESneo2, pIRESneo2-MT-1B and pIRESneo2-MT-2A after amplification with MT-2A specific primers are listed in Table B.2. The results presented in Table 4.3 show the normalised fold change expression of MT-1B and MT-2A respectively in the pIRESneo2-MT-1B and -MT-2A transfected clone pools compared to the pIRESneo2 transfected pool. The statistical significance ($p<0.05$) according to the Student t-test compared to pIRESneo2 control cells indicate that the MT-2A expression in both the pIRESneo2-MT-1B and

pIRESneo2-MT-2A clone pools, as well as MT-1B expression in the pIRESneo2-MT-1B clone pool are significant (n=3).

Table 4.3: Normalised expression ratios for MT-1B and MT-2A in transfected cells

Clones	Expression ratio ± SD	
	MT-1B	MT-2A
pIRESneo2	1.00 ± 1.56	1.00 ± 0.28
pIRESneo2-MT-1B	133 112 ± 0.29*	1.07 ± 0.30*
pIRESneo2-MT-2A	1.20 ± 0.63	2.16 ± 0.11*

The median normalised fold change in MT expression ± SD is indicated relative to the expression of GAPDH and β-2-microglobulin housekeeping genes (data not shown). Expression ratios are indicated as the mean ± SD (n = 3). MT-1B indicates expression of MT-1B mRNA and MT-2 denotes expression of MT-2A mRNA in the various transfected clone pools. *denotes statistical significance (p<0.05) according to the Student t-test for multiple groups, compared to pIRESneo2 control cells.

It is evident that pIRESneo2-MT-1B shows a very high expression level (low Ct level) of MT-1B mRNA compared to pIRESneo2 control cells and pIRESneo2-MT-2A cells, both of which displayed very low levels of amplification. The reason for the high relative expression level of MT-1B in the pIRESneo2-MT-1B pool relative to pIRESneo2 and pIRESneo2-MT-2A can be attributed to the very low base expression level of MT-1B expression in normal HeLa cells. This data correlates with previous results published by Heguy *et al.* (1986) and coincides with results from a recent study by Olivier (2004). The overexpression of MT-1B in the pIRESneo2-MT-1B clone pool can therefore be seen clearly.

The two fold difference in normalised expression values for MT-2A expression in the pIRESneo2-MT-2A clone pool compared to pIRESneo2 and pIRESneo2-MT-1B clone pools indicate quite a big difference in the protein concentration due to existing high base-level expression of MT-2A. Even though the base-level expression of MT-2A in the control cells were relatively high compared to MT-1B

expression in the same cells, this does not necessarily indicate different levels of overexpression but only different base expression levels for these two MT isoforms. This coincides again with the findings of Heguy *et al.* (1986) and Olivier (2004) and also suggests that MT-2A is the main isoform of metallothioneins expressed in HeLa cells. This isoform also appears to be the most (or only) inducible with cadmium and ROS in HeLa cells.

4.2.3. CONFIRMATION OF METALLOTHIONEIN PROTEINS

Table 4.4 indicates the metallothionein protein levels of the various transfected clone pools as well as normal untransfected HeLa cells as determined by the ELISA assay. Metallothionein protein levels are expressed as µg metallothionein per µg total protein (n = 3). It can be seen from the table that the deviation between these three values for each cell line differs quite extensively. The assay showed poor reproducibility with the linearity of standard curves often not optimal. The standard curve utilised for these specific values included concentrations ranging from 200 – 0.195 x 10^{-3} µg MT.µg protein^{-1} and being linear only in the range of 100 - 1.53 x 10^{-3} µg MT.µg protein^{-1} (r^2 = 0.99). The assay proved to be problematic, even after extensive optimisation and modifications (Olivier, 2004).

The results indicate that the values for pIRESneo2, -MT-1B and -MT-2A all lie above the linear detection range of the method. From the data it can be observed that the MT levels are much higher in the transfected cells than in the HeLa cell line. According to these results the median of the MT levels for the pIRESneo2 and pIRESneo2-MT-2A pools are the same and pIRESneo2-MT-1B being a little lower compared to them. On the contrary, a much higher increase in MT protein levels in the pIRESneo2-MT-1B and -MT-2A transfected clone pools was expected. It can be expected that MT levels in pIRESneo2 pools might be higher than that of normal HeLa cells as these cells are under more stress of constant transcription and translation of the bicistronic mRNA of the plasmid. Even so, the MT levels of the pIRESneo2-MT-1B and pIRESneo2-MT-

2A pools were expected to be much higher than that of the pIRESneo2 pool. It is possible to explain the lower protein level in the pIRESneo2-MT-1B pool with a previous report (Haq *et al.*, 2003). The report suggests that even though the majority of evidence indicate that MT expression is transcriptionally regulated, some evidence indicate that post-transcriptional events, of unknown nature that modulate MT mRNAs, are also important in MT gene expression.

However, from the detection limit of the assay together with the poor reproducibility of the assay the only conclusion that can be drawn from the data is that it is not accurate and cannot be relied upon. Taking into account the real-time PCR results together with the confirmation of the presence of the cDNA sequences in plasmid form, it can be suggested that MT-1B and MT-2A has been successfully overexpressed in the cells, even though the ELISA results were, unfortunately, not in agreement with these results.

Table 4.4: Metallothionein protein levels in transfected clone pools

Clones	µg MT/µg protein	Median
HeLa cells	0	0.023
	0.023	
	0.055	
pIRESneo2	0.185	0.288
	0.288	
	0.476	
pIRESneo2-MT-1B	0.254	0.254
	0.270	
	0.022	
pIRESneo2-MT-2A	0.419	0.288
	0.288	
	0.004	

4.3. SUMMARY

In this chapter the transfection and analysis of HeLa cells with the expression vectors for MT-1B and MT-2A is described. Selection of the cells was carried out on a combined pool of clones as well as on single clones for each of the different transfectants (pIRESneo2, pIRESneo2-MT-1B and pIRESneo2-MT-2A). PCR analyses of these clones and clone pools confirmed the presence of the pIRESneo2 and respective MT-containing pIRESneo2 expression vectors in plasmid form. From the real-time PCR it can be concluded that a high level of overexpression for MT-1B is present in the pIRESneo2-MT-1B clone pool. The pIRESneo2-MT-2A clone pool showed some degree of MT-2A overexpression but not nearly that of MT-1B overexpression in the pIRESneo2-MT-1B pool. This can be explained in terms of the high base expression level of MT-2A expression in normal HeLa cells compared to the base expression level of MT-1B. Metallothionein protein levels could not be accurately detected with the ELISA method and did not verify the overexpression in the transfectant clone pools. However the protocol for this assay was problematic even after extensive optimisation. Hence, in light of the RNA expression results it was assumed that the respective overexpression of MT-1B and MT-2A in HeLa cells had been achieved successfully.

CHAPTER FIVE

INVESTIGATION OF SELECTED FUNCTIONAL PROPERTIES OF METALLOTHIONEINS OVEREXPRESSING HeLa CELLS

5.1. MATERIALS AND METHODS

To determine the contribution of MT overexpression in HeLa cells, selected biochemical parameters relating to a deficiency in complex I were measured as described in this chapter. As indicated in Chapter 2, this included the measurement of ROS production, caspase activity and mitochondrial membrane potential. In addition, cell viability was also measured. All analyses were carried out on the pIRESneo2, pIRESneo2-MT-1B and pIRESneo2-MT-2A clone pools together with normal HeLa cells. The protocols followed in this study were performed according to the specifications included with the respective kits utilised or according to published protocols. Modifications to these protocols are indicated throughout. Statistical analyses for all the assays, except confocal microscopy, were carried out as described in Section 4.1.5. As some assays of rotenone-treated cells coincided with a study that ran parallel to this one (Olivier, 2004) and because a comparison of the data between these two studies was essential, some of these assays were performed together (complex I activity and confocal microscopy) as will be clear from the results.

5.1.1. ROTENONE AND *t*-BHP TITRATIONS

Complex I deficiency was induced by means of 24 hour incubations with rotenone (Sigma-Aldrich) in such a way that several final concentrations of rotenone in equal quantities dissolved in EtOH were added to equal amounts of media. In this way final concentrations of 0, 10, 100, 500, 1000 and 2500 nM rotenone were incubated with HeLa cells. Positive controls for ROS induction were *t*-butylhydroperoxide (*t*-BHP, Sigma-Aldrich), at 0.5, 0.8, 1.0 and 1.5 mM

incubated for 3 hours. These *t*-BHP incubations were also included in the MTT assay.

5.1.2. CELL HARVESTING AND COUNTING

A 25 cm^2 flask with approximately 100% cell confluency was trypsinised, washed and collected as described in Section 4.1.1.2. The cell pellet was resuspended in 500 µl 1 x PBS and transferred to a micro-centrifuge tube. Trypan Blue dye exclusion was used to count viable cells. The principle is that live viable cells do not take up Trypan Blue, whereas non-viable (dead) cells do. Each square of the hemacytometer, with cover-slip in place, represents a total volume of 10^{-4} cm^3. Since 1 cm^3 is equivalent to approximately 1 ml, the subsequent cell concentration per ml will be determined using the calculations represented in Equation 5.1.

Equation 5.1: Counting of viable cells

Cells/ml	=	average count per square x dilution factor x 10^4
Total cells	=	cells/ml x original volume of fluid from which cell sample was removed.

This was done by adding 100 µl of a cell suspension to 250 µl of 0.4 % (w/v) Trypan Blue solution (BioWhittaker™) and 150 µl 1 x PBS. It was incubated at room temperature for 5-10 minutes. With the cover-slip in place, approximately 7.5 µl of a cell suspension was pipetted into the side of the cover-slip placed over the hemacytometer which allows the fluid to fill the chamber by capillary force. The cells in the 1 mm centre square were counted together with four corner squares. Non-viable cells stained blue and was not counted. The cell on top and left touching the middle lines of the perimeter of each square were counted. There were seldom any non-viable cells before incubations and the percentage viability was therefore not really a factor when seeding cells. Although data of subsequent assays were normalised to protein content, the number of cells in

assays proved to be crucial in the sensitivity and reproducibility of assays such as ROS detection and MTT tests.

5.1.3. SELECTED RESPIRATORY CHAIN ENZYME ASSAYS

The NADH:ubiquinone oxidoreductase (complex I) activity was determined both directly and via the measurement of complex I and III activity together, taking into account the activity of complex III alone. The principles and protocols of these important measurements are discussed in the following sections. OXPHOS activity is indicated in reference to citrate synthase activity (discussed in Section 5.1.4) and total protein content (as discussed in Section 4.1.4.1). All OXPHOS assays were performed on a Uvikon XS Double beam spectrophotometer (BIO-TEK Instruments). OXPHOS analyses were conducted on normal HeLa cells.

5.1.3.1. Preparation of enriched mitochondrial fraction

The normal HeLa cells collected after rotenone titrations were carried out, as described in Sections 5.1.1, were resuspended in 3 ml ice-cold SET buffer [0.25 M sucrose (Sigma-Aldrich), 2 mM EDTA (ethylenediamine-tetra-acetic acid dipotassium salt, Fluka), 10 mM Tris® (Roche), pH 7.4] and transferred to a glass homogeniser (Potter Eveljam tissue grinder). The cells were disrupted with 15 strokes of the motor driven plunger, keeping the homogenizer in ice. The homogenate was centrifuged for 10 minutes at 600 x g and 4 °C. The supernatant was retained on ice and centrifuged for 10 minutes at 10 000 x g and 4 °C. The pellet was resuspended in 100 µl SET buffer, collected in a microcentrifuge tube and centrifuged for 10 minutes at 10 000 x g and 4 °C. 0.5 ml Hypotonic [25 mM potassium phosphate consisting of KH_2PO_4 (Merck) and K_2HPO_4 (Sigma-Aldrich), pH 7.2, 5 mM $MgCl_2$ (Saarchem)] buffer was added and centrifuged at 600 x g and 4 °C for 2 minutes. The pellet was then resuspended in 100 µl hypotonic buffer and stored at -70 °C. The mitochondrial preparation was thawed on ice three times before all enzyme assays were carried out.

5.1.3.2. NADH:ubiquinone oxidoreductase (Complex I) activity

Complex I (NADH:ubiquinone oxidoreductase) activity can be measured with the rotenone-sensitive NADH oxidation in the presence of antimycin A and potassium cyanide. The NADH oxidation allows the electrons to be transferred to coenzyme Q1. The addition of antimycin A and KCN prevents the transfer of the electrons to complexes III and IV. Two identical samples are measured simultaneously; one for the measurement of the rotenone-sensitive complex I activity (A1) and one to which rotenone is added to measure all rotenone-insensitive NADH oxidation (A2). The NADH oxidation rate was calculated from the slope of absorbance decrease over time using an extinction coefficient for NADH of 6.81 mM^{-1} cm^{-1} at 340 nm, taking into account the contribution of CoQ-1 reduction to the absorption (Ragan *et al.*, 1987) as indicated in Equation 5.3 (Rahman *et al.*, 1996). The complex I activity was calculated taking into account the protein content and citrate synthase activity as indicated in Equations 5.2 and 5.3.

The reaction was started by mixing 482.5 µl water with 10 µl mitochondrial preparation (as prepared in Section 5.1.3.1) for each sample and placed in a 1 ml cuvette. The mixture was incubated for 3 minutes and the spectrophotometer blanked. Next, 2.5 µl 10 mM coenzyme Q1 (in EtOH, Sigma-Aldrich) was added to each sample. For the sample (A1), 5 µl 100 % EtOH was added. For the rotenone sample (A2), 5 µl 0.75 mM rotenone (Sigma-Aldrich) was added. Then 87.5 µl assay reagent was added to each sample. The assay reagent contained the following: 50 µl 0.5 M KPi (19 ml 0.5 M KH_2PO_4 (Merck) and 81 ml 0.5 M K_2HPO_4 (Sigma-Aldrich), pH 7.4), 12.5 µl 5 mM NADH (Roche, Grade I, 100 %), 10 µl 50 mM KCN (potassium cyanide, BDH, in 100 mM KPi, pH 7), 10 µl 0.5 mM antimycin A (in EtOH, Sigma-Aldrich) and 5 µl 10 % BSA (Bovine serum albumin, fraction V; fatty acid free; Boehringer Mannheim). NADH oxidation were measured at 340 nm for 10 minutes or until the linearity of the decrease in absorbance decreased (Rahman *et al.*, 1996).

Equation 5.2: Calculation of Complex I activity

CI Activity = [(A1-A2)/6.81] / [(v / 1000 x mg protein) x V] = µmole / min / mg

A1 = difference in absorbance in sample without rotenone. A2 = difference in absorbance in sample with rotenone. 6.81 $mM^{-1}.cm^{-1}$ = extinction coefficient for NADH, taking into account the contribuition of CoQ-1 reduction. v = volume of sample preparation added. V = total reaction volume.

Equation 5.3: Calculation of Complex I activity per citrate synthase activity

CI activity per UCS = CI activity*/citrate synthase activity
= µmole / min / UCS

UCS = units citrate synthase activity. *expressed as µmole.min^{-1}.mg^{-1} total protein.

5.1.3.3. Ubiquinol:ferricytochrome c oxidoreductase (Complex III) activity

Complex III was assayed by the rate of reduction of cytochrome *c* by decylbenzylquinol (Rahman *et al.*, 1996). The reaction mixture consisted of 90 µl assay reagent [50 µl 0.5 M KPi (pH 7.4), 20 µl 25 mM n-dodecylmaltoside (Boehringer Mannheim), 10 µl 50 mM KCN, 5 µl 10 % BSA and 5 µl 0.25 mM rotenone] and MilliQ water (to have a final reaction volume of 500 µl) in a 1 ml cuvette. The cuvette was left in the cell changer for 5 to 10 minutes to allow temperature to equilibrate to 30 °C, after which 10 µl mitochondrial pellet (as prepared in Section 5.1.3.1) was added. Subsequently, 5 µl reduced decylbenzylquinol was added. The reaction was then started by the addition of 4 µl 2 mM cytochrome *c* (Sigma-Aldrich, horse heart, type VI). The linear increase in absorbance at 550 nm was measured for 10 minutes (A1). A duplicate sample containing water instead of sample was utilised as blank (A2). The complex III activity was calculated as indicated by Equations 5.3 and 5.4.

Equation 5.4: Calculation of complex III and I+III activities

Activity = [(A1-A2)/29.5] / [(v / 1000 x mg protein)] x V = µmole/min/mg

A1 = difference in absorbance in sample without rotenone. A2 = difference in absorbance in sample with rotenone. 29.5 $mM^{-1}.cm^{-1}$ = extinction coefficient for cytochrome c. v = volume of sample preparation added. V = total reaction volume.

5.1.3.4. Complex I and III activity

The measurement of the combined activity of complexes I+III can be measured by the rotenone-sensitive reduction of cytochrome *c* (Rustin, *et al.*, 1994). For this assay, the blank, consisting of 10 µl mitochondrial preparation (as prepared in Section 5.1.3.1) and MilliQ water (to have a final reaction volume of 500 µl) in a 1 ml cuvette, was incubated at 37 °C for 3 minutes. Subsequently 100 µl Medium F [50 mM Tris®-HCl, 5 $mg.ml^{-1}$ BSA], 40 µM oxidized cytochrome *c* and 0.8 mM NADH was added and the linear increase in rotenone-sensitive cytochrome C reduction was measured for 2 minutes at 550 nm (A1). The rotenone-insensitive reduction was then measured for 2 minutes (A2) after the addition of 3 µM. The combined activity of complexes I and III was calculated as indicated in Equation 5.3 and 5.4.

5.1.4. CITRATE SYNTHASE ACTIVITY

Due to the complex nature of respiratory chain deficiencies, it is necessary to measure the activity of at least one mitochondrial enzyme not involved in this chain (reference enzyme) such as citrate synthase. This distinguishes between a low number of mitochondria, thus general low activity in the sample, or a specific deficient OXPHOS enzyme activity (Ruitenbeek *et al.*, 1989). Citrate synthase is located in the matrix of the mitochondria and catalyzes the reaction by which acetyl-CoA (acetyl-coenzyme A) condenses with oxaloacetate to form citrate that enters the Krebs cycle. The CoA, containing a sulhydryl group, reacts with DTNB

(Ellman's reagent) to produce a yellow complex that can be measured at 412 nm. The activity can then be calculated as shown in Equation 5.5 (Bergmeyer, 1981; Robinson *et al.*, 1987). The protein content was determined as described in Section 4.1.4.1 with a 10 x dilution of the mitochondrial preparation.

The mitochondrial preparation was thawed on ice. Meanwhile, the following was mixed and placed in a 1 ml glass cuvette at 30 °C: 413 µl water, 50 µl DTNB [5,5'-dithiobis-(2-nitrobenzoic acid), Boehringer Mannheim GmbH, 0.4 $mg.ml^{-1}$ in 1 M Tris®-HCl (Roche), pH 8, freshly prepared], 2 µl Triton® X100 [10 % in water, prepared fresh, BDH], 5 µl acetyl-CoA [6 mM in water, Roche] and 5 µl mitochondrial preparation. The difference in absorbance at 412 nm was measured for 2 minutes (A1). Freshly prepared 25 µl oxaloacetate (1.32 $mg.ml^{-1}$ in water, Boehringer Mannheim GmbH) was added and the absorbance at 412 nm was recorded for 3 minutes (A2). A Uvikon XS Double beam spectrophotometer (BIO-TEK Instruments) was used. The protein concentration was determined as described in Section 4.1.4.1 with a 10 x dilution of the mitochondrial preparation.

Equation 5.5: Calculation of citrate synthase activity

$$\frac{(A1 - A2)}{13.6} \times V / (\text{mg protein} \times v) \times 1000 = \mu\text{mole/min/mg activity}$$

A1 = linear increase in absorbance at 412 nm before addition of oxaloacetate. A2 = linear increase in absorbance at 412 nm after addition of oxaloacetate. V= total volume (µl) in cuvette. v = volume (µl) mitochondrial preparation. Extinction coefficient of TNB = 13.6 $mM^{-1}.cm^{-1}$. Note that µmoles/min/mg is also expressed as units CS (UCS) per mg.

5.1.5. CELL VIABILITY ASSAY (MTT TEST)

The utilisation of a tetrazolium salt in a quantitative colorimetric assay for cell survival and proliferation was first described by Mosmann in 1983. MTT (3-(4,5-Dimethylthiazol-2-yl)-2,5-diphenyltetrazolium bromide) is reduced by active mitochondria to form a blue formazan product and can therefore be used to

measure cytotoxicity, proliferation or activation as mitochondrial reducing activity. Berridge and Tan (1993) found that malate, glutamate and succinate, but also NADH and NADPH were substrates in supporting MTT reduction by subcellular components. Liu and coworkers (1997) also suggested MTT reduction can also occur outside the mitochondria and instead that it is taken up by cells through endocytosis and reduced by an N-ethylmaleimide-sensitive flavin oxidase.

The absorbancies of the samples were measured at 560 (formazan) and 645 nm (background). The difference in absorbance values were used to determine the percentage cell viability relative to the blank samples, taking into account the protein content of these samples. The harvested cells were counted (Section 5.1.2), seeded into 96-well plates at 25 000 cells per well (final volume of 100 µl media per well as described in Section 4.1.1.2) and incubated overnight in order for the cells to adhere. On the next day, rotenone incubations were started as described in Section 5.1.1. After 21 hours the *t*-BHP incubations were started. 30 minutes before the end of the incubations of the positive control (6% acetic acid, Saarchem[1]) was added to the appropriate wells. The plate was then centrifuged for 5 minutes at 1 000 x g. The supernatant was discarded and the wells washed by the addition of 200 µl 1 x PBS and repeating the centrifugation step. The supernatant was removed and 20 µl 5 mg/ml MTT (Sigma-Aldrich) in PBS was added to each well. The cells were then incubated for 5 hours at 37 °C. To each well 100µl DMSO (Dimethyl sulphoxide, Saarchem) was added and the absorbance measured at 560 and 630 nm with a BioTek fluorescence (FL 600) plate reader.

The protein determinations of these samples were done on an extra duplicate set of samples treated exactly as the MTT-samples but without the addition of MTT and the protein concentration determined as discussed in Section 4.1.4.1.

[1] Saarchem (PTY) Ltd. is a company of Merck, JHB, South Africa.

5.1.6. ROS LEVELS AND MEMBRANE POTENTIAL

Intracellular accumulation of ROS was measured fluorometrically and studied with confocal microscopy. The nonfluorescent dye 2',7'-dichlorofluorescin diacetate (DCFDA) is freely permeable to cells. DCFDA is hydrolyzed to 2',7'-dichlorofluorescin (DCF) inside the cells by intracellular esterases. Oxidation of the reduced dyes can then occur in the presence of ROS, especially hydroxyl radicals, to produce a green fluorescent DCF (Zhang *et al.*, 2000). High levels of ROS can lead to the decreased membrane potential and formation of mtPTPs that can be visualised with confocal microscopy. The fluorometric quantification of this ROS production is described in Section 5.1.6.1 and the visualisation of ROS and membrane potential with confocal microscopy in Section 5.1.6.2.

5.1.6.1. Fluorometric quantification of ROS levels

The harvested cells were counted (Section 5.1.3) and seeded into 96-well plates with 25 000 cells per well (final volume of 100 µl) and incubated overnight in order for the cells to adhere. On the next day, rotenone incubations were executed as described in Section 5.1.1. After 21 hours the *t*-BHP incubations were started. After the elapsed 24 hour incubation time DCFDA [Sigma-Aldrich, in DMSO (Sigma-Aldrich) stored at -70 °C], prepared in media, was added to each of the wells to a final concentration of 10 µM. The plate was incubated for 30 minutes at 37 °C and washed with 200 µl 1 x PBS. The PBS was removed and a final 100 µl 1 x PBS added to each well. The excitation was set at 485 nm and emission was read at 530 nm with a BioTek fluorescence (FL 600) plate reader.

5.1.6.2. Confocal microscopy

To examine the ROS production in or near the mitochondria, a mitochondrial stain called MitoTracker®[1] CM-H_2XROS red was co-incubated with the DCFDA probe. The MitoTracker® probe contains a mildly thiol-reactive chloromethyl moiety that keeps the dye associated with active mitochondria after passively diffusing across the plasma membrane. The reduced probes are nonfluorescent until they enter the lipid environment of the functional mitochondria.

Opening of the mtPTP, which may occur as a result of high ROS levels, causes depolarisation of the membrane or collapse of mitochondrial membrane potential which subsequently leads to a reduction in fluorescence (Crompton, 1999). To visualise mitochondrial membrane potential tetramethylrhodamine methylester (TMRM), a membrane permeant cationic fluorophore was used. It loads into polarized mitochondria electrophoretically due to the negative membrane potential of the mitochondria.

5.1.6.2.1. Visualisation of ROS production

The harvested cells were counted (Section 5.1.3), seeded in 6-well plates with 200 000 cells per well (final volume of 2 ml media per well) and incubated overnight in order for the cells to adhere. Each well contained a glass cover slip (Menzel-Glaser, 31 mm, #1) onto which the cells attached. On the next day, 0, 100 and 1000 nM rotenone incubations were started as described in Section 5.1.1. After the elapsed incubation time, DCFDA (final concentration 5 µM) together with MitoTracker® CM-H_2XROS (final concentration 1 µM, Molecular Probes[2]) was added to the wells and incubated at 37 °C for 30 minutes. The cells were washed four times with 2 ml culture media and the cover slips placed into a specially designed chamber. The Nikon (pcm 2000) inverted confocal microscope with a krypton-argon-helium neon laser was utilised to study the

[1] MitoTracker® is a registered trademark of Molecular Probes, Inc., Leiden, The Netherlands.
[2] Molecular probes, Inc., Eugene, OR, U.S.A.

cells. The green emission was set at 505 nm and the red emission at 565 nm. The pinhole was set at 0.5 µM. The laser gain was set at 1.6 for the green DCFDA probe and at 2.7 for the red MitoTracker® probe.

5.1.6.2.2. Visualisation of membrane potential

Cells were prepared and incubated in the same way as described in the previous section. After the elapsed incubation time, TMRM (tetramethylrhodamine, methyl ester, Molecular probes) to 0.5 µM final concentration were incubated at 37 °C for 30 minutes. The cells were washed and viewed as described in the previous section. The pinhole was set at 0.5 µM, the laser gain was set at 1.7 for the green MitoTracker® probe and at 2.1 for the red TMRM probe. The laser gain was set at 2.1 for the red TMRM probe and the neutral density filter set at 10 %.

5.1.7. CASPASE 3/7 ACTIVITY

The measurement of the cysteine aspartic acid-specific protease or caspases 3 and 7 was performed with the use of the Apo-ONE®[1] Homogeneous Caspase-3/7 Assay kit (Promega). The assay is based on cleavage of the pro-fluorescent caspase-3/7 substrate rhodamine 110, bis-(N-CBZ-L-aspartyl-L-glutamyl-L-valyl-L-aspartic acid amide) (Z-DEVD-R110). The removal of the Asp-Glu-Val-Asp peptides by capase-3/7 activity, and excitation at 499 nm, causes the intense fluorescence of the rhodamine 110 leaving group with a maximum emission at 521 nm.

The harvested cells were counted (Section 5.1.2), seeded into 96-well plates with 25 000 cells per well (final volume of 100 µl) and incubated overnight in order for the cells to adhere. On the next day, rotenone titrations on the various cell lines were carried out as discussed in Section 5.1.1. The positive control cells were

[1] Apo-ONE is a registered trademark of Promega Corporation, Madison, WI, U.S.A.

incubated with 1 $\mu g.ml^{-1}$ staurosporine (Sigma-Aldrich) in the media for the final 2 hours. Subsequently the Apo-ONE® Homogeneous Caspase-3/3 Assay kit was utilised according to the manufacturer's specifications. Measurements were recorded every 30 minutes for at least 3 hours with a BioTek fluorescence (FL 600) plate reader.

5.2. RESULTS AND DISCUSSION

5.2.1. RESPIRATORY CHAIN ENZYME ANALYSES

5.2.1.1. Complex I activity

The results generated for the rotenone-sensitive measurement of complex I (NADH:ubiquinone oxidoreductase) activity in HeLa cells can be seen in Table 5.1. Activity is indicated as a percentage relative to the control group (0 nM rotenone treated HeLa cells). Even though a decrease in activity with increasing rotenone administration can be seen, SD are very high and the percentage activity for the 1000 nM treated cells are much higher for the control group.

This was not expected, especially in the light of the irreversible binding of rotenone to complex I, and does not correlate with the results of combined complex I+III activity discussed hereafter. The method showed poor reproducibility, giving different results with the same mitochondrial preparations. The most problematic however, was the relatively high rotenone-insensitive NADH oxidation compared to the rotenone-sensitive oxidation. This problem is not uncommon and has been described previously by Chretien and co-workers (2003) to be mainly due to contaminating non-mitochondrial NADH:ubiquinone oxidoreductase activity of up to 90 % in cultured skin fibroblasts. They proposed the permeabilisation of plasma membranes without affecting mitochondrial membranes by the addition of digitonin and Percoll. Unfortunately, this preparative method proved even more unsuccessful compared to mitochondrial isolation as utilised in this study.

Since this assay has previously been performed successfully on fibroblasts in the same laboratory, we therefore conclude that this method is not applicable to HeLa cells in particular. Therefore further investigations into complex I activity via the combined complex I+III activity had to be carried out as described in Section 5.2.1.2.

Table 5.1: Rotenone-sensitive NADH:ubiquinone oxidoreductase activity in HeLa cells after rotenone titrations

Rotenone (nM)	Mean ± SD(µmole/min/UCS)	% activity	*p*
0	478 ± 198	100.0	-
10	341 ± 286	71.46	0.53
100	287 ± 384	60.15	0.49
1 000	1119 ± 982	234.3	0.33
2 500	-611 ± 691	0.00	0.06

Activities are expressed as a percentage relative to 0 nM rotenone treated cells (control). Statistical significant difference ($p < 0.05$ being significant) in mean values ± SD ($n = 3$) compared to the control cells is indicated as determined with the Student t-test for independent groups.

5.2.1.2. Combined complex I+III and complex III activity

Figure 5.1 depicts the activities of combined complex I+III and complex III activity in HeLa cells, respectively. The activities are indicated as a percentage, relative to the control group (0 nM rotenone treated cells). The figure shows the percentage rotenone-insensitive complex III activity that was unaffected, relative to the rotenone-sensitive combined complex I+III activity decreasing with an increase in rotenone dosage. Mean values ± SD ($n = 2$) for the combined complex I+III activity showed statistical significance ($p < 0.05$) for all the rotenone concentrations relative to the control group as determined with the Student t-test. According to the results, even a low concentration of 10 nM rotenone can reduce complex I activity to less than 50 % after only 24 hours. This data corresponds to previous studies on fibroblast cultures (Koopman, 2004). It can therefore be assumed that the titration concentrations utilised (0 to 2500 nM) successfully resulted in increased complex I deficiency and could be utilised to create an *in vitro* model of complex I (NADH:ubiquinone oxidoreductase) deficiency with various levels of deficiency. This model could then be utilised to investigate the

possible protective role of MTs using various parameters regarding ROS and apoptosis.

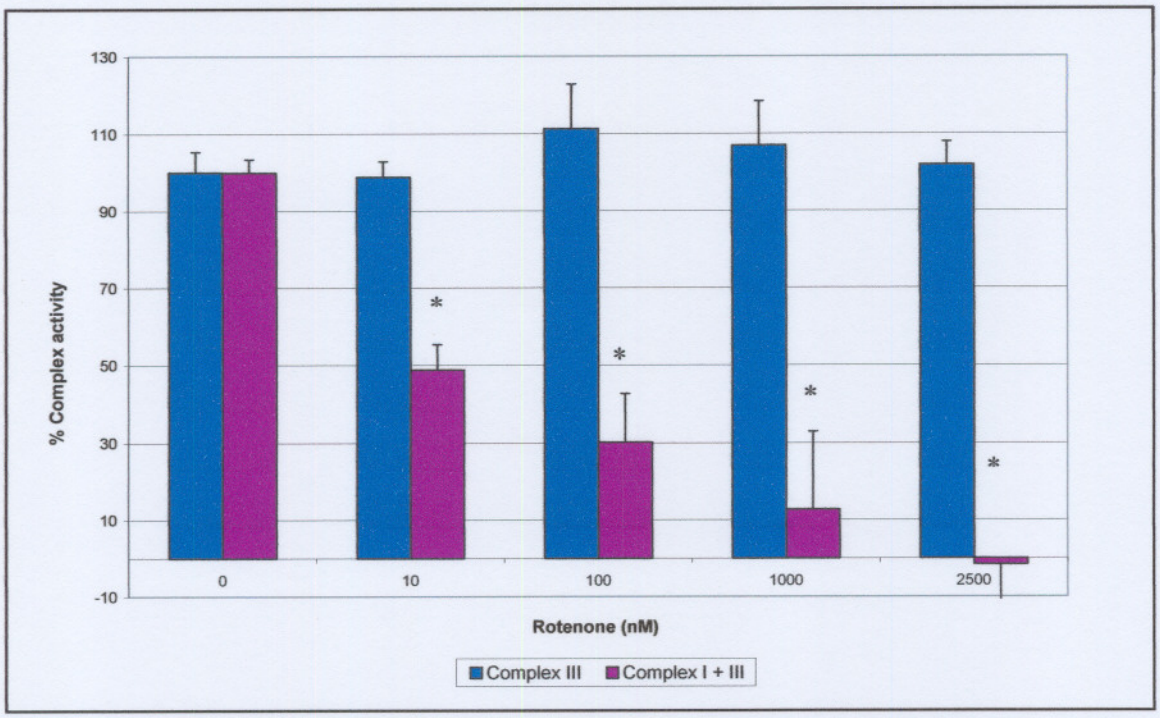

Figure 5.1. Complex I+III activities and complex III activities in HeLa cells incubated with rotenone. Combined complex I+III activities (blue) are rotenone-sensitive, whilst complex III (purple) activities are rotenone-insensitive. Activities are expressed as a percentage relative to control cells treated with 0 nM rotenone. Asterisks (*) signify mean values ± SD (n = 2) which were statistically significantly different from the control group as determined with the Student t-test ($p < 0.05$) for independent groups.

5.2.2. Cell viability

The cell viability as determined with the MTT assay is illustrated in Figure 5.2 for both rotenone and *t*-BHP titrations. Results are indicated as % cell viability compared to that of the 0 nM rotenone-treated cells. In this, as well as all further comparisons between cell lines, the base vector (pIRESneo2)-transfected cells were regarded as the correct control line to compare the effect of MT-1B and MT-2A overexpression as it is the cell line that has one variable difference compared to the test cell lines. According to the Shapiro-Wilk W test all the data sets had a normal distribution, therefore a Student t-test for multiple independent groups

was performed to determine which mean ± SD (n = 3) values are statistically significant (p<0.05) relative to the control group for each cell line. All four cell lines (HeLa cells together with pIRESneo2-, pIRESneo2-MT-1B- and pIRESneo2-MT-2A transfected clone pools) showed a decrease in cell viability with an increase in rotenone or *t*-BHP concentrations. Even though the viability of the pIRESneo2 transfected cells is higher than anticipated, statistical analysis shows no outliers with most values being significant, even for the other cell lines.

Two different positive controls were originally considered for this assay. The first, Triton X100®, could not be utilised because it loosened the cells from the wells. This caused erroneous results as all the cells were washed away before detection. The second positive control, glacial acetic acid, produced good toxicity results without loosening the cells. It can be seen from the figure that untransfected HeLa cells have superior cell viability compared to all transfected clone pools. MT-1B overexpression did not show any increased cell viability compared to the HeLa cells or the pIRESneo2 transfected clone pool. The pIRESneo2-MT-2A transfected pools, however, showed a clear tendency towards enhanced cell viability compared to the pIRESneo2 transfected pool and even the pIRESneo2-MT-1B transfected clone pool. This tendency can be observed even more clearly with the *t*-BHP treated cells in which the MT-2 overexpression shows twice the cell viability of that of pIRESneo2 overexpression. It is clear from the results that the rotenone treated cells did not show as much a decrease in cell viability as expected.

This may be due to the fact that, in a state of reduced ATP generation as observed following rotenone treatment, apoptosis may proceed until cellular ATP stores are depleted or reduced to a point where cell death becomes necrotic rather, or in addition to, apoptotic (Isenberg & Klaunig, 2000). It is possible that this state of necrosis has not been reached yet in these cells, as cell viability only decreased to about 70% and the MTT assay is sensitive to necrosis rather than apoptosis. According to Kweon *et al.* (2004) and Long *et al.* (2004), *t*-BHP treatment causes extensive ROS production and concomitant loss of most intracellular lactate dehydrogenase (LDH) indicating loss of membrane integrity

and therefore causing necrotic cell death rather than apoptosis. Due to the fact that the MTT assay is known for measuring necrosis rather than apoptosis, the results therefore suggest that MT-2A overexpression could have a protective effect against putatively ROS-induced necrosis in complex I deficient cell lines. The protection against (ROS-induced) cell damage induced by *t*-BHP clearly underlines this property in this particular analysis.

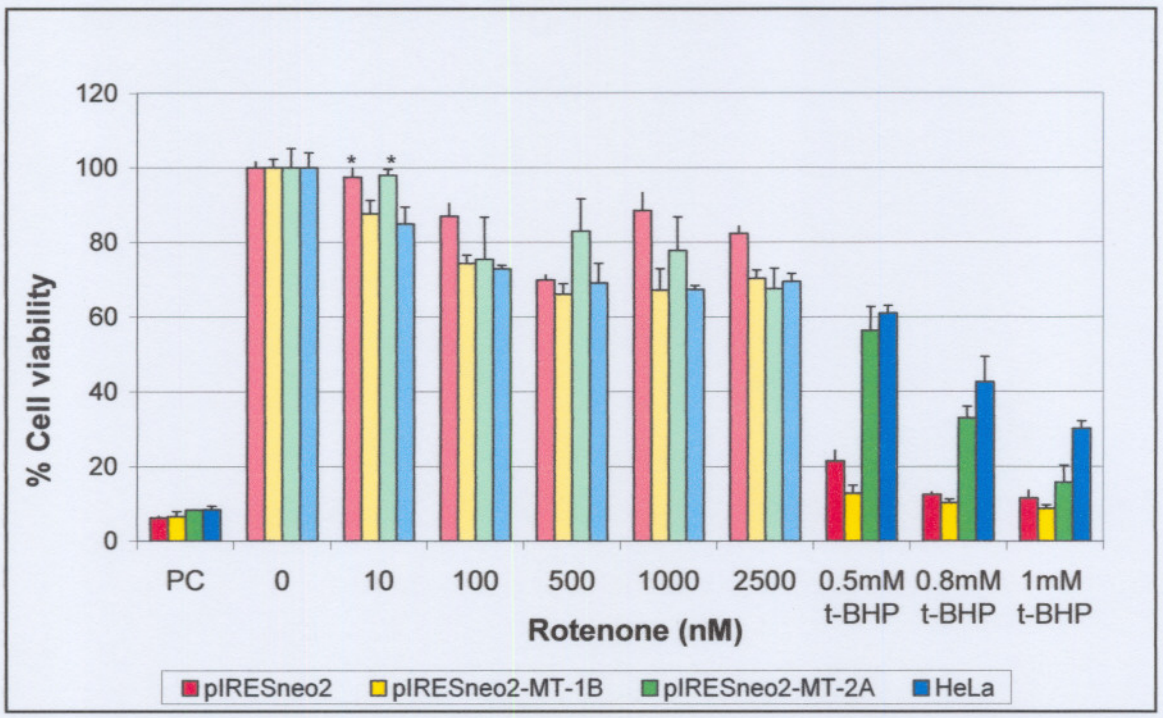

Figure 5.2. Effect of rotenone and *t*-BHP on cell viability in HeLa cells and transfected clone pools. The percentage cell viability of the various cell clones after incubations with rotenone and *t*-BHP were assessed with the MTT assay. Results are expressed relative to the 0 nM rotenone treated cells. HeLa cells (blue), together with pIRESneo2 transfected cells (red) acted as negative controls. The pIRESneo2-MT-1B transfected cells and pIRESneo2-MT-2A transfected cells are respectively indicated in yellow and green. The positive control (PC) was treated with 6 % acetic acid. Asterisks (*) signify mean values ± SD (n = 3) not significant, with all other values statistically significantly different from the 0 nM groups as determined with the Student t-test ($p < 0.05$) for independent groups.

5.2.3. ROS PRODUCTION

5.2.3.1. Fluorometric quantification of ROS levels

Figure 5.3 shows ROS production with increase in rotenone treatment in HeLa cells, pIRESneo2, pIRESneo2-MT-1B and pIRESneo2-MT-2A transfected clone pools. It indicates the relative fluorescence units per µg total protein against the rotenone, as well as *t*-BHP concentrations which acted as positive controls. What is clear from the figure is that the production of ROS increases with an increase in rotenone concentration. According to the Shapiro-Wilk W test the distribution of the data sets were normal, therefore a Student t-test for multiple independent groups was performed for each cell line. This indicated that most mean values ± SD (n = 8) values are statistically significant ($p<0.05$) relative to the control group (0 nM rotenone treatment) for each different cell line with no outliers. However, the assay showed poor inter-assay reproducibility as it was repeated several time with results varying to such an extent that differences between the cell lines were not always the similar. Nevertheless, there was a tendency towards increasing ROS production with increase in rotenone concentration. The values for the positive control did not always show a linear increase in ROS production (data not shown). It is also not expected for HeLa cells to show more ROS production that the pIRESneo2 transfected clone pool (as can be seen in Figure 5.6), due to its constant transcriptional and translational stress to produce the recombinant proteins. This, however, was not the case in previous analyses.

Two critical factors have been identified for this method. Firstly, too little cells do not show accurate results, due to the plate reader only measuring fluorescence over a few millimetres in diameter in the middle bottom part of the well. If cells are not present at that particular site, inaccurate results are received. In addition, too many cells also showed a protective effect on each other, making clumps due to overgrowing, causing the probe to accumulate unspecifically as revealed by confocal microscopy. Due to different growth rate in the different cell pools, some cell populations will be denser than others, and lower levels of ROS can be

found due to this protective effect. The second problem was identified with the experiments carried out with confocal microscopy. It sometimes identified some DCFDA crystal formations in the samples. If such crystals would be present in the wells, this automatically reduces the surrounding DCFDA concentration in the wells, having lower efficiency of probe binding to the ROS present.

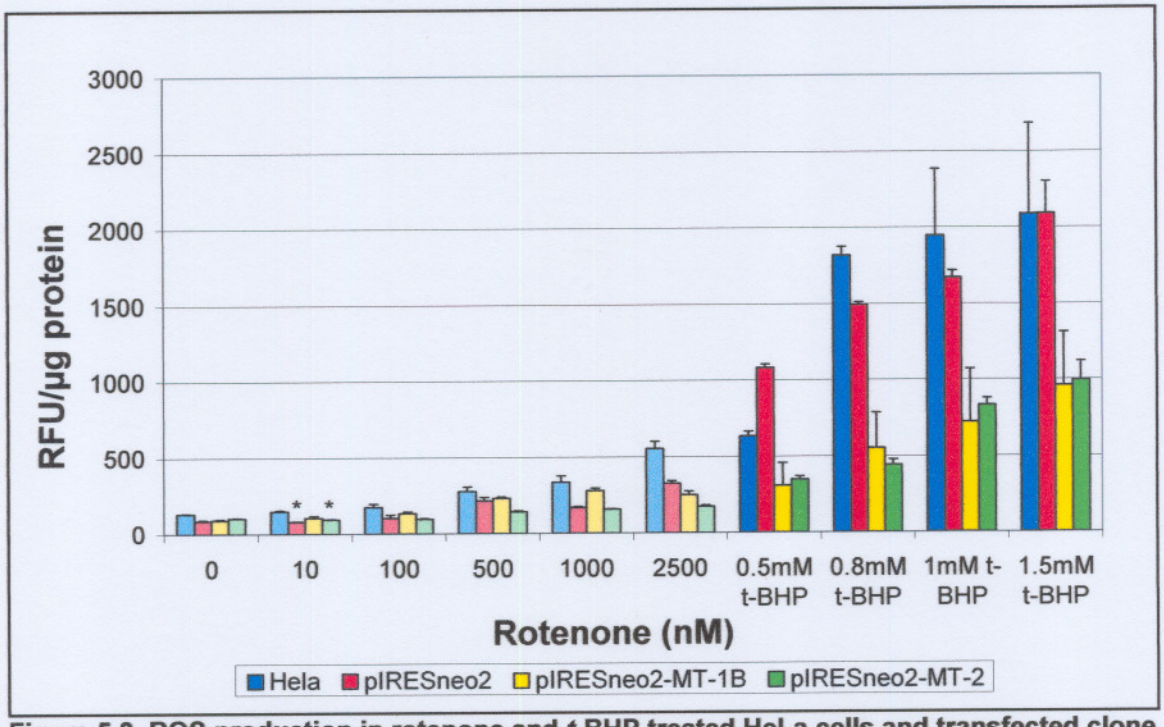

Figure 5.3. ROS production in rotenone and *t*-BHP treated HeLa cells and transfected clone pools. Values are indicated as relative fluorescence units (RFU) per µg total protein. HeLa cells (blue) together with pIRESneo2 transfected cells (red) acted as negative controls. The pIRESneo2-MT-1B transfected cells and pIRESneo2-MT-2A transfected cells are respectively indicated in yellow and green. The positive controls were cells treated with various concentrations of *t*-BHP, as indicated. Asterisks (*) signify mean values ± SD (n = 8) which are not significant, with all other values statistically significantly different from the 0 nM groups as determined with the Student t-test ($p < 0.05$) for independent groups.

From the figure it can be observed that the pIRESneo2-MT-1B and pIRESneo2-MT-2A cells have less than halve the ROS production present in the pIRESneo2 cells in the positive controls. This can not be observed so clearly with the rotenone incubations, although there is a tendency that both these cell lines have a smaller increase in rotenone-induced ROS production. This suggests that MT-1B and MT-2A does have a protective role against ROS, but,

especially due to the unexpected result with the pIRES pool (control), it does not give conclusive proof that ROS produced from a complex I deficiency is scavenged successfully by MT-1B or MT-2A. If these results were to be considered to be correct, this could indicated that MT protection is effective at high levels of ROS production. Even though it was suspected that MT-2A is the main protector, it is unclear from these results whether this assumption would be correct. In light of the poor reproducibility however, this analysis would probably have to be optimised and conducted several times in order to generate accurate results.

5.2.3.2. Visualization of ROS production with confocal microscopy

The visualisation of ROS present in the HeLa cells, pIRESneo2, pIRESneo2-MT-1B and pIRESneo2-MT-2A transfected clone pools with treatment of rotenone at 0, 100 and 1000 nM can be seen in Figure 5.4. Red fluorescence indicates active mitochondria treated with MitoTracker® CM-H_2XROS. Green fluorescence indicates ROS production due to binding of the green DCFDA probe. A decrease in active mitochondria and an increase in green labelled ROS production were expected with an increase in rotenone concentration, especially in the case of the pIRESneo2 control cells. However, due to the fact that different cells needed to be studied, due to the 24 hour incubations with rotenone and the practical limitations of probe labelling and cell culturing in the microscope chamber, the results can be biased to a certain extent. It can be observed in the 1000 nM rotenone treated pIRESneo2 cells that different results can be obtained if the analyst does not investigate objectively. Even though one photographic representation shows one dead cell, indicating very few cells of which most is dead and with no ROS production, the other photograph shows several cells in less critical condition with high levels of ROS production compared to the 0 nM control cells. Another problem was the low signal of green DCFDA fluorescence compared to the red fluorescence. It could indicate less ROS, or just a weaker probe.

However, it can be seen that there is a tendency towards more ROS production or stress in the pIRESneo2 cells with an increase in rotenone concentration. In the more severely affected cells the absence of fluorescence can be attributed to the fact that intracellular esterases are needed to convert the DCFDA probe to fluoresce and that these enzymes may already be inactivated due to stress. The 100 and 1000 nM concentrations of rotenone seemed to induce less ROS or stress in the pIRESneo2-MT-1B and pIRESneo2-MT-2A cells compared to the pIRESneo2 cells as can be seen from their morphology. With rotenone treatment or under stress conditions the HeLa cells became more spherical. The green fluorescence detected in pIRESneo2-MT-2A cells are only due to background fluorescence and the pIRESneo2-MT-1B cells treated with 100 nM rotenone shows one of the crystals mentioned in Section 5.2.3.1.

Even though a tendency towards ROS scavenging or protection could be observed for MT-2A and MT-1B from the results provided in Sections 5.2.3.1 and 5.2.3.2, the extent to which this protection takes place takes place could, with microscopy, not accurately be determined quantitatively or qualitatively due to experimental difficulties or limitations. It is suggested that optimised ROS measurement with the fluorescence plate reader method would be more accurate and less biased.

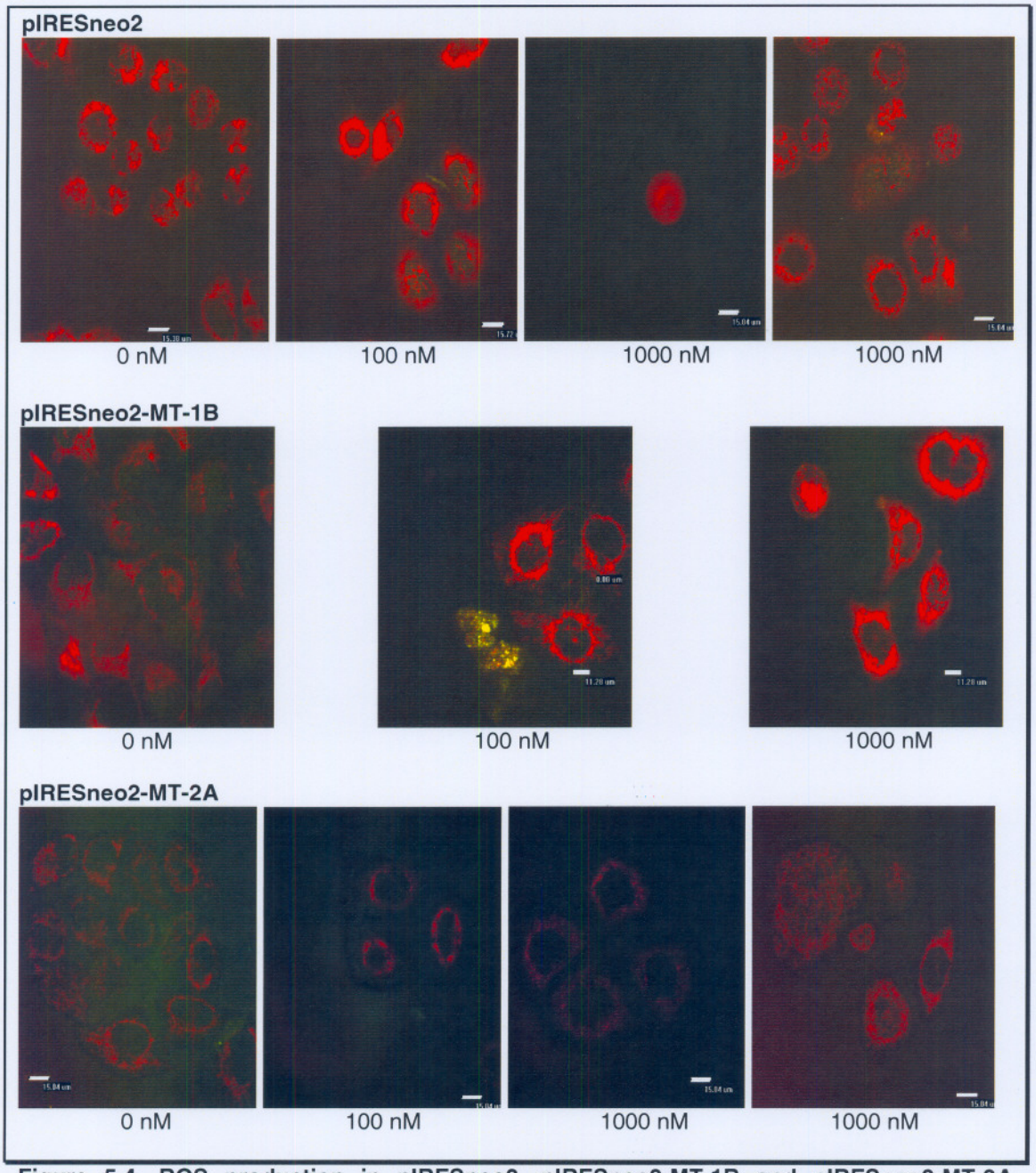

Figure 5.4. ROS production in pIRESneo2, pIRESneo2-MT-1B and pIRESneo2-MT-2A transfected clone pools treated with rotenone. Red fluorescence indicates mitochondria treated with MitoTracker® CM-H_2XROS. Green fluorescence indicates ROS production due to the binding of the green DCFDA probe. All cells were treated with respectively 0, 100 and 1000 nM rotenone over a 24 hour incubation. The pIRESneo2-MT-1B photograph for 100 nM shows a crystal mentioned in Section 5.2.3.1.

5.2.4. MITOCHONDRIAL PERMEABILITY TRANSITION PORE

The decrease in mitochondrial membrane potential after rotenone treatment can be seen in Figure 5.5. The HeLa cells and pIREsneo2, pIRESneo2-MT-1B and pIRESneo2-MT-2A transfected clone pools were treated with 0, 100 and 1000 nM rotenone respectively over a 24 hour incubation period. The red fluorescence indicates mitochondrial membrane potential or polarized mitochondria that load the TMRM probe. Less intensity therefore indicate a reduction in membrane potential or formation of the mtPTP. Though this depolarization of the membranes is visible in the pIRESneo2 transfected cells, it is not as clear cut with the pIRESneo2-MT-1B and pIRESneo2-MT-2A transfected clone pools. Again, as with confocal microscopic visualisation of ROS production described in Section 5.2.3.2, results can be biased.

The pIRESneo2-MT-1B transfected cells treated with 1000 nM rotenone can be seen in two photographic representations. The first photograph indicates spherical cells with more depolarization compared to the control (0 nM rotenone treated) cells. The second however show some cells with normal morphology and much more membrane potential (less mtPTP). Even so, such healthy cells could not be visualised with the pIRESneo2 cells and it is possible that the variation could be due to the difference in MT expression in different transfected clones present in the pIRESneo2-MT-1B clone pool. This would indicate the substantial protection of the membrane potential by MT-1B. The pIRESneo2-MT-2A transfected cells also appeared to have relatively normal morphology after 100 and 1000 nM rotenone treatment and relatively high fluorescent signal, indicating protection of the membrane potential or less mtPTP formation.

These results support those of apoptosis induction or caspase 3/7 activity as discussed in Section 5.2.5, suggesting that both MT-1B and MT-2A has protective function against mtPTP formation and subsequent apoptosis induction, but that MT-2A seems to show this protective effect to a greater extent as indicated by the previous assays. It should be noted that this method was

previously attempted with fluorometric detection, but further optimisation is required before it can be implemented.

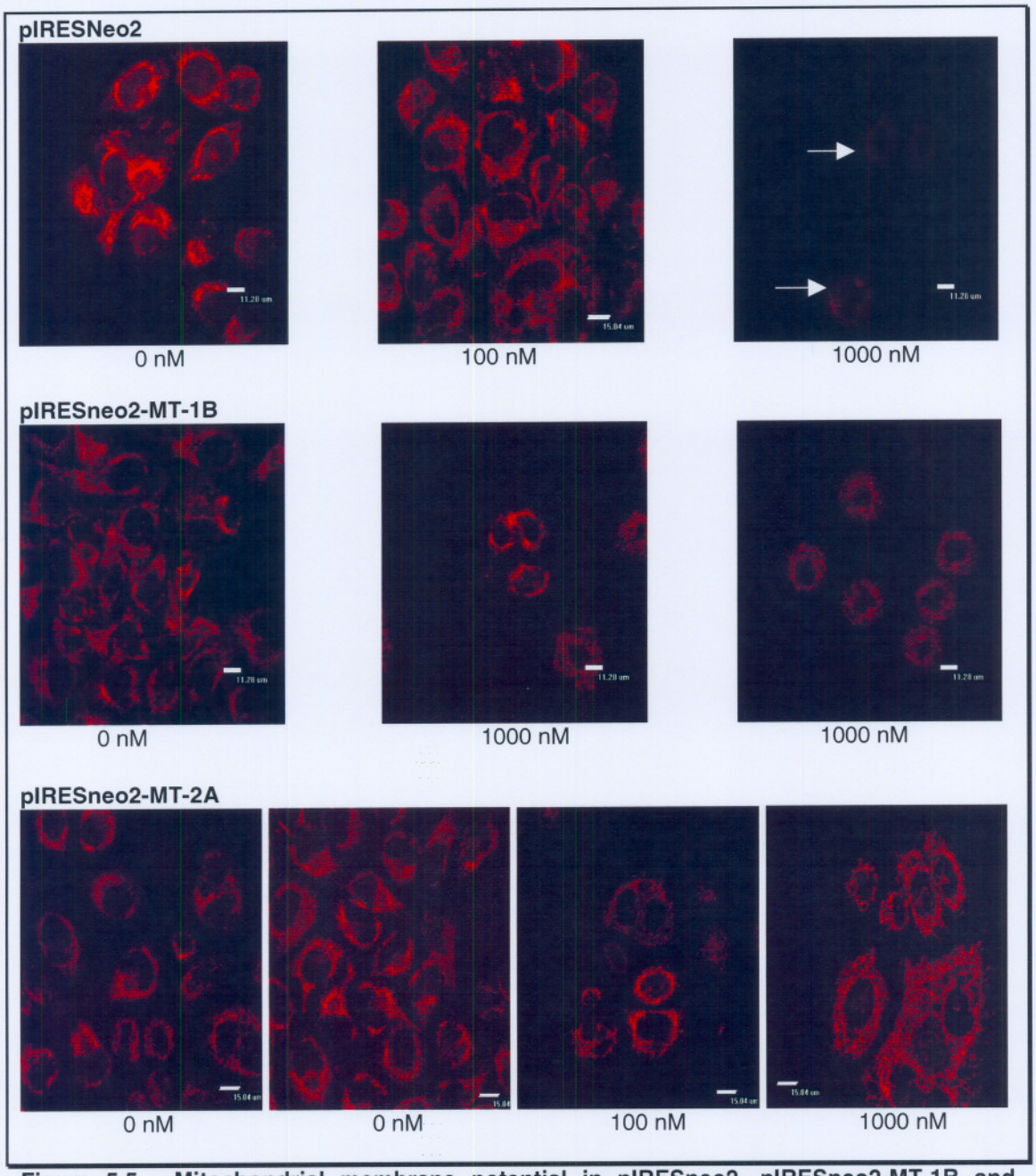

Figure 5.5. Mitochondrial membrane potential in pIRESneo2, pIRESneo2-MT-1B and pIRESneo2-MT-2A transfected clone pools treated with rotenone. Mitochondrial membrane potential or polarized mitochondria allows the TMRM probe to become fluorescent and can be observed as red fluorescence. Less intensity indicates a reduction in membrane potential. All cells were treated with respectively 0, 100 and 1000 nM rotenone over a 24 hour incubation.

5.2.5. CASPASE ACTIVITY

The effect of rotenone-induced complex I deficiency on apoptosis induction, as measured by caspase-3/7 activation, can be seen in Figure 5.6. The figure shows the caspase 3/7 activity for HeLa cells, pIRESneo2, -MT-1B and -MT-2A transfected clone pools as absorbance units per minute per µg total protein. The positive control was cells treated with 1 $\mu g.ml^{-1}$ staurosporine for 2 hours. Values are indicated as the mean ± SD (n = 2) with statistical significance ($p < 0.05$) relative to the 0nM rotenone treated control group as determined with the Student t-test for multiple independent groups. Most values showed statistical significance with relatively low standard deviations.

All four cell lines show relatively the same caspase activity after staurosporine treatment and show various degrees of increase in caspase activity with increase in rotenone dosage. The caspase activity is somewhat higher for pIRESneo2 transfected cells than for normal HeLa cells, as expected. As mentioned previously, these cells are under more stress to constantly transcribe and translate the bicistronic mRNA of the plasmids. The pIRESneo2-MT-1B transfected cells showed considerably less caspase activity than the pIRESneo2 pool, from 125 nM rotenone treatment and higher, indicating protection against apoptosis to a certain extent. The pIRESneo2-MT-2A transfected cells showed even more protection against the complex I-dependant apoptosis up and to 100 nM rotenone treatment. However, the caspase activity (apoptosis induction) for pIRESneo2-MT-2A transfected cells is half of that of the pIRESneo2 transfected cells from 250 nM rotenone and higher.

This would imply that MT-2A overexpression has a significant protective role against the detrimental effects that lead up to apoptosis induction in cells with a complex I deficiency, as suggested in the hypothesis of this study. This would also indicate that MT-2A, rather than MT-1B is the main protector against apoptosis in complex I deficient cells and could possibly explain the low and un-

inducible levels of MT-1B in rotenone treated HeLa cells as reported previously by Heguy *et al.* (1986) and Olivier (2004).

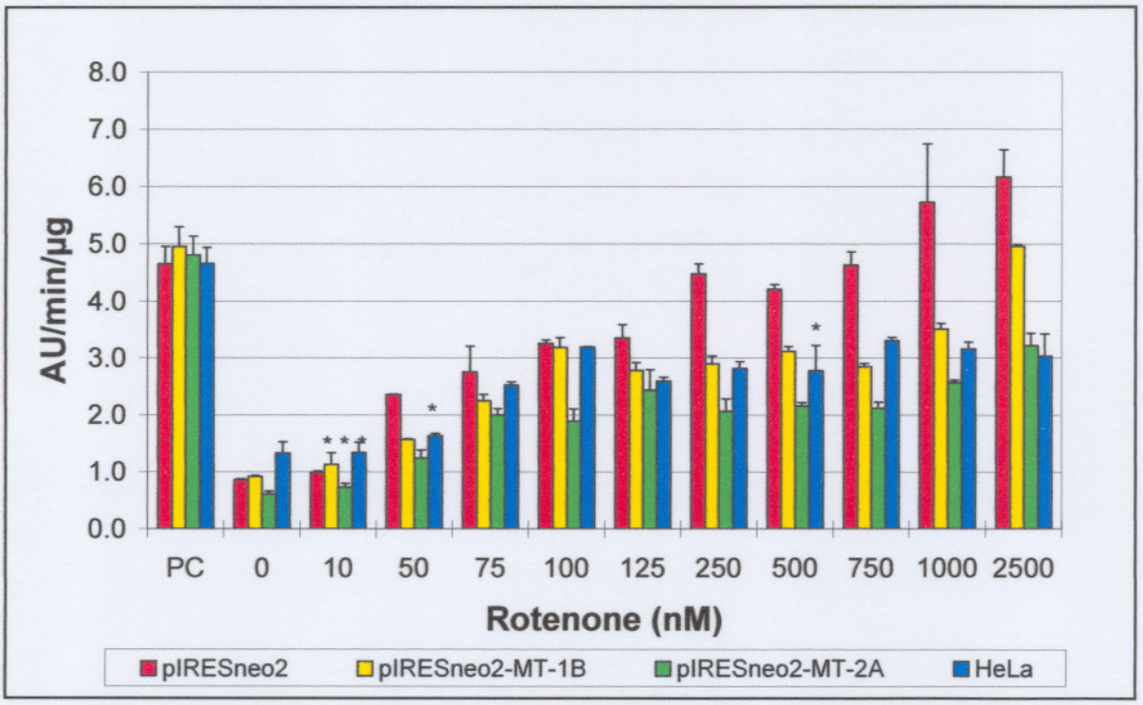

Figure 5.6. Effect of rotenone on caspase activity in HeLa cells and transfected clone pools. Caspase activity is indicated as relative fluorescence units per minute per µg total protein. HeLa cells (blue) together with pIRESneo2 transfected cells (red) acted as negative controls. The pIRESneo2-MT-1B transfected cells and pIRESneo2-MT-2A transfected cells are respectively indicated in yellow and green. The positive control (PC) was treated with 1 $\mu g.ml^{-1}$ staurosporine. Asterisks (*) signify mean values ± SD ($n = 2$) not significant, with all other values statistically significantly different from the 0 nM groups as determined with the Student t-test ($p < 0.05$) for independent groups.

5.3. SUMMARY

In this chapter the investigation into the functional properties of MT-1B and MT-2A in the pIRESneo2-MT-1B and pIRESneo2-MT-2A transfected clone pools, characterised in Chapter 4, is described. It confirmed the decrease in NADH:ubiquinone oxidoreductase (complex I) activity with increase in rotenone concentration administered. The cell viability assay indicated that MT-2A overexpression in transfected HeLa cells supported much higher cell viability

levels with rotenone and especially *t*-BHP treatment than in control cells. Caspase 3/7 activity was also significantly lower in MT-2A overexpressing cells. These results suggest that MT-2A might have a protective effect against necrosis and especially apoptosis in complex I deficient cells. MT-1B overexpression also showed less caspase activity than the control cells, but did not show increased cell viability compared to control cells with rotenone treatment. This suggests that even though MT-1B has some protective effect against apoptosis, it does not have the same extent of protection MT-2A has.

The results generated with ROS measurement in the cells treated with rotenone and *t*-BHP did not indicate conclusive proof of MT-1B or MT-2A having a protective or scavenging ability. However, a tendency towards better cellular morphology after rotenone treatment could be seen with the confocal microscopic visualisation of ROS in the pIRESneo2-MT-1B and pIRESneo2-MT-2A transfected cells. These cells also showed less ROS production after *t*-BHP treatment than the pIRESneo2 control cells. This protection however was not as visible in the rotenone treated cells. The formation of mtPTP appeared to be much less in the rotenone treated pIRESneo2-MT-1B and pIRESneo2-MT-2A transfected cells relative to the control cells (0 nM rotenone) as well as compared to the pIRESneo2 treated cells. This again supports the protective effect of the MTs against apoptosis in the complex I deficient cells.

It does however appear that MT-2A generally seems to be a somewhat more effective protector than MT-1B, possibly accounting for the low and un-inducible expression levels of MT-1B in the rotenone treated HeLa cells as reported previously. The role of this protection however cannot undoubtedly be attributed to ROS scavenging in this study.

CHAPTER SIX

CONCLUSIONS

Many diseases have been classified to be caused by deficiency of the mitochondrial respiratory chain. Of these disorders, complex I deficiency is frequently the cause (Triepels *et al.*, 2001b). One of the major consequences of such a deficiency is the production of ROS, its deleterious effects on the mitochondria and consequential induction of apoptosis (Wallace, 1999). Metallothioneins have been identified as one of the scavengers of such reactive oxygen species, probably due to its high cysteine content Thomas *et al.*, 1986; Ghoshal & Samson, 2001). In light of recent work by van der Westhuizen *et al.* (2003) it has been proposed that these metallothioneins may have a ROS-related protective effect in complex I deficient cell lines. In a closely related project by Olivier (2004) the expression of MTs with a rotenone-induced complex I deficiency in HeLa cells was investigated. The aim of this project was therefore to investigate the putative protective role of metallothioneins in a complex I deficient cell line and ascertain whether this protection was targeted against ROS or ROS-related consequences. It was also necessary to establish whether different MT isoforms would lead to different levels of protection in this complex I deficient cell line.

For these purposes the MT-1B and MT-2A cDNA sequences were cloned into the pIRESneo2 expression vector (as discussed in Chapter 3) and the clone pools of the transfected cells characterised (as presented in Chapter 4). In this chapter the use of an ELISA method to measure metallothionein protein levels, that was unsuccessful, is discussed. Another option to measure the same protein levels could be to use Western blotting. Southern blotting could be used to confirm the presence of the MT cDNA, with the aid of radioactive detection as it is more sensitive than fluorescent detection, especially in light of the relatively low expression values even of MT-2A in normal HeLa cells.

Complex I deficiency was induced in transfected cells and various analyses performed to determine the contribution of overexpressed MT-1B and MT-2A to selected parameters in the cells (see Chapter 5). Studies of cell viability as measured with the MTT reaction of these rotenone treated clone pools indicated that MT-2A overexpression supported higher cell viability levels than that of the pIRESneo2 control cells or the pIRESneo2-MT-1B transfected cells. This MT-2A overexpression showed an even greater protective effect in the *t*-BHP treated cells, which causes high endogenous ROS levels leading to necrotic rather than apoptotic cell death. Taking these results into consideration, it can be suggested that MT-2A has a protective effect against ROS and ROS-induced necrosis. Such a protective role for MT-1B could not be observed from these cell viability assays.

Direct ROS production analyses in rotenone treated cells did not indicate conclusive proof of MT-1B or MT-2A having a protective or scavenging ability. The MT-1B and MT-2A overexpression did, however, appear to lower ROS production in the *t*-BHP treated cells. A tendency towards better cellular morphology after rotenone treatment could also be observed with the confocal microscopic visualisation of ROS in the pIRESneo2-MT-1B and pIRESneo2-MT-2A transfected cells. However, some difficulties have been experienced with these two methods, and conducting these analyses again could perhaps clarify these results. Ideally flow cytometry could also be used to measure the DCF fluorescence in each cell, therefore compensating for the background levels of fluorescence in the media and the limitations of measurement in the fluorometric and confocal microscopic methods performed in this study.

Caspase 3/7 activity was significantly lower in MT-1B and especially MT-2A overexpressing cells compared to the control pIRESneo2 cells. This would imply that MTs protect against apoptosis in complex I deficient cells and is probably the strongest evidence for a protective effect, in this study, as rotenone, at relatively low levels, is known to induce apoptosis (Li *et al.*, 2003; Isenberg & Klaunig, 2000). Cell viability measurements for MT-1B overexpression however did not support this protective role for MT-1B.

Taking these results into consideration, it is suggested that even though MT-1B has a protective effect against apoptosis, it does not have the same extent of protection MT-2A has, particularly when considering results from the *t*-BHP incubations. The MTT assay is much more selective to measure necrosis, and apoptosis is not reflected to the same extent as necrosis in this assay. This would indicate that MT-1B, in some way, protects against apoptosis, whilst MT-2A protects against both apoptosis and ROS-induced necrosis. This could also indicate why rotenone treated cells did not show more than 30 % decrease in cell viability in contrast to what was expected. In a state of reduced ATP generation as observed following rotenone treatment, apoptosis may proceed until cellular ATP stores are depleted or reduced to a point where cell death becomes necrotic rather than apoptotic (Isenberg & Klaunig, 2000). It is possible that this state of necrosis has not been reached in these cells, as cell viability decreased only to approximately 70%. It should also be noted that DNA fragmentation studies need to be conducted in the future to support these apoptosis (caspase 3/7 activity) results.

The formation of the mtPTP is thought to be a consequence, or perhaps even a cause, of apoptosis. The formation of mtPTP, visualised as decreased membrane potential, appeared to be much less in the rotenone treated cells overexpressing MT-1B and 2A respectively, relative to pIRESneo2 control cells. This again supports the protective effect of the MTs against apoptosis in rotenone-induced complex I deficient cells. Whether one of these two MT isoforms is more effective in this protective role was not clear from this particular experiment. To support this data, the use of flow cytometric analyses would again be a good alternative.

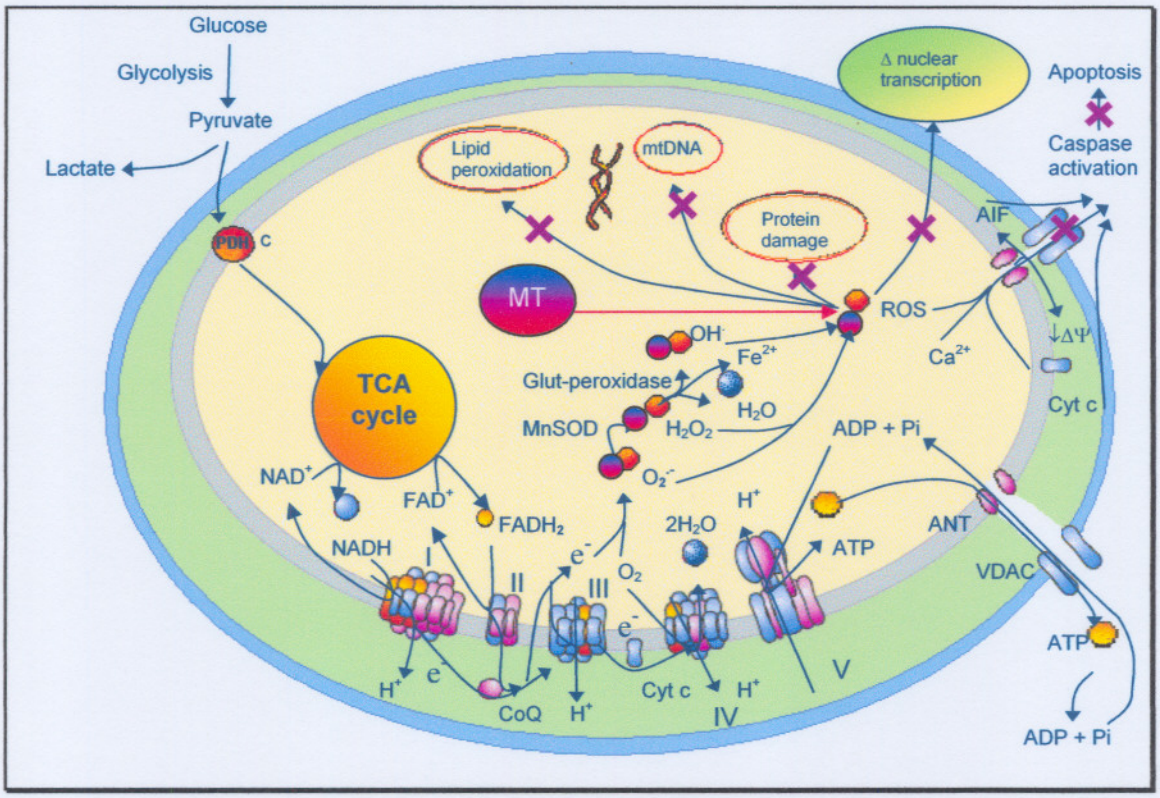

Figure 6.1. Simplified schematic representation of the mitochondrial metabolism indicating the effect of MT overexpression. Through its primary scavenging of ROS, MTs (blue-pink circle) secondarily protect against mitochondrial permeability pore formation and apoptosis (indicated with a purple cross). Its scavenging of ROS could also possibly inhibit oxidation of DNA, lipids and proteins, indicate with a purple cross (adapted from Wallace, 1999).

The evidence presented in this study supports the hypothesis that MTs, and particularly both MT-1B and MT-2A has some protective effect in complex I deficient cells (Figure 6.1). This protection is probably due to ROS scavenging through the formation of disulfide bonds between the free thiol groups of the MTs and ROS ($O_2^{\cdot-}$ and H_2O_2, but particularly $OH^{\cdot}$), although this study did not conclusively prove direct ROS protection. It does appear, however, that MT-2A seems to be more effective in protection against ROS, mtPTP formation, apoptosis and ROS-induced necrosis than MT-1B. This could suggest why MT-1B are expressed in very low, barely detectable, levels in HeLa cells compared to relatively high expression of MT-2A in these cells. This MT-1B expression also showed to be un-inducible by rotenone, cadmium and zinc (Olivier, 2004). Heguy *et al.* (1986) stated that methylation of the MT-1B gene

could be the reason for this observation. Therefore, in normal cells, except in liver and kidney cells where MT-1B expression levels are higher, MT-2A could be the main protector against the deleterious biochemical effects found with complex I deficiency. A possible explanation for this difference in efficiency to bind and scavenge ROS may be found in the difference in structure between the two isoforms. They differ by nine amino acids. Most of these differences occur directly next to one, or in between, two cysteine residues. MT-1B also has one more cysteine residue than MT-2A. This would affect the structural environment surrounding the cysteine residues to which ROS is thought to bind, possibly causing 'knobs' obstructing this binding of ROS.

Even though various other analyses could be conducted to verify the results generated in this study, it would be feasible to consider extending the study to *in vivo* models. This would not only allow the use of various other methods of detecting oxidative stress or the consequences thereof, such as, antioxidant capacity, antioxidant enzyme modulation, serum reactive oxygen metabolites, glutathione redox state and macromolecular (DNA, lipid, protein) damage that does not ordinarily seem to be successful in cell culture work. Most importantly, it would also indicate whether this protective effect of MT-1B and especially MT-2A in complex I deficiency would be significant in an *in vivo* model. Such a study could be performed at the Division of Biochemistry at the North-West University, as it is equipped with all the necessary facilities.

Another possible follow-up on this study could be to determine the protective role of MTs in deficiencies or diseases other than complex I deficiency. The use of *t*-BHP for such studies holds strong possibilities in light of the relatively high level of MT-2A protection in cells treated with this agent as well as its relatively frequent use in ROS related studies.

Another notion to consider in future studies would be to target MTs as therapeutic agents *in vivo*. The wide range of agents capable of inducing metallothioneins could facilitate such treatment modalities. An *in vivo* model such as described above would also create the opportunity to ascertain which possible MT

expression inducers could be considered for treatment. Apart from this protective role, in the nearer future, MT-2A expression levels could be considered as a biomarker for ROS levels not only in complex I deficiency, but also any other disease connected to ROS production. Even though expensive, the use of real-time PCR would be an excellent choice due to its simple, rapid, accurate and very sensitive nature once the method has been optimised for the specific sample nature, such as type of tissue or cell culture.

In conclusion, during this study (as outlined in Chapter 2) a problem has been identified from current literature and a hypothesis formulated about the function of MT expression. From the aims and objectives a defined *in vitro* model was used to investigate this hypothesis and, although supporting evidence would be useful, sufficient scientific evidence was generated during this study to support this hypothesis (Chapters 3 to 5).

REFERENCES

Abel, J., & de Ruiter, N. 1989. Inhibition of hydroxyl-radical-generated DNA degradation by metallothionein. *Toxicology letters.* 47(2): 191-196.

Anderson, S., Bankier, A.T., Barrell, B.G., de Bruijn, M.H.L., Coulson, A.R., Drouin, J., Eperon, I.C., Nierlich, D.P., Roe, B.A., Sanger, F., Schreier, P.H., Smith, A.J.H., Staden, R., Yong, I.G. 1981. Sequence and organization of the human mitochondrial genome. *Nature.* 290: 457-465.

Andreu, A.L., & Gonzalo-Sanz, R. 2004. Mitochondrial disorders: a classification for the 21st century. *Neurologia.* 19(1): 15-22.

Andrews, G.K. 2000. Regulation of Metallothionein Gene Expression by Oxidative Stress and Metal Ions. *Biochemical Pharmacology.* 59: 95-104.

Atlas, R.M. 1997. Principles of Microbiology. 2nd edition. NY: McGraw-Hill. 476.

Bauman, J.W., Liu, J., Liu, Y.P., Klaassen, C.D. 1991. Increase in metallothionein production by chemicals that induce oxidative stress. *Toxicology and applied pharmacology.* 10:347-354.

Bergmeyer, H.U. 1981. Methods of Enzymatic analysis. 3rd edition. Weinheim: Verlag Chemie GmbH. 353-355.

Berridge, M.V., Tan, A.S. 1993. Characterization of the cellular reduction of 3-(4,5-dimethylthiazol-2-yl)-2,5-diphenyltetrazolium bromide (MTT): subcellular localization, substrate dependence, and involvement of mitochondrial electron transport in MTT reduction. *Archives of Biochemistry and Biophysics.* 303(2): 474-482.

Binz, P.-A., Kägi, J.H.R. 2001. Molecular Evolution of Metallothioneins: Contributions from coding and non-coding Regions. http://www.unizh.ch/~mtpage/poster/posterevol.html. 2004.

BIOEDIT Sequenc Aliignment Editor. http://www.mbio.ncsu.edu/BioEdit/bioedit.html. 2004.

Bogenhagen, D.F., Applegate, E.F., Yoza, B.K. 1984. Identification of a promoter for transcription of the heavy strand of human mtDNA: in vitro transcription and deletion mutagenesis. *Cell.* 36: 1105-1113.

Bogenhagen, D., & Clayton, D.A. 1974. The Number of Mitochondrial Deoxyribonucleic Acid Genomes in Mouse L and Human HeLa Cells: Qantitative isolation of mitochondrial deoxyribonucleic acid. *The Journal of Biological Chemistry.* 249(24): 7991-7995.

Brown, T. & Mackey, K. 1997. Analysis of RNA by Northern and Slot Blot hybridization. *In* Ausubel, F.M., Brent, R., Kingston, R.E., Moore, D.D., Seidman, J.G., Smith J.A., Struhl, K., *ed.* Current Protocols in Molecular Biology. NY: Wiley. 4.9.1-4.9.7.

Bustin, S.A. 2000. Absolute quantification of mRNA using real-time reverse transcription polymerase chain reaction assays. *Journal of Molecular Endocrinology.* 25: 169–193.

Butcher, H., Kennette, W., Colling, O., Demoor, J., Koropatnick, J. 2003. A sensitive time-resolved fluorescent immunoassay for metallothionein protein. *Journal of Immunological Methods*. 272: 247-256.

Carelli, V., Ross-Cisneros, F.N., Sadun, A.A. 2004, Mitochondrial dysfunction as a cause of optic neuropathies. *Progress in Retinal and Eye Research*. 23(1): 53-89.

Chen, S.H., Lin, C.Y., Cho, C.S., Lo, C.Z., Hsiung, C.A. 2003. 3(13): 3751-3754.

Cherian, M.G., Jayasurya, A., Bay, B-H. 2003. Metallothioneins in human tumors and potential roles in carcinogenesis. Mutation Research. 533: 201-209.

Chinnery, P.F., Thorburn, D.R., Samuels, D.C., White, S.L., Dahl, H.M., Turnbull, D.M., Lightowlers, R.N., Howell, N. 2000. The inheritance of mitochondrial DNA heteroplasmy: random drift, selection or both. *Trends in Genetics*. 16(11): 500-505.

Chinnery, P.F. 2002. Inheritance of mitochondrial disorders. *Mitochondrion*. 2(1-2): 149-155.

Chretien, D., Bénit, P., Chol, M., Lebon, S., Rötig, A., Munnich, A., Rustin, P. 2003. Assay of mitochondrial respiratory chain complex I in human lymphocytes and cultured skin fibroblasts. *Biochemical and Biophysical Research Communications*. 301: 222-224.

Coyle, P., Philcox, J. C., Carey, L. C., Rofe, A. M. 2002. Metallothionein: The multipurpose protein. *Cellular and Molecular Life Sciences*. 59: 001-21.

Crompton, M. 1999. The mitochondrial permeability transition pore and its role in cell death. *Biochemical Journal*. 341: 233-249.

Dalton, T.P., Shertzer, H.G., Puga, A. 1999. Regulation of gene expression by reactive oxygen species. *Annual reviews in Pharmacological toxicology*. 39: 67-101.

DiMauro, S. 2004a. Mitochondrial diseases. *Biochimica et Biophysica Acta*. 1658: 80-88.

Esposti, M.D. 1998, Inhibitors of NADH–ubiquinone reductase: an overview. *Biochimica et Biophysica Acta-Bioenergetics*. 1364(2): 222-235.

Freshney, R.I. 2000. Culture of animal cells: A manual of basic technique. 4th edition. NY: Wiley-Liss Inc. 196-198; 455-458.

Frey, T.G., & Mannella, C.A. 2000. The internal structure of mitochondria. *Trends in Biochemical Science*. 25(7): 319-324.

Ghoshal, K., & Samson, T.J. 2001. Regulation of metallothionein gene expression. *Progress in nucleic acid research and Molecular Biology*. 66: 358.

Greenamyre, J.T., Betarbet, R., Sherer, T.B. 2003. The rotenone model of Parkinson's disease: genes, environment and mitochondria. *Parkinsonism Related Disorders*. 2: S59-64.

Gray, M. W., Burger, G., Lang, B.F. 1999. Mitochondrial evolution. *Science*. 283(5407): 1476-1481.

Grigorieff, N. 1998. Three-dimensional structure of bovine NADH:ubiquinone oxidoreductase (complex I) at 22 A in ice. *Journal of Molecular Biology*. 277(5): 1033-46.

Grigorieff, N. 1999. Structure of the respiratory NADH:ubiquinone oxidoreductase (complex I). Current Poinion in Structural Biology. 9:476-483.

Hackenbrock, C.R. 1966. Ultrastructural bases for metabolically linked mechanical activity in mitochondria. I. Reversible ultrastructural changes with change in metabolic steady state in isolated liver mitochondria. *Journal of Celular Biology.* 30: 269–297.

Halgren, R.G., Fielden, M.R., Fong, C.J., Zacharewski, T.R. 2001. Assesment of clone identity and sequence fidelity for 1189 IMAGE cDNA clones. *Nucleic Acids Research.* 29: 582-588.

Hamer, D.H. 1986. Metallothionein. *Annual Review of Biochemistry.* 55: 913-951.

Haq, F., Mahoney, M., Koropatnick, J. 2003. Signaling events for metallothionein induction. *Mutation Research.* 533: 211-216.

Heguy, A., West, A., Richards, R.I., Karin, M. 1986. Structure and tissue-specific expression of the human metallothionein 1B gene. *Molecular and cellular biology.* 6(6): 2149-2157.

Hirst, J., Carroll, J., Fearnley, I.M., Shannon, R.J., Walker, J.E. 2003. The nuclear encoded sub-units of complex I from bovine heart mitochondria. *Biochimica et Biophysica Acta.* 1604: 135– 150.

Ide, T., Tsutsui, H., Kinugawa, S., Utsumi, H., Kang, D., Hattori, N., Uchida, K., Arimura, K-I., Egashira, K., Takeshita, A. 1999. Mitochondrial electron transport complex I is a potential source of oxygen free radicals in the failing myocardium. *Circulation Research.* 85: 357-363.

Isenberg, J.S., & Klaunig, J.E. 2000. Role of the Mitochondrial Membrane Permeability Transition (MPT) in Rotenone-Induced Apoptosis in Liver Cells. *Toxicological sciences.* 53: 340-351.

Jacob, S.T., Ghoshal, K., Sheridan, J.F. 1999. Induction of Metallothionein by stress and its molecular mechanisms. *Gene expression.* 7: 301-310.

Kägi, J.H.R., & Vallee, B.L. 1960. Metallothionein: a Cadmium- and Zinc-containing protein form Equine renal cortex. *Journal of Biological Chemistry.* 236(9): 2435-3442.

Kägi, J.H.R., & Vallee, B.L. 1961. Metallothionein: a Cadmium- and Zinc-containing protein form Equine renal cortex. *Journal of Biological Chemistry.* 235(12): 3460-3465.

Kägi, J.H.R., Himmelhoch, S.R., Whanger,P.D., Bethune, J.L., Vallee, B.L. 1974. Equine Hepatic and Renal metallothioneins. *Journal of Biological Chemistry.* 249(11): 3537-3542.

Karin, M., Andersen, R.D., Slater, E., Smith, K., Herschman, H.R. 1980. Metallothionein mRNA induction in HeLa cells in response to zinc or dexamethasone is a primary induction response. *Nature.* 286: 295-297.

Karin, M., Eddy, R.L., Henry, W.M., Haley, L.L., Byers, M.G., Shows, T.B. 1984. Human metallothionein genes are clustered on chromosome 16. *Proceedings of the National Academy of Sciences of the United States of America.* 81: 5494-5498.

Kling, P.G., & Olsson, P. 2000. Involvement of differential metallothionein expression in free radical sensitivity of RTG-2 and CHSE-214 cells. *Free Radical Biology & Medicine.* 28(11): 1628-1637.

Kondoh, M., Inoue, Y., Atagi, S., Futakawa, N., Higashimoto, M., Sato, M. 2001. Specific induction of metallothionein synthesis by mitochondrial oxidative stress. *Life Sciences.* 69: 2137–2146.

Koopman, W.J. 2004. Verbal communication with the supervisor. Department of Biochemistry and Pediatrics, University Medical Center Nijmegen, The Netherlands.

Kristián, T. 2004. Metabolic stages, mitochondria and calcium in hypoxic/ischemic brain damage. *Cell Calcium.* 369(3-4): 221-233.

Kweon, M-H., Jung, M-J., Sung, H-C. 2004. Cytoprotective effects of heme oxygenase-1 induction by 3-*O*-caffeoyl-1-methylquinic acid. *Free Radical Biology and Medicine.* 36(1): 40-52.

Lambert, A.J., & Brand, M.D. 2004. Inhibitors of the quinone-binding site allow rapid superoxide production from mitochondrial NADH:ubiquinone oxidoreductase (complex I). *Journal of Biological Chemistry.* 279(38): 39414-39420.

Li, N., Ragheb, K., Lawler, G., Sturgis, J., Rajwa, B., Melendez, J.A., Robinson, J.P., 2003. Mitochondrial complex I inhibitor rotenone induces apoptosis through enhancing mitochondrial reactive oxygen species production. *Journal of Biological Chemistry.* 278(10): 8516-8525.

Liu, Y., Peterson, D.A., Kimura, H., Schubert, A. 1997. Mechanism of Cellular 3- (4,5-Dimethylthiazol-2-yl) -2,5-Diphenyltetrazolium Bromide (MTT) Reduction. *Journal of Neurochemistry.* 69(2): 581-593.

Liu, Y., Fiskum, G., Schubert, D. 2002. Generation of reactive oxygen species by the mitochondrial electron transport chain. *Journal of Neurochemistry.* 80: 780-787.

Long, A.C., Colitz, C.M.H., Bomser, J.A., 2004. Apoptotic and Necrotic Mechanisms of Stress-Induced Human Lens Epithelial Cell Death. *Experimental Biology and Medicine.* 229: 1072-1080.

Loschen, G., Flohe, L., Chance, B. 1971. Prespiratory chain linked production in pigeon heart mitochondria. *Federation of European Biochemical Societies Letters.* 18: 261-264.

Loschen, G., Azzi, A., Flohe, L. 1974. Superoxide radicals as precursors of mitochondrial hydrogen peroxide. *Federation of European Biochemical Societies Letters.* 42: 68-72.

Luft, R., Ikkos, D., Palmieri, G., Ernster, L., Afzeleus, B. 1962. A case of severe hypermetabolism of nonthyroid origin with a defect in the maintenance of mitochondrial respiratory control: a correlated clinical, biochemical, and morphological study. *Journal of Clinical Investigation.* 41(9): 1776-1804.

Maniatis, T., Fritsch, E.F., Sambrook, J. 1982. Molecular cloning: a laboratory manual. NY: Cold Spring Harbor Laboratory Press. 249-251, A468.

Mitchell, P. 1961. Coupling of phosphorylation to electron and hydrogen transfer by a chemi-osmotic type of mechanism. *Nature.* 191: 144-148.

Mitchell, P. 1979. Keilin's respiratory chain concept and its chemiosmotic consequences. *Science.* 206: 1148-1158.

Mosmann, T. 1983. Rapid colorimetric assay for cellular growth and survival: Application to proliferation and cytotoxicity assays. *Journal of Immunological Methods.* 65(1-2): 55-63.

Munnich, A., Rötig, A., Chretien, D., Saudubray, J., Cormier, V., Rustin, P. 1996. Clinical presentations and laboratory investigations in respiratory chain deficiency. *European Journal of Pediatrics.* 155: 262-274.

Munnich, A., & Rustin, P. 2001. Clinicla spectrum and diagnosis of mitochondrial disorders. *American Journal of Medical Genetics.* 106: 4-17.

NCBI, National Center for Biotechnology Information, National Institutes of Health, http://www.ncbi.nlm.nih.gov, 2004.

Nicholls, D.G., & Ferguson, S.J. 2002. Bioenergetics. Elsevier Science; Academic Press. 108; 113-118; 121; 258-261.

Old, R.W., & Primrose, S.B. 1989. Principles of Gene Manipulation: An introduction to Genetic Engineering. 4th edition. London: Blackwell Scientific publications. 26.

OLIGONUCLEOTIDE PROPERTIES CALCULATOR, http://www.basic.nwu.edu/biotools/oligocalc.html, 2004.

Olivier, Y. 2004. Analysis of metallothionein expression levels in NADH:ubiquinone oxidoreductase deficiency. Potchefstroom: North-West University. (Dissertation-M.Sc.)

Perkins, G.A., & Frey, T.G. 2000. Recent structural insight into mitochondria gained by microscopy. *Micron: The International Research and Review Journal for Microscopy,* 31: 97–111.

Perkins, G., Renken, C., Martone, M.E., Young, S.J., Ellisman, M., Frey, T. 1997. Electron Tomography of Neuronal Mitochondria: Three-Dimensional Structure and Organization of Cristae and Membrane Contacts. *Journal of Structural Biology.* 119(3): 260-272.

Pfaffl, M.W., Horgan, G.W., Dempfle, L. 2002. Relative exression software tool (REST) for groupwise comparison and statistical analysis of relative expression results in real-time PCR. *Nucleic Acids Research.* 30(9): e36.

Piccolo, G., Banfi, P. Azan, G., Rizzuto, R., Bisson,, R., Sandona, D., Bellomo, G. 1991. Biological markers of oxidative stress in mitochondrial myopathies with progressive external ophthalmoplegia. *Journal of the Neurological Sciences.* 105: 57-60.

Pitkanen, S., Merante, F., McLeod, D.R., Applegarth, D., Tong, T., Robinson, B.H. 1996. Familial cardiomyopathy with cataracts and lactic acidosis: a defect in complex I (NADH-dehydrogenase) of the mitochondria respiratory chain. *Pediatric Research.* 39(3): 513-521.

Pulkes, T., & Hanna, M.G. 2001. Human mitochondrial DNA diseases. *Advanced Drug Delivery Reviews.* 49(1-2): 27-43.

Quiafe, C.J., Findley S.D., Erickson J.C., Froelick G.J., Kelly E.J., Zambrowicz B.P., Palmiter R.D. 1994. Induction of a new metallothionein isoforms (MT-IV) occurs during differentiation of stratified squamous epithelia. *Biochemistry.* 33: 7250-7259.

Radonic, A., Thulke, S., Mackay, I.M., Landt, O., Siegert, W., Nitsche, A. 2004. Guideline to reference gene selection for quantitative real-time PCR. *Biochemical Biophysical Research Communication.* 313: 856-862.

Ragan, C.I., Wilson, M.T., Darley-Usmar, V.M., Lowe, P.N. 1987. *In* Darley-Usmar, V.M., Rickwood, D., Wilson, M.T., *eds.* Mitochondria: A practical approach. Oxford: IRL Press: 89.

Raha, S., Robins, B.H. 2000. Mitochondria, oxygen free radicals, disease and ageing. *Trends in Biochemical Science.* 25: 502-508.

Rahman, S., Blok, R.B., Dahl, H.H., Danks, O.M., Kirby, D.M., Chow, C.W., Christodoulou, J., Thorburn, D.R. 1996. Leigh syndrome: clinical features and biochemical and DNA abnormalities. *Annual Neurology.* 39: 343–351.

Robinson, B.H. 1998. Human Complex I deficiency: Clinical spectrum and involvement of oxygen free radicals in the pathogenicity of the defect. *Biochimica et Biophysica Acta.* 1364; 271–286.

Robinson, J.B., JR., Brent, L.G., Sumegi, B., Srere, P.A. 1987. *In*: Darley-Usmar, V.M., Rickwood, D., Wilson, M.T., *eds.* Mitochondria: A practical approach. Oxford: IRL Press. 160.

Rossman, T.G., Concharova, E.I., Nádas, A., Dolzhanskaya, N. 1997. Chinese hamster cells expressing antisense to metallothionein become spontaneous mutators. *Mutation research.* 373: 75-85.

Ruitenbeek, W., Trijbels, J.M.F., Fischer, J.C., Sengers, R.C.A., Janssen, A.J.M., Kerkhof C.M.C. 1989. Mitochondrial myopathies: Multiple enzyme defects in the respiratory chain. *Journal of Inherited Metabolic Disease.* 12(Suppl 2): 352-354.

Ruitenbeek, W., Wendel, u., Trijbels, F., Sengers, R. 1996. Mitochodnrial energy metabolism. *In* Blau, N., Duran, M., Blaskovics, M.E., *ed.* Physician's Guide to the Laboratory Diagnosis of Metabolic Diseases. Chapman & Hall Medical. 391; 404-405.

Rustin, P., Chretine, D., Bourgeron, T., Gérard, B., Rötig, A., Saudubray, J.M., Munnich A. 1994. Biochemical and molecular investigations in respiratory chain deficiencies. *Clinica Chimica Acta.* 228: 35-51.

Sanger, F., Nicklen, S., Coulson, A.R. 1977. DNA sequencing with chain-terminating inhibitors. *Proceedings of the National Academy of Sciences of the United States.* 74(12): 5463-5467.

Sato, M., Sasaki, M., Hojo, H. 1995. Antioxidative roles of Metallothionein and Manganese Superoxide dismutase induced by Tumor Necrosis Factor-α and Interleukin-6. *Archives of biochemistry and biophysics.* 316(2): 738-744.

Satoh, M., Naganuma, A., Imura, N. 1988. Metallothionein induction prevents toxic side effects of cisplatin and adriamycin used in combination. *Cancer Chemotherapy and Pharmacology.* 21: 176-178.

Scheffler, I.E. 2001a. A century of mitochondrial research: achievements and perspectives. *Mitochondrion*. 1(1): 3-31.

Scheffler, I.E. 2001b. Mitochondria make a come back. *Advanced Drug Delivery Reviews*. 49(1-2): 3-26.

Sjöstrand, F.S. 1953. Electron microscopy of mitochondria and cytoplasmic double membranes. *Nature*. 171: 30-31.

Smith, P.K., Krohn, R.I., Hermanson, G.T., Mallia, A.K., Gartner, F.H., Provenzano, M.D., Fujimoto, E.K., Goeke, N.M., Olson, B.J., Klenk, D.C. 1985. Measurement of protein using bicinchoninic acid. *Analytical Biochemistry*. 150(1): 76-85.

STATISTICA (data analysis software system), version 6. StatSoft, Inc. http://www.statsoft.com, 2004.

Stennard, F.A., Holloway, A.F., Hamilton, J., West, A.K. 1994. Characterization of six additional human metallothionein genes. *Biochimica et Biophysica Acta*. 1218: 357-365.

Stoscheck, C.M. 1990. Quantitation of protein. *In* Deutscher, M.P., *ed.* Methods in enzymology. San Diego: Academic. 60-62.

Sugimoto, N., Nakano, S., Yoneyama, M., Honda, K. 1996. Improved thermodynamic parameters and helix initiation factor to predict stability of DNA duplexes. *Nucleic Acids Research*. 24(22): 4501–4505.

Taanman, J.W. 1999. The mitochondrial genome: structure, transcription, translation and replication. *Biochimica Biophysica Acta*. 1410(2): 103-23.

Thein, S.L. & Wallcace, R.B. 1986. The use of synthetic oligonucleotides as specific hybridisation probes in the diagnosis of genetic disorders. *In*: Human genetic diseases: a practical approach. Davies, K.E., *ed.* Oxford: IRL Press, 33-50.

Thomas, J.P., Bachowski, G.J., Girotti, A.W. 1986. Inhibition of cell membrane lipid peroxidation by cadmium- and zinc-metallothioneins. *Biochimica et Biophysica Acta*. 884:448-461.

Thornalley, P.J., & Vašák, M. 1985. Possible role for metallothionein in protection against radiation-induced oxidative stress: Kinetics and mechanism of its reaction with superoxide and hydroxyl radicals. *Biochimica et Biophysica Acta*. 827(1): 36–44.

Triepels, R.H., Hanson, B.J., van den Heuvel, L.P., Sundell, L., Marusich, M.F., Smeitink, J.A., Capaldi, R.A. 2001a. Human Complex I Defects Can Be Resolved by Monoclonal Antibody Analysis into Distinct Subunit Assembly Patterns. *Journal of Biological Chemistry*. 276(12): 8892-8897.

Triepels, R.H., Van Den Heuvel, L.P., Trijbels, J.M., Smeitink, J.A. 2001b. Respiratory chain complex I deficiency. *American Journal of Medical Genetics*. 106(1):37-45.

Vallee, B.L. 1995. The function of metallothionein. *Neurochemistry International*. 27(1): 23-33.

Van der Heiden, M.G., & Thompson, C.B. 1999. Bcl-2 proteins: regulators of apoptosis or of mitochondrial homeostasis. *Nature Cell Biology*. 1(8): E209-E216.

Van der Westhuizen, F.H., & Pretorius, P.J. 2002. Simple, rapid technique for cloning eukaryotic colonies. Technical Tips Online. http://research.bmn.com/tto. 142 (1):T02489.

Van der Westhuizen, F.H., Van den Heuvel, L.P., Smeets, R., Veltman, J.A., Pfundt, R., Van Kessel, A.G., Ursing, B.M., Smeitink, J.A.M. 2003. Human mitochondrial complex I deficiency: Investigating transcriptional responses by microarray. *Neuropediatrics*. 34: 14-22.

Vandesompele, J., De Preter, K., Pattyn, F., Poppe, B., Van Roy, N., De Paepe, A., Speleman, F. 2002. Accurate normalization of real-time quantitative RT-PCR data by geometric averaging of multiple internal control genes. *Genome Biology*. 3: research0034.1–research0034.11.

Voet, D., & Voet, J.G. 1995. Biochemistry. 2nd edition. NY: John Wiley & Sons. 564-565.

Wallace, D.C. 1999. Mitochondrial diseases in man and mouse. *Science*. 283: 1482-1488.

Wallace, D. C., & Lott, M. T. "MITOMAP: A Human Mitochondrial Genome Database" http://www.mitomap.org, 2004.

Zhang, CY., Gong, Y-X., Ma, H., An, C-C., Chen, D-Y. 2000. Trichosanthin induced calcium-dependent generation of reactive oxygen species in human choriocarcinoma cells. *Analyst*. 125: 1539–1542.

APPENDIX A

SEQUENCING RESULTS OBTAINED FOR CLONING

Figure A.1 shows an example of a section from a sequence electropherogram received for pIRESNeo2-MT-1B clone 1 with the pIRES3' primer utilised for sequencing. The sequencing results obtained during the cloning process as discussed in Chapter 3 are indicated below.

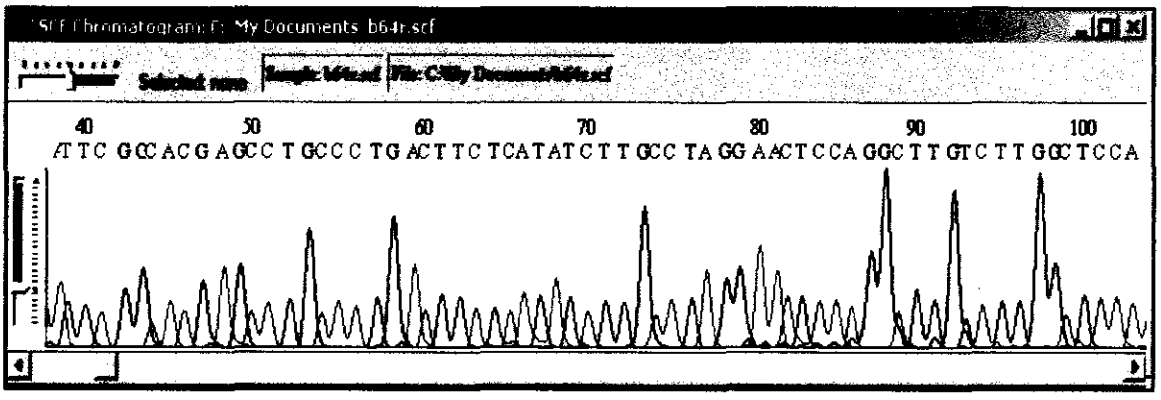

Figure A.1. Example of an electropherogram of sequence analysis of pIRESneo2-MT-1B clone 1 with the pIRES3' reverse primer.

Nucleotide	Sequence
3 3′	TGA CAT GAT TAC GAA TTT AAT ACG ACT CAC TAT AGG GAA TTT GGC
0	
	*Eco*R I
48	CCT CGA GGC CAA GAA TTC GGC ACG AGC CTG CCC TGA CTT CTC ATA
15	
93	TCT TGC CTA GGA ACT CCA GGC TTG TCT TGG CTC CAA ATG GAT CCC
30	M D P
138	AAC TGC TCC TGC ACC ACA GGT GGC TCC TGT GCC TGC GCC GGC TCC
45	N C S C T T G G S C A C A G S
183	TGC AAG TGC AAA GAG TGC AAA TGT ACC TCC TGC AAG AAG TGC TGC
60	C K C K E C K C T S C K K C C
228	TGC TCT TGC TGC CCC GTG GGC TGT GCC AAG TGT GCC CAG GGC TGT
75	C S C C P V G C A K C A Q G C
273	GTC TGC AAA GGC TCA TCA GAG AAG TGC CGC TGC TGT GCC TGA TGT
90	V C K G S S E K C R C C A *
318	TGG GAG AGC CCT GCT CCC AGA CAT AAA TAG AGC AAC CAG TAC TAA
363	CCT GGA TTT TTT TTT TTA ACT ACC CTG ACC GGT TTG CTA CAT TCT
408	TTT TTC TAT TCA ATA TGT GAA AGA CAA TAA AAC ACT TTT GAC TTG
	Pac I
453	AAA AAA AAA AAA AAA AAA AAA AAA GAT CTT TAA TTA AGC GGC CGC
498	AGG TTT ATT CCC TTA AGG GGG GGT AAA TTT TAG CT- GGG CAT GGG
543	CCG TGG TTT TAA AAC GTC GGG ACG GGG AAA AAC CCG GGG GTT CCC
588	CAA TTT AAT CCC CTT GGA GAA AAA AAA AAA AAA AAA 5′

Figure A.2. Sequencing of pT7T3D-PAC-MT-1B with the Universal primers. The sequence is indicated in the 3′-5′ direction, and the sequence of human MT-1B cDNA, (which corresponds exactly with the sequence of NCBI (NM_005947)), is indicated in blue text. The amino acid sequence of MT-1B is indicated underneath the nucleotide sequence. The underlined text shows the restriction sites of *Pac* I and *Eco*R I where the MT-1B cDNA sequence was ligated into.

Nucleotide	Sequence
2	GGT ACC GAG CTC GGA TCG ATC CTA CGA ACT CCA GGC TTG TCT TGG
1	
47	CTC CAA ATG GAT CCC AAC TGC TCC TGC ACC ACA GGT GGC TCC TGT
16	M D P N C S C T T G G S C
92	GCC TGC GCC GGC TCC TGC AAG TGC AAA GAG TGC AAA TGT ACC TCC
31	A C A G S C K C K E C K C T S
137	TGC AAG AAG TGC TGC TGC TCT TGC TGC CCC GTG GGC TGT GCC AAG
46	C K K C C C S C C P V G C A K
182	TGT GCC CAG GGC TGT GTC TGC AAA GGC TCA TCA GAG AAG TGC CGC
61	C A Q G C V C K G S S E K C R
227	TGC TGT GCC TGA TGT TGG GAG AGC CCT GCT CCC AGA CAT AAA TAG
76	C C A *
272	AGC AAC CAG TAC TAA CCT GGA TTT TTT TTT TTA ACT ACC CTG ACC
91	
317	GGC CTA GGA ACT CCA GGC TTG TCT TGG CTC CAA ATG GAT CCC AAC
106	M D P N
362	TGC TCC TGC ACC ACA GGT GGC TCC TGT GCC TGC GCC GGC TCC TGC
121	C S C T T G G S C A C A G S C
407	AAG TGC AAA GAG TGC AAA TGT ACC TCC TGC AAG AAG TGC TGC TGC
136	K C K E C K C T S C K K C C C
452	TCT TGC TGC CCC GTG GGC TGT GCC AAG TGT GCC CAG GGC TGT GTC
151	S C C P V G C A K C A Q G C V
497	TGC AAA GGC TCA TCA GAG AAG TGC CGC TGC TGT GCC TGA TGT TGG
166	C K G S S E K C R C C A *
542	GAG AGC CCT GCT CCC AGA CAT AAA TAG AGC AAC CAG TAC TAA CCT
587	GGA TTT TTT TTT TTA ACT ACC CTG ACC GGT CGT ACG TCT CCG GAT
632	TCA AAT TCG GAT CCG CGG CCG CAT AAA TAA CTG ATC CAG GGG GCT
677	GGA ATT AAC CCC CCT GTC TGC GAG GGC CAT CTG TTG GGG GGA GAA
722	CCC CCT CTC AAA AGC GGG CAT GAC TTC TGC GCT AAG ATT GCC AGT
757	TTT CAA AAA ACG AGG AGG ATT TGA TAT TCA CCT GGC CCG CGG TGA
812	TGC CTT TGA GGG TGG CCG CGT CCA TCT GGT CAG AAA AGA CAA TCT
857	TTT TGT TGT CAA GCT TGA GGT GTG GCA GGC TTG AGA TCT GGC CAT
902	ACA CTT GAG TGA CAA TGA CAT CCA CTT TGC CTTT CTC TCC ACA GGGT
947	GTC CAC TCC CAG GTCC AAC TGC AGG

Figure A.3. Sequencing of pIRESneo2-MT-1B clone 3 with primers T7 and pIRES-3´. The MT-1B (GenBank accession number NM_005947) cDNA nucleotide sequence as well as the amino acid sequence is indicated in blue text. This corresponds exactly to the NCBI sequence, though a double insert was ligated with a small fragment of the primer cleaved for ligation (yellow highlighted text) after *Pin*A I restriction. The neighbouring vector sequence (where the insert was ligated into) is indicated in normal black text, with purple text indicating nucleotides that do not correspond to the vector sequence. The extra nucleotides indicated in sequencing that do not correspond to the vector sequence, is indicated in red text.

```
>gi|27414494|ref|NM_005947.1|  Homo sapiens metallothionein 1B (functional)
(MT1B), mRNA
          Length = 404

 Score =  539 bits (272), Expect = e-150
 Identities = 272/272 (100%)
 Strand = Plus / Plus


Query: 184 gcctaggaac tccaggcttg tcttggctcc aaatggatcc caactgctcc tgcaccacag 243
           ||||||||||| ||||||||||| ||||||||||| ||||||||||| ||||||||||| ||||||||||
Sbjct: 25  gcctaggaac tccaggcttg tcttggctcc aaatggatcc caactgctcc tgcaccacag 84


Query: 244 gtggctcctg tgcctgcgcc ggctcctgca agtgcaaaga gtgcaaatgt acctcctgca 303
           ||||||||||| ||||||||||| ||||||||||| ||||||||||| ||||||||||| ||||||||||
Sbjct: 85  gtggctcctg tgcctgcgcc ggctcctgca agtgcaaaga gtgcaaatgt acctcctgca 144


Query: 304 agaagtgctg ctgctcttgc tgccccgtgg gctgtgccaa gtgtgcccag ggctgtgtct 363
           ||||||||||| ||||||||||| ||||||||||| ||||||||||| ||||||||||| ||||||||||
Sbjct: 145 agaagtgctg ctgctcttgc tgccccgtgg gctgtgccaa gtgtgcccag ggctgtgtct 204


Query: 364 gcaaaggctc atcagagaag tgccgctgct gtgcctgatg ttgggagagc cctgctccca 423
           ||||||||||| ||||||||||| ||||||||||| ||||||||||| ||||||||||| ||||||||||
Sbjct: 205 gcaaaggctc atcagagaag tgccgctgct gtgcctgatg ttgggagagc cctgctccca 264


Query: 424 gacataaata gagcaaccag tactaacctg ga 455
           |||||||||| |||||||||| |||||||||| ||
Sbjct: 265 gacataaata gagcaaccag tactaacctg ga 296
```

Figure A.4. Analysis of pIRESneo2-MT-1B clone 1 sequence with pIRES3' primer from 5'-3' as analysed with Basic Local Alignment Search Tool from NCBI. Query indicates the sequence analysed whilst Sbjct refers to the Genbank sequence NM 005947 it was compared to.

Nucleotide	Sequence
	TTA TAC CCC CCC CCC CCA TAG GGA GAC CCA AGC TTG GTA CCG AGC
2	
1	
47	TCG GAT CGA TCC GGT TTG CTA CAT TCT TTC CTA GGA ACT CCA GGC
16	5′ 3′
92	TTG TCT TGG CTC CAA ATG GAT CCC AAC TGC TCC TGC ACC ACA GGT
31	M D P N C S C T T G
137	GGC TCC TGT GCC TGC GCC GGC TCC TGC AAG TGC AAA GAG TGC AAA
46	G S C A C A G S C K C K E C K
182	TGT ACC TCC TGC AAG AAG TGC TGC TGC TCT TGC TGC CCC GTG GGC
61	C T S C K K C C C S C C P V G
227	TGT GCC AAG TGT GCC CAG GGC TGT GTC TGC AAA GGC TCA TCA GAG
76	C A K C A Q G C V C K G S S E
272	AAG TGC CGC TGC TGT GCC TGA TGT TGG GAG AGC CCT GCT CCC AGA
91	K C R C C A *
317	CAT AAA TAG AGC AAC CAG TAC TAA CCT GGA TTT TTT TTT TTA ACT
362	ACC CTG ACC GGA GAA TGT AGC AAA CCG GTC GTA CGT CTC CGG ATT
	3′ 5′
407	CGA ATT CGG ATC CGC GGC CGC ATA GAT AAC TGA TCC AGT GTG CTG
452	GAA TTA ATT CGC TGT CTG CGA GGG CCA GCT GTT GGG GTG AGT ACT
497	CCC TCT CAA AAG CGG GCA TGA CTT CTG CGC TAA GAT TGT CAG TTT
542	CCA AAA ACG AGG AGG ATT TGA TAT TCA CCT GGC CCG CGG TGA TGC
587	CTT TGA GGG TGG CCG CGT CCA TCT GGT CAG AAA AGA CAA TCT TTT
632	TGT TGT CAA GCT TGA GGT GTG GCA GGC TTG AGA TCT GGC CAT ACA
677	CTT GAG TGA CAA TGA CAT CCA CTT TGC TTT CTC TAG CGC ACA GGG
722	TGT ...

Figure A.5. Sequencing of pIRESneo2-MT-1B clone 1 with primers T7 and pIRES-3′. The MT-1B (GenBank accession number NM_005947) cDNA nucleotide sequence as well as the amino acid sequence is indicated in blue text. This corresponds exactly to the NCBI sequence. The neighbouring vector sequence (where the insert was ligated into) is indicated in normal black text. Purple text indicates nucleotides that do not correspond to the vector sequence. The extra inserts (yellow highlighted text) ligated between the vector ends and insert ends corresponds to the 3′ to 5′ sequences of the 3′ primer site (MT-1B-rev) that was cleaved with *Pin*A I for ligation purposes.

```
>gi|31543214|ref|NM_005953.2|  Homo sapiens metallothionein 2A (MT2A), mRNA
          Length = 372

 Score =  496 bits (250), Expect = e-137
 Identities = 268/274 (97%)
 Strand = Plus / Minus


Query: 1   tcgcgttctt tacatctggg agcggggctg tcccagcatc aggcgcagca gctgcacttg 60
           ||||||||||| |||||||||| |||||||||| |||||||||| |||||||||| ||||||||||
Sbjct: 281 tcgcgttctt tacatctggg agcggggctg tcccagcatc aggcgcagca gctgcacttg 222


Query: 61  tccgacgccc ctttgcagat gcagccctgg gcacacttgg cacagcccac agggcagcag 120
           |||||||||| |||||||||| |||||| ||| |||||||||| |||||||||| ||||||||||
Sbjct: 221 tccgacgccc ctttgcagat gcagccttgg gcacacttgg cacagcccac agggcagcag 162


Query: 121 gagcagcagc ttttcttgca ggaggtgcat ttgcactctt tgcatttgca ggagccggcg 180
           |||||||||| |||||||||  || |||||| |||||||||| |||||||||| ||| ||||||
Sbjct: 161 gagcagcagc ttttcttgca cgaagtgcat ttgcactctt tgcatttgca ggaaccggcg 102


Query: 181 caggtgcagg agtcaccggc ggcgcaggag cagttgggat ccatggcgag ctgaagaggc 240
           |||||||||| |||||||||| |||||||||| |||||||||| |||||||| | ||||||||||
Sbjct: 101 caggtgcagg agtcaccggc ggcgcaggag cagttgggat ccatggcgtg ctgaagaggc 42


Query: 241 ggctagagtc gggaccggtt gcacgcgggttcgc 274
           |||||||||| ||||| |||| ||||||||||||||
Sbjct: 41  ggctagagtc gggacaggtt gcacgcgggttcgc 8
```

Figure A.6. Analysis of pIRESneo2-MT-2A clone 3 sequence with pIRES3' primer from 3'-5' as analysed with Basic Local Alignment Search Tool from NCBI. Query indicates the sequence analysed whilst Sbjct refers to the Genbank sequence NM 005953 it was compared to. Nucleotides that do not correspond in this comparison were found to correspond in a duplicate sample and with forward primers.

Nucleotide	Sequence
1	GCC CAA AGC TTG GTA CCG AGC TCG GAT CGA TGC GAA CCC GCG TGC
1	
46	AAC CGG TCC CGA CTC TAG CCG CCT CTT CAG CTC GCC ATG GAT CCC
16	M D P
91	AAC TGC TCC TGC GCC GCC GGT GAC TCC TGC ACC TGC GCC GGC TCC
31	N C S C A A G D S C T C A G S
136	TGC AAA TGC AAA GAG TGC AAA TGC ACC TCC TGC AAG AAA AGC TGC
46	C K C K E C K C T S C K K S C
181	TGC TCC TGC TGC CCT GTG GGC TGT GCC AAG TGT GCC CAG GGC TGC
61	C S C C P V G C A K C A Q G C
226	ATC TGC AAA GGG GCG TCG GAC AAG TGC AGC TGC TGC GCC TGA TGC
76	I C K G A S D K C S C C A *
271	TGG GAC AGC CCC GCT CCC AGA TGT AAA GAA CGC G**AA TTC AGG TTT**
316	**GTG GAA TTC GGA TCC GCG GCC GCA TAG ATA ACT GAT CCA GTG TGC**
361	**TGG AAT TAA TTC GCT GTC TGC GAG GGC CAG CTG TTG GGG TGA GTA**
406	**CTC CCT CTC AAA AGC GGG CAT GAC TTC TGC GCT AAG ATT GTC AGT**
451	**TTC CAA AAA CGA GGA GGA TTT GAT ATT CAC CTG GCC CGC GGT GAT**
496	**GCC TTT GAG GGT GGC CGC GTC CAT CTG GTC AGA AAA GAC AAT CTT**
541	**TTT GTT GTC AAG CTT GAG GTG TGG CAG GCT TGA GAT**

Figure A.7. Sequencing of pIRESneo2-MT-2A clone 3 with primers T7 and pIRES-3′. The MT-2A (GenBank accession number NM_005953) cDNA nucleotide sequence as well as the amino acid sequence is indicated in blue text. This corresponds exactly to the NCBI sequence. The neighbouring vector sequence (in which the insert was inserted to) is indicated in normal black text. Purple text indicates nucleotides that do not correspond to the vector sequence. The extra insert (yellow highlighted text) ligated between the 3′ insert end and the 5′ vector end corresponds to a section of the 3′ to 5′ sequence of the 3′ primer site (MT-2-rev) that was cleaved with *Eco*R I for ligation purposes.

APPENDIX B

NORTHERN AND REAL-TIME ANALYSES TO ANALYSE MT mRNA EXPRESSION

B.1. NORTHERN ANALYSIS

Originally it was decided to confirm the MT-1B and MT-2A mRNA expression in the transfected clone pools with the use of Northern blotting[1]. However, the method exhibited various difficulties resulting in the use of real-time PCR instead. Section B.1 describes the modified protocol for the analysis and Section B.2 shows the result of the MT-1B expression analysis in the various clones.

B.1.1. Materials and methods

Formaldehyde gel electrophoresis (1.2 % agarose) of the isolated RNA samples (see Section 4.1.3) was run according to Brown & Mackey (1997).

The specific MT-1B and MT-2A cDNA utilised for probe labelling was amplified with the MT-1B- and MT-2A-specific primers as described in Sections 3.1.2.2 and 3.1.2.3 and extracted from agarose gels after electrophoresis by means of a DNA extraction kit (Fermentas) according to the manufacturer's specifications. The Gene Images™[2] Random Prime Labelling Module (Amersham Biosciences) was subsequently modified to a PCR amplification step to label the extracted cDNA's with the MT-1B-fwd/MT-1B-rev and MT-2A-fwd/MT-2A-rev primers. The PCR reaction contained the following to a final volume of 50 µl: nucleotide mix [5 x stock solution of fluorescein-11-dUTP (Fl-dUTP), dATP,dCTP, dGTP and dTTP in Tris®-HCl, pH 7.8, 2-mercaptoethanol and $MgCl_2$], 20 pmoles of each of the

[1] Northern blotting was standardised and performed in collaboration with O. Levanets.
[2] Gene Images™ is a trademark of Amersham Biosciences UK Limited, Buckinghamshire, UK.

primers, 45 ng PCR product, 1 unit Taq polymerase and RNase-free water. The reaction was amplified as indicated in Table 4.1 for 25 cycles.

Table B.1: PCR conditions for amplification of MT-1B and MT-2A probes

PCR step	# of cycles	Action	Temperature (°C)	Duration (min)
1	1	Initial denaturation	94	2:00
		Denaturation	94	0:30
2	25	Annealing	59	0:30
		Extension	72	0:30
3	1	Final extension	72	5:00
4	1	Cooling	4	Hold

= number of cycles.

Hybridisation and stringency washes were carried out according to the protocol included with the Gene Images™ Random Prime Labelling Module (Amersham Biosciences), which was originally utilised during the labelling procedure. Following the stringency washes, the Gene Images™ CDP-Star™[1] detection module (Amersham Biosciences) was used to detect the fluorescein-labelled probe according to the manufacturer's specifications with at least 3 hour film exposures. The film was then developed in a High Contrast Film Developer (Phenisol film developer, Ilford ™) and immediately fixed with the Rapid fixer (5 x film & paper fixer, Ilford).

[1] CDP-Star is a trademark of Tropix Inc., Bedford, MA, U.S.A.

B.1.2. Results

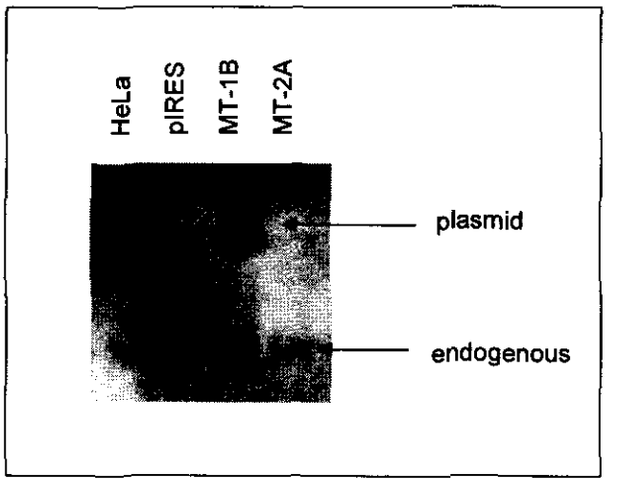

Figure B.1. Northern blot for MT-1B mRNA expression. The MT-1B mRNA expression due to the pIRESneo2-MT-1B plasmid (plasmid) showed a strong signal. Expression of normal MT-1B (endogenous) in HeLa cells, pIRESneo2, -MT-1B and -MT-2A transfected clone pools showed very low signal intensity.

B.2. REAL-TIME PCR ANALYSIS

Figure B.2 depicts fluorescence measurements (relative fluorescent units) against cycle number for amplification of pIRESneo2, pIRESneo2-MT-1B and pIRESneo2-MT-2A with MT-1B and MT-2A specific primers respectively (n = 3). The threshold setpoint was set at 60 for all analyses. The Ct values indicated in this figure are listed in Table B.2.

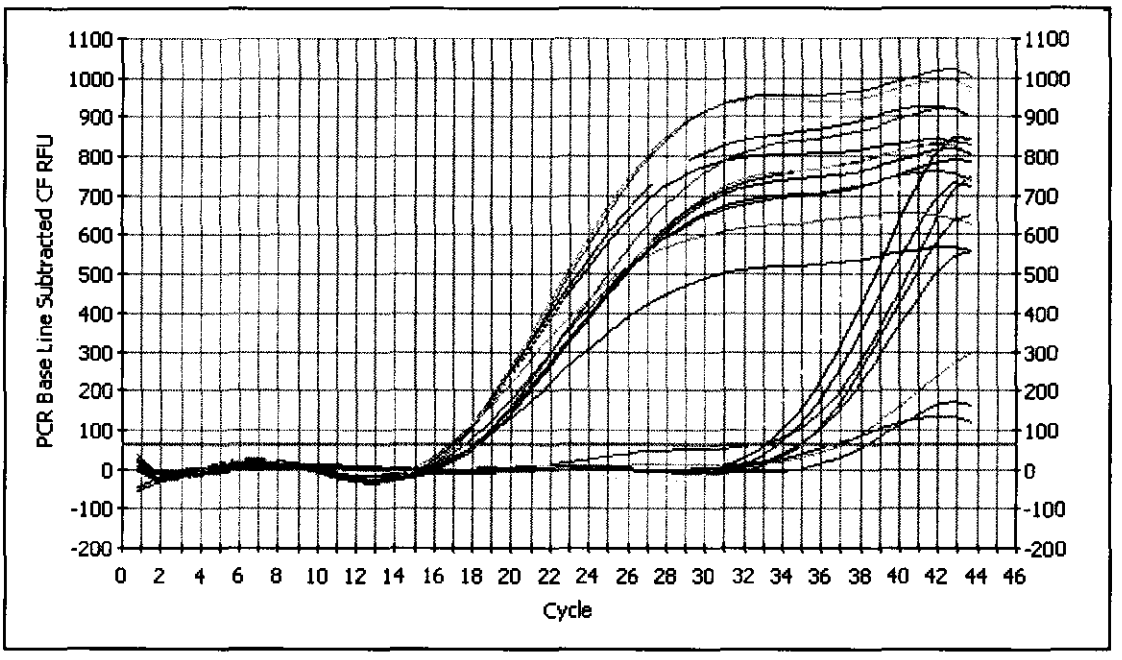

Figure B.2. Example of real-time PCR results for pIRESneo2, pIRESneo2-MT-1B and pIRESneo2-MT-2A with MT-1B and MT-2A specific primers. Threshold setpoint is indicated as an orange line. Results are indicated individually by differently colored lines. Table B.2 indicates the Ct values obtained from these results.

Table B.2: Real-time PCR results for MT-1B and MT-2A expression indicated as Ct values

PCR Quantification Spreadsheet Data for FAM-490					
Well	**Identifier**	**Ct**	**Well**	**Identifier**	**Ct**
	MT-1B primers			**MT-2A primers**	
F01	pIRESneo2	32.4	**G01**	pIRESneo2	18.1
F02	pIRESneo2	36.9	**G02**	pIRESneo2	18.2
F03	pIRESneo2	34.8	**G03**	pIRESneo2	18.2
F04	pIRESneo2-MT-1B	16.9	**G04**	pIRESneo2-MT-1B	17.9
F05	pIRESneo2-MT-1B	17	**G05**	pIRESneo2-MT-1B	18
F06	pIRESneo2-MT-1B	17.1	**G06**	pIRESneo2-MT-1B	18
F07	pIRESneo2-MT-2A	33.7	**G07**	pIRESneo2-MT-2A	16.9
F08	pIRESneo2-MT-2A	33	**G08**	pIRESneo2-MT-2A	16.9
F09	pIRESneo2-MT-2A	34.8	**G09**	pIRESneo2-MT-2A	17.5
F10	HeLa	32.1	**G10**	HeLa	16.8
F11	(-) control	38.2	**G11**	(-) control	36.4

APPENDIX C

REFERENCE FOR VALIDATION OF HOUSEKEEPING GENES SUITABILITY

Validation of housekeeping genes suitability as normalization controls in rotenone-induced Complex I deficient HeLa cells

Oksana Levanets[a], Antonel Olckers[b], Francois H. van der Westhuizen[a,*]

[a]Division of Biochemistry, School for Chemistry and Biochemistry, North-West University, Potchefstroom, South Africa

[b]Center for Genome Research, North-West University, Pretoria, South Africa

*Corresponding author: [a]Division of Biochemistry, School for Chemistry and Biochemistry, North-West University, Hoffmanstreet, Potchefstroom, 2520, South Africa. Tel: +27 18 2992318, Fax +27 18 2992316, E-mail: bchfhvdw@puk.ac.za

Abstract

The contribution of transcriptional responses to the cellular consequences in mitochondrial disease has clearly become evident in recent years. One of the tools to investigate these responses, quantitative real-time PCR (RT-PCR) is regarded as one of the most reliable and rapid methods but requires reference genes for normalization. We evaluated the expression variation of five commonly used housekeeping genes in rotenone-induced complex I deficient HeLa cells. 18S rRNA was found to be the most stable gene, followed by β-microglobulin, GAPDH, β-actin and RNA polymerase II. Although the selection of housekeeping genes for the normalization of expression data depends on the specific experimental conditions and cell line, these results may by useful for selecting suitable housekeeping genes when investigating transcriptional responses in mitochondrial deficiencies.

Keywords: Quantitative real-time PCR; Reference genes; Housekeeping genes; Transcription analysis; Mitochondrial complex I deficiency; Rotenone.

1. Introduction

The cell biological consequences of deficiencies of the oxidative phosphorylation (OXPHOS) system are complex and include a diversity of cellular processes such as metabolic and signal transduction imbalances as well as oxidative stress-related damage (Briére et al., 2004). The disease expression depends on several factors, including the genotype and tissues affected. Much interest currently exists in the contribution of mitochondrial and nuclear transcriptional responses to the phenotype expression of mitochondria-related diseases, of which NADH:ubiquinone oxidoreductase (complex I) deficiency is one of the most frequently encountered (Triepels et al., 2001; Loeffen et al., 2000). Although limited data still exists, it is becoming evident that nuclear-mitochondrial communication may play a distinct role in the pathology of the complex I deficiency (van der Westhuizen et al., 2003; Heddi et al., 1999; Collombet et al., 1997).

For the investigation of transcriptional responses many techniques allow quantitative analysis of mRNA expression such as Northern blotting, *in situ* hybridization, RNase protection, microarray analysis and competitive RT-PCR. Quantitative real-time PCR has become a powerful tool for transcription quantification in recent years due to its high accuracy, broad dynamic range, and sensitivity. Independent of the techniques used, quantifications are generally normalized using so-called housekeeping genes as invariant controls to account for sample handling, loading and experimental variation. This practice is being questioned as it becomes increasingly clear that some housekeeping genes may vary considerably in certain biological samples (Bustin, 2002). Therefore, identifying suitable control genes has become one of the important problems in such investigations. To assist these types of studies we investigated the stability of expression of certain commonly used housekeeping genes, including glyceraldehyde-3-phosphate dehydrogenase (GAPDH), β-actin, β-2-microglobulin (β-2-MG), RNA polymerase II (RP2) and 18S rRNA, in rotenone-induced complex I-deficient HeLa cells.

2. Materials and methods

2.1. Cell culture and rotenone treatments

HeLa cells were cultured in Dulbecco's Modified Eagles medium (DMEM) containing 5% (v/v) fetal calf serum and antibiotics (penicillin, 250U/ml; streptomycin, 250μg/ml) in a humidified incubator at 37 °C and 5%

CO_2. To cultures that were approximately 70% confluent in 25 cm^2-flasks rotenone was added at various final concentrations ranging between 0 and 10 µM. These incubations enabled the induction of complex I deficient cell lines with rotenone-sensitive residual enzyme activities of approximately 100% (at 0 nM rotenone), 50% (10 nM), 30% (100 nM), 12% (1000 nM) and 0% (2.5 µM and higher), as measured in enriched mitochondrial preparations and normalized against citrate synthase activity (Rahman et al., 1996). As a control for the induction of oxidative stress, *tert*-butyl hydroperoxide (*t*-BHP) at concentrations ranging between 0.5 and 1.0 mM were included in the array of incubations. Separate sets of incubations were performed for 24 and 48 hours.

2.3. RNA isolation and cDNA synthesis

Total RNA was isolated using QIAzol™ reagent (Qiagen, Hilden, Germany) according to instructions and the RNA integrity was electrophoretically verified by ethidium bromide staining. 3 µg of RNA was reverse transcribed with 200U M-MLV Reverse Transcriptase (Promega, Madison, WI) in a volume of 40 µl using 0.5 µg random hexamer primers (Promega) according to manufacturer's instructions.

2.4. Quantitative real-time PCR

The sequences of all primers used for the PCR are listed in Table 1. Real-time quantitative PCR was performed using an iCycler iQ™ (Bio-Rad, Hercules, CA) in a final volume of 20 µl using the SYBR Green method. The PCR reaction consisted of 10 µl iQ™ SYBR® Green Supermix (Bio-Rad, Hercules, CA), 500 nM of forward and reverse primers, and 75 ng of cDNA (3 ng for 18S rRNA primers). A four-step experimental run protocol was used: 1) initial denaturation (3 min. at 95 °C); 2) 35 cycles of denaturation at 95 °C for 20 sec, primer annealing at 60 °C for 10 sec, extension at 72 °C for 20 sec and an additional step at 82 °C (84 °C for 18S rRNA primers) with a single fluorescense measurement; 3) final extension at 72 °C for 5 min; 4) melting curve analysis (55-95 °C with a heating rate of 0.5 °C per 5 sec and fluorescent measurement every 5 sec). A high temperature fluorescence measurement point at the end of the fourth segment was performed to improve SYBR Green quantification (Pfaffl et al., 2002). Fluorescence was measured following each cycle and displayed graphically (iCycler iQ Real-time Detection System Software, version 3.0, BioRad, Hercules, CA). The software determined a cycle threshold (Ct) value, which identified the number of PCR cycles where the fluorescence signal exceeds the detection threshold value for that sample. This threshold is set to the log linear range of the

amplification curve and kept constant for data analysis throughout the study. Every assay included a no-template control, five serial dilution points (in steps of 5-fold) of a cDNA mixture, as well as each of the test cDNA's. All samples were amplified in triplicates and the mean value was used for further calculations.

2.5. Calculations and statistical analysis

Results (Ct values) from iCycler iQ Real-time Detection System were analyzed by Statistica Version 6.1 software (StatSoft, Tulsa, OK) and BestKeeper software tool (Pfaffl et al., 2004). PCR efficiency for each primers set was calculated by serial dilutions method using REST software tool (Pfaffl et al., 2002). The relative expression quantities for each sample were calculated by the comparative Ct method and gene expression stability was analyzed using GeNorm software tool (Vandesompele et al., 2002).

3. Results

Quantitative real-time RT-PCR was performed on total RNA samples obtained from HeLa cells that were treated with various rotenone concentrations, resulting in residual complex I activities ranging between 0 and 100%, as well as *t*-BHP-induced oxidative stress. To ensure comparability between the analyses of all five housekeeping genes, we first determined the reaction efficiency of each individual assay by measuring serial dilutions of 75 ng cDNA in triplicate (Pfaffl et al., 2002). All PCR reactions displayed efficiency between 88% and 100%. The variations in the cycle threshold (Ct) values, which represent the cycle where a significant increase in amount of PCR product occurs, are summarized in Figure 1. Comparing the median expression values (Ct values) of the housekeeping genes, as shown in Figure 1, the variability for housekeeping gene expression was clearly less in the case of the 18S rRNA as compared to the other genes. Ct values were also expressed as relative expression quantities and analyzed using the GeNorm software tool. The results of this analysis are presented as GeNorm expression stability values (or gene stability measures, M), which are defined as average pairwise variations of a particular gene with all other control genes as summarized in Table 2 (Vandesompele et al., 2002). Genes with the lowest M values have the most stable expression. Figure 2 shows the standard deviation expressed as a fold change from the mean and range expressed as maximum variability for housekeeping genes after rotenone treatment. The most stable housekeeping gene in these conditions was 18S

rRNA with a maximum variability of 1.3 fold change. The most variable genes were RNA polymerase II and β-actin (1.97 and 1.96 fold change, respectively).

4. Discussion

One of the essential consequences of mitochondrial disease is altered expression of some genes involved in bioenergetics (van der Westhuizen et al., 2003; Heddi et al., 1999; Collombet et al., 1997). Investigations of transcriptional responses will no doubt contribute to our understanding of the disease and with the tools currently available present exciting challenges. Real-time PCR is one of the most accurate and commonly used methods to evaluate changes in gene expression. A parallel quantification of a housekeeping gene is a commonly used approach for the validation of the expression of tested gene. The first comparisons of the levels of gene expression were based on the assumption that constant expression of housekeeping genes exist in all the tissues and cells under all conditions. But it became clear that various incubating conditions and different stress or pathological states of the organism strongly influence the expression of housekeeping genes (Thellin et al., 1999; Bustin, 2002; Radonic et al., 2004). To avoid these problems evaluating expression stability of several housekeeping genes under the experimental conditions should be performed before selecting the most stable gene or a panel of genes for normalization (Bustin, 2002).

To define suitable internal controls for gene expression quantification in an *in vitro* complex I deficient model we titrated HeLa cells with rotenone. *In vitro* modulation of mitochondrial electron transport is often used to investigate underlying mechanisms of these diseases (Mojet et al., 1997; Luetjens et al., 2000; Chinopoulos and Adam-Vizi, 2001). Rotenone is commonly used specific and irreversible inhibitor of complex I has been shown to induce apoptosis via the production of reactive oxygen species in several cell lines (Li et al., 2003). For analysis of housekeeping genes expression stability we have chosen commonly used genes representing different biological activities including glycolysis, cytoskeleton structure and kinetics, immune response, gene expression and protein biosynthesis. Our study of internal controls stability in conditions of induced mitochondrial complex I deficiency revealed 18S rRNA to be the most stable and most suitable for normalization of tested genes expression quantification both for 24 and 48 h treatments. The maximum fold change in expression level for 18S rRNA under conditions where low to high levels of complex 1 activity, oxidative stress and apoptosis occur, was only 1.3 times. Using 18S rRNA as an internal control, however, has some disadvantages. Firstly, it's

possible to use only total RNA for quantification and to synthesize cDNA with random primers. Secondly, 18S rRNA gene contains no introns and transcript amplification therefore is susceptible to false results from contaminating DNA. And thirdly, due to the high abundance of rRNA transcripts, using 18S rRNA as an internal control for studies of genes expressed at relatively low levels requires additional dilution of cDNA templates or lower primer concentrations for its amplification. As expected, 18S rRNA was the most abundant of transcripts (lowest Ct value even after 25 times cDNA dilution), and RNA polymerase II transcript appeared to be the least abundant.

RNA polymerase II and β-actin appeared to be the most variable in our experimental conditions, but even for these genes expression variability levels (maximum 1.97 and 1.96 fold changes, respectively) allow use them for normalization in quantification experiments.

In conclusion, according to our data, the rank of housekeeping genes expression stability in conditions of rotenone-induced complex I deficient HeLa cells is 18S rRNA, β-microglobulin, GAPDH, β-actin, RNA polymerase II. As none of the genes has transcription variation of more than two all of these genes should be suitable as internal controls in similar experiments. However, each of these genes has some advantages and disadvantages as internal controls which must be considered. Although current opinion suggests the preferable use of a housekeeping gene panel for obtaining more accurate results in quantification, we believe our data could be useful when considering a normalization strategy for investigations of transcriptional responses in mitochondrial disease.

Acknowledgements

The authors would like to thank the National Research Foundation of South Africa for financial support (GUN 2053704). We would also like to thank the staff of the School of Pharmacy, North-West University, for use of PCR apparatus and the staff of the Mitochondrial Research Laboratory, North-West University, for assistance.

References

Bustin, S.A., 2002. Quantification of mRNA using real-time reverse transcription PCR (RT-PCR): trends and problems. J. Mol. Endocrinol. 29, 23-39.

Brière, J.J., Chrétien, D., Bénit, P., Rustin, P., 2004. Respiratory chain defects: what do we know for sure about their consequences in vivo? Biochimica et Biophysica Acta (BBA) – Bioenergetics In Press.

Chinopoulos, C., Adam-Vizi, V., 2001. Mitochondria deficient in complex I activity are depolarized by hydrogen peroxide in nerve terminals: Relevance to Parkinson's disease. J. Neurochem. 76, 302-306.

Collombet, J.M., Faure-Vigny, H., Mandon, G., Dumoulin, R., Boissier, S., Bernard, A., Mousson, B., Stepien, G., 1997. Expression of oxidative phosphorylation genes in muscle cell cultures from patients with mitochondrial myopathies. Mol. Cell. Biochem. 168, 73-85.

Heddi, A., Stepien, G., Benke, P.J., Wallace, D.C., 1999. Coordinate induction of gene expression in tissues of mitochondrial disease. J. Biol. Chem. 274, 22968-22976.

Li, N., Ragheb, K., Lawler, G., Sturgis, J., Rajwa, B., Melendez, J.A., Robinson, J.P., 2003. Mitochondrial complex I inhibitor rotenone induces apoptosis through enhancing mitochondrial reactive oxygen species production. J. Biol. Chem. 278, 8516-8525.

Loeffen, J.L., Smeitink, J.A., Trijbels, J.M., Janssen, A.J., Triepels, R.H., Sengers, R.C., van den Heuvel, L.P., 2000. Isolated complex I deficiency in children: clinical, biochemical and genetic aspects. Hum. Mutat. 15, 123-34.

Luetjens, C.M., Bul, N.T., Sengpiel, B., Munstermann, G., Poppe, M., Krohn, A.J., Bauerbach, E., Kriegstein, J., Prehn, J.H., 2000. Delayed mitochondrial disfunction in excitotoxic neuron death: Cytochrome *c* release and a secondary increase in superoxide production. J. Neurosci. 20, 5715-5723.

Mojet, M.H., Mills, E., Duchen, M.R., 1997. Hypoxia-induced catecholamine secretion in isolated newborn rat adrenal chromaffin cells is mimicked by inhibition of mitochondrial respiration. J. Physiol. 504, 175-189.

Pfaffl, M.W., Horgan, G.W., Dempfle, L., 2002. Relative expression software tool (REST) for group-wise comparison and statistical analysis of relative expression results in real-time PCR. Nucleic Acids Res. 30, e36.

Pfaffl, M.W., Tichopad, A., Prgomet, C., Neuvians, T.P., 2004. Determination of stable housekeeping genes, differentially regulated target genes and sample integrity: BestKeeper--Excel-based tool using pair-wise correlations. Biotechnol. Lett. 26, 509-515.

Table 1

Gene specific primers used for real-time PCR.

Gene	Primers	Sequence	Accession number	Reference	Amplicon size, bp
GAPDH	GAPDH-Fwd	GAAGGTGAAGGTCGGAGTC	NM_002046	Radonic et	226
	GAPDH-Rev	GAAGATGGTGATGGGATTTC		al., 2004	
β-actin	Beta-Act-Fwd	AGCCTCGCCTTTGCCGA	NM_001101	Radonic et	174
	Beta-Act-Rev	CTGGTGCCTGGGGCG		al., 2004	
β-2-microglobulin	Beta-2-MG-Fwd	AGCGTACTCCAAAGATTCAGGTT	NM_004048	Radonic et	306
	Beta-2-MG-Rev	ATGATGCTGCTTACATGTCTCGAT		al., 2004	
RNA polymerase II	RP2-Fwd	GCACCACGTCCAATGACAT	X63564	Radonic et	267
	RP2-Rev	GTGCGGCTGCTTCCATAA		al., 2004	
18S rRNA	18SrRNA-Fwd	GTGCATGGCCGTTCTTAGTT	X03205	Generated	187
	18SrRNA-Rev	CGGACATCTAAGGGCATCAC		by Primer3 software	

Table 2

GeNorm analysis of housekeeping genes expression stability. Results are shown as GeNorm expression stability values or M, the internal control gene-stability measure, defined as average pairwise variation of a particular gene with all other control genes (Vandesompele et al., 2002). Genes with the lowest M values have the most stable expression.

Gene	M (24 h)	M (48 h)
18S rRNA	0.466	0.402
Beta-2-microglobulin	0.548	0.503
GAPDH	0.575	0.506
Beta-actin	0.682	0.512
RNA polymerase II	0.730	0.532

Figure 1

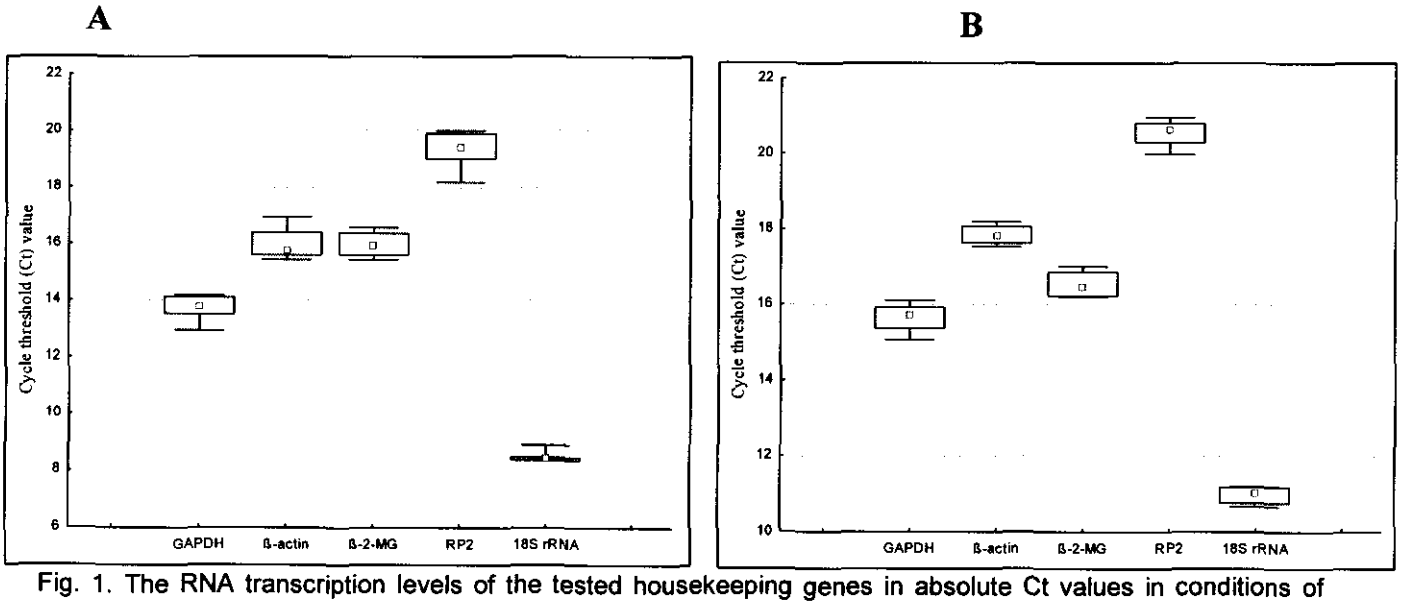

Fig. 1. The RNA transcription levels of the tested housekeeping genes in absolute Ct values in conditions of rotenone-induced complex I deficiency in HeLa cells (A, 24 h induction; B, 48 h induction). The median values are indicated by small squares, 25 - 75% percentiles are indicated by the boxes and minimum and maximum values indicated by whiskers.

Figure 2

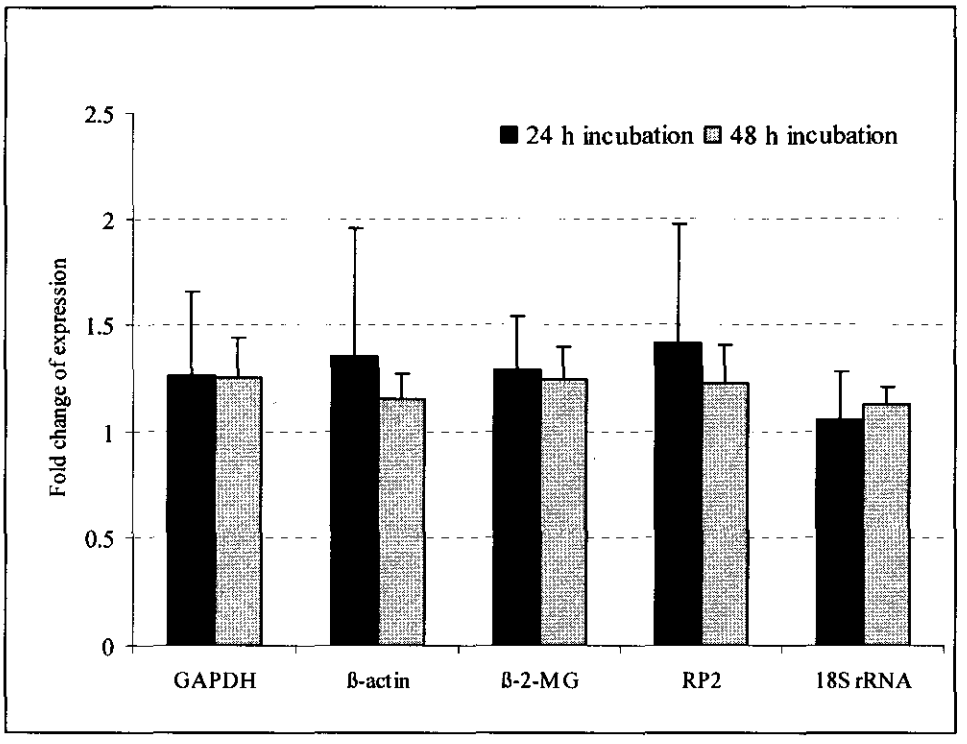

Fig. 2. Changes in housekeeping genes expression in rotenone-induced complex I deficient HeLa cells. Variability of genes expression shown as an average fold change from the mean (columns) and maximum fold change (error bars).